SPECTRAL FEATURE EXTRACTION OF BIOMEDICAL SIGNALS

Ishan Ranjan

A Thesis
in
The Department
of
Electrical and Computer Engineering

Presented in Partial Fulfillment of the Requirements
for the Master of Applied Science at
Concordia University
Montreal, Quebec, Canada

January 1991

National Library
of Canada

Acquisitions and
Bibliographic Services Branch

395 Wellington Street
Ottawa, Ontario
K1A 0N4

Bibliothèque nationale
du Canada

Direction des acquisitions et
des services bibliographiques

395, rue Wellington
Ottawa (Ontario)
K1A 0N4

Your file Votre référence

Our file Notre référence

ISBN 0-315-90908-0

Canada

ABSTRACT

Algorithms are developed and tested to interpret EEG signals. The basis of the study is the interest doctors and biomedical engineers have in spectral feature extraction of these signals.

The work here deals with spectral modeling of brain or EEG signals. Methods based on a combination of linear prediction and homomorphic filtering are applied to simulated and real EEG signals. Another active area of research in EEG signal analysis is noise cancellation. An attempt has been made to minimise muscle noise in EEG signals using adaptive filtering. Some encouraging results are obtained with real data studies. Sequential adaptive spectral estimation of EEG signals is also studied using different adaptive algorithms.

In recent years, multidimensional spectral estimation has become an area of considerable interest. Progress has been made in the developement of parametric methods for multidimensional spectral estimation in general and bispectrum estimation in particular. Here an algorithm for bispectrum estimation based on parametric models is studied and is used for detecting quadratic phase coupling in EEG signals.

ACKNOWLEDGEMENTS

The author is indebted to his supervisors, Dr. E.I. Plotkin, Professor,Department of Electrical and Computer Engineering and Dr. M.N.S. Swamy, Dean, Faculty of Engineering and Computer Science, for the advice and guidance they have given throughout the course of this study.

The author is also very grateful to Dr. Plotkin and Dr. Swamy for providing graduate student support through their NSERC grants. The additional support provided by Concordia University in the form of International Student Fee Remissions is also gratefully acknowledged.

The author is thankful to Dr. J. Gotman, Professor of Applied Neurology, Montreal Neurological Institute for providing data for the study and to Dr. Kenneth Hickey Jr. for familiarizing the author with the clinical experiment.

The assistance and helpful suggestions provided by Dr. S.V. Narasimhan, Dr. Dov Wulich, Mr. Tong Wen and Mr. Xing Chen are also appreciated.

Table of Contents

LIST OF FIGURES vii
LIST OF TABLES ix

CHAPTER 1 INTRODUCTION 1
1.1. Brief Description of Research 1
1.2. Organization of the Thesis 3

CHAPTER 2 REVIEW OF EXISTING RESEARCH 4
2.1. Introduction 4
2.2. EEG Signal Characterstics 5
2.3. EEG Signal Processing - a review 7
2.3.1. Introduction 7
2.3.2. Time Domain Analysis 7
2.3.3. Frequency Domain Analysis 9
2.3.4. Parametric Models for EEG Analysis 12
2.3.5. Nonstationary EEG Analysis 19
2.3.6 Transients in EEG and their Detection 20
2.3.7. Artefacts in EEG and their Elimination 21
2.4. References 24

CHAPTER 3 SOFTWARE SIMULATION OF EEG SIGNALS 34
3.1. Introduction 34
3.2. The Basic Model 35
3.3. Implementation 36
3.4. Examples and Results 41
3.5. References 47

CHAPTER 4 SPECTRAL ESTIMATION OF EEG SIGNALS 48
4.1. Introduction 48
4.2. Spectral Modeling by Homomorphic Prediction 49
4.3. Spectral Modeling by Pole Zero Decomposition 55
4.4. Results 58
4.5. References 71

CHAPTER 5 MUSCLE ARTEFACT CANCELLATION FROM EEG SIGNALS 73
5.1. Introduction 73

5.2. Simulation of Muscle Artefact 74
5.3. Filtering of Muscle Artefact from EEG 78
5.4. Studies with Simulated Data 81
5.5. Studies with Real Data 86
5.6. References 91

CHAPTER 6 ADAPTIVE SPECTRAL ESTIMATION OF EEG SIGNALS 93
6.1. Introduction 93
6.2. LMS Gradient Adaptive Algorithm 94
6.3. LMS - Lattice Adaptive Algorithm 99
6.4. LMF - Lattice Adaptive Algorithm 100
6.5. Simulation Results 101
6.6. Conclusions 106
6.7. References 107

CHAPTER 7 BISPECTRUM ESTIMATION OF EEG SIGNALS 109
7.1. Introduction 109
7.2. Bispectrum Estimation - a review 111
7.2.1. Introduction 111
7.2.2. Cumulants and Higher Order Spectra 111
7.2.3. Bispectrum : Definition and Properties 112
7.2.4. Bispectrum Estimation Procedures 113
7.2.5. Use of Bispectrum in Signal Processing 116
7.3. Bispectrum Estimation based on Parametric Model 121
7.3.1. Introduction 121
7.3.2. AR Model for Bispectrum Estimation 121
7.3.3. Third Order Recursion Method 125
7.4. Detection of Quadratic Phase Coupling 129
7.4.1. Introduction 129
7.4.2. Quadratic Phase Detection in EEG Signals 130
7.5. Conclusions 132
7.6. References 136

CHAPTER 8 CONCLUSIONS 139

LIST OF FIGURES

Fig.3.1 Schematic diagram of EEG simulator (Zetterberg, 1973) 40

Fig.3.2 Simulated EEG signals for given set of parameters 43

Fig.4.1 Canonic representation of a homomorphic system 51

Fig.4.2 Negative derivative phase spectrum for all pole filters 51

Fig.4.3 Comparison of spectrum of EEG estimated by homomorphic prediction 60

Fig.4.4 Estimated pole - zero spectrum for EEG signals 61

Fig.4.5 Real EEG signals recorded (Montreal Neurological Institute, 1990) 62

Fig.4.6 Component spectrum for real EEG by different methods 64

Fig.5.1 Logmagnitude spectrum of the impulse response of filters (Johnson, 1979) 76

Fig.5.2 Simulated muscle noise sampled at 200 Hz 77

Fig.5.3 The LMS-TDL predictor with decorrelation delay. 80

Fig.5.4 Burg spectrum for different stages of filtering of the EEG signal 83

Fig.5.5 Burg spectrum for different stages of filtering of the EEG signal 89

Fig.5.6a Muscle noise contaminated real EEG segment 91

Fig.5.6b Lowpass filtered muscle noise contaminated EEG signal 91

Fig.5.6c LMS - TDL predictor output 91

Fig.5.6d LMS - lattice predictor output 91

Fig.6.1 The LMS - TDL prediction filter 97

Fig.6.2 Computed spectrum from prediction filter coefficients 103

Fig.7.1 Flowchart of parametric bispectrum estimation method 127

Fig.7.2 Detection of quadratic phase coupling in EEG signals using bispectrum 133

LIST OF TABLES

Table 3.1 Parameters of EEG registration 44

Table 3.2 Parameters of realised EEG filters 44

Table 3.3 The parameters of individual EEG activities 45

Table 3.4 The parameters of simulated EEG data 45

Table 3.5 Parameters of the simulated EEG signal 46

Table 4.1 Different EEG signal spectrum by homomorphic prediction. 65

Table 4.2 Different EEG signal spectrum by pole-zero decomposition. 66

Table 4.3a Estimated poles and zeros by different methods. 67

Table 4.3b Estimated poles and zeros by different modeling methods. 67

Table 4.3c Estimated zeros by different modeling methods. 68

Table 4.3d Estimated zeros by different modeling methods. 69

Table 4.3e Estimated zeros by different modeling methods. 69

Table 4.3f Estimated zeros by different modeling methods. 70

Table 5.1 Parameters of EEG registration 82

Table 5.2 Frequencies estimated by Burg's method for EEG signal. 85

Table 5.3 Frequencies estimated by Burg's method for EEG signal. 90

Table 6.1 Parameters of EEG registration 104

Table 6.2 Frequencies estimated by Burg's method for EEG signal. 104

Table 6.3 Frequencies estimated by Burg's method for EEG signal. 105

Table 8.1 Degree of phase coupling of EEG during REM sleep. 135

CHAPTER 1

INTRODUCTION

1.1 A Brief Description of the Research

The subject matter of the thesis falls in the general area of spectral analysis which finds applications in a wide variety of fields, especially in the area of brain research. Brain signals, or EEGs as they are called have become an indispensable tool in clinical neurophysiology, pharmacology and other related areas. The EEG is mainly contained of frequency related activities i.e. alpha, beta, theta and delta, which are wide sense stationary, the nonstationary spike and waves, and transients. Further, the stationary EEG segments are preceeded and suceeded by nonstationary transients.

The main objective of EEG signal and spectral analysis is to extract valid information from the EEG record and present it in a convenient form to the neurologist, in order to enable proper diagnosis. For this purpose, many analysis techniques have been used and with the advent of the Fast Fourier Transform and minicomputers, spectral analysis techniques have become important. In the last decade, parametric representation of the EEG signals has become popular from the point of view of data reduction, as the data to be handled is quite large. In addition to this, parametric representation also provides effective computer classification of EEG signals by pattern recognition techniques. Further, parametric techniques unlike the nonparametric ones can be easily extended to nonstationary signals and are indirectly useful for the detection of transients. These advantages have led to the developement of improved parametric techniques which are applicable to signals in general and EEG in particular. Also, techniques existing in the allied areas are being evaluated for EEG signal analysis. From these considerations, in the present study spectral analysis of EEG signals based on parametric models has been chosen as the main objective. The following topics are covered:

1. Spectral modeling of EEG signals

Two methods of spectral modeling, homomorphic prediction and pole zero modeling by pole zero decomposition, both based on a combination of linear prediction and homomorphic filtering are

considered. These methods are applied to simulated and real EEG signals. The results of the two methods are compared with Burg's maximum entropy all pole modeling method. The results indicate that the pole-zero modeling by linear prediction technique without prior homomorphic filtering results in erroneous spectral estimates, whereas the methods that are considered here provide accurate spectral estimates of the logmagnitude spectrum of the EEG signal.

2. Noise cancellation based on adaptive filtering

An active area of research in EEG signal analysis is noise cancellation. This is because the presence of noise affects the performance of both the time domain and the frequency domain analysis of EEG signals. The different types of noise present are occular noise, ECG pulsation and muscle noise - which is due to the contraction of scalp and neck muscles. Of the various kinds of noise present, muscle noise is found to be quite frequent and its magnitude is also often many times that of the EEG signal itself. Different methods for minimizing the noise in EEG signal records have been reported in literature. In the present study, muscle noise has been minimized by using an approach that involves lowpass filtering to remove noise that lies outside the EEG signal frequency band and LMS adaptive filtering to remove the muscle noise inside the EEG signal frequency band. The performance of such a filtering technique is studied both for simulated and real EEG signals. Also the effect of muscle noise on the parametric model based representation of the EEG signal is studied and the improvement achieved by the filtering technique is dealt with.

3. Adaptive Spectral Estimation of EEG signals

The Least Mean Fourth (LMF) adaptive algorithm proposed by Widrow provides lower convergence error than the Least Mean Square (LMS) adaptive algorithm for the same speed of convergence. This adaptive algorithm has been considered for sequential adaptive spectral estimation of EEG signals. In this attempt, the LMF adaptation has been extended to the lattice structure since this particular structure has advantages like higher speed of convergence and better stability properties as compared to the tapped delay line structure.

4. Detection of Quadratic Phase Coupling in EEG signals

Recently, there has been considerable interest and progress made in the developement of parametric methods for bispectrum estimation. In the present work, an algorithm for bispectrum estimation based on parametric models is studied and is used for detecting quadratic phase coupling in real EEG signals. The detection of this phase coupling is important in analysis of sleep records.

1.2 Organization of the Thesis

A certain amount of work has been done in the field of Spectral analysis of EEG signals. Chapter 2 presents an extensive review of the literature in this area. The developement of a software simulation technique for EEG signals is discussed in Chapter 3.

Chapter 4 deals with spectral estimation of EEG signals. Two methods of parametric spectral modeling are discussed. On the other hand, Chapter 5 deals with adaptive muscle noise cancellation from the EEG signal. In this chapter, a hybrid approach for muscle noise cancellation is discussed and simulations are carried out on both simulated and real EEG signals. Chapter 6 involves a study of adaptive spectral estimation of EEG signals.

A parametric method for bispectrum estimation is studied in Chapter 7. This chapter involves a review of bispectrum estimation techniques that have been discussed in literature. It also involves the implementation of a parametric method for bispectrum estimation and quadratic phase coupling.

Chapter 8 deals with Conclusions and possibilities for future research.

CHAPTER 2

REVIEW OF EXISTING RESEARCH

2.1 Introduction

The main objective of EEG signal processing is to extract valid information from the EEG signal records and present them in a convenient form to the neurologist so that proper diagnosis is possible. Spectral analysis and modeling plays a crucial role in EEG signal processing. This is because EEG basically consists of frequency related components and its characterization is also done in terms of its spectral parameters.

Berger's extensive study of EEG records from scalp electrodes has revealed that the frequency content of EEG is of crucial importance in its assesment. The rythmic activity corresponding to frequency centred around 10 Hz. and ranging from 8 to 14 Hz. is called alpha (α) activity and is found to be prominent in the middle and posterior part of the brain in the normal wakeful state. This activity gets attenuated by increase in the degree of vigilance or decrease in the degree of wakefulness. There is a high frequency rythmic activity confined to 14 to 30 Hz. called the beta (β) activity having a different type of spatial distribution and not influenced by wakefulness, similar to the alpha activity. The low frequency activities in the range 1 to 3 Hz. and 4 to 8 Hz. are called delta (δ) and theta (θ) activities respectively. These activities appear depending on the location on the scalp and state of the subject. The other factors that determine the nature of the EEG signal are the age and state of the patient, hereditary factors, influences on the brain (e.g. injuries, functional disturbences, diseases, stimuli, chemical influence and drugs) and artefacts.

In addition to the above frequency related activities mentioned, EEG also contains specific transients or paroxysmals which occur spontaneously. These are considered to be superimposed on the frequency related activities. The transients are called spikes, sharp waves and spike-and-wave activity depending on their characterstics. These appear mainly in patients with some kind of epileptic attacks. These transients have unique features for each type of epilepsy.

It is possible to detect the functional disturbance in the brain and judge it's severity, localization and spread based on the frequency content of the EEG by simultaneously recording EEG from the different parts of the brain.

In visual analysis, after considering the extrinsic parameters e.g. the age and patients state of alertness and well being, the following EEG signal parameters and their inter-relationships are considered for the interpretation of the EEG record :

Frequency or wavelength

Amplitude

Waveform

Locus

Interhemispheric coherence

Character of wave occurence

Regulation

Reactivity

Any computer analysis must also consider all these factors and their relationship or establish those which are essential in achieving of equal or of better significance. Towards this goal, signal processing techniques which are powerful and efficient play an important role.

2.2 EEG Signal Characterstics

EEG is often analysed as a time series in the same way as speech and seismic signals. It can not be expressed by any mathematical relationship - it is nondeterministic and needs statistical treatment. EEG, being a random signal, is treated as a stochastic process like signals in other feilds such as speech and geophysics. For analysis of stochastic process to be easy and valid, requirements of stationarity and gaussianity are very important. Stationarity calls for the joint probability density function of all orders to be independent of time origin. Since the Gaussian process is completely specified by the first and second order statistics - namely the mean and autocorrelation function, if these two are

independent of time origin, the Gaussian process is stationary in the strict sense. But for processes other than Gaussian, in general if the mean and autocorrelation are independent of time origin, the process is called wide sense stationary or weakly stationary. As Gaussian process requires only first and second order statistics, it simplifies the theoretical analysis. For non-Gaussian processes, higher order statistics like bicovariance are required.

Also in practice, it is not possible to deal with ensembles and so another property called ergodicity, which implies that a single sample function characterizes the ensemble, is required. This demands that all the ensemble averages be equal to their respective time averages. Ergodicity assumes stationarity. Hence for simple and valid analysis, gaussianity and stationarity are the assumptions made. Attempts have been made to study whether these requirements are met in case of the EEG signal.

It has been reported that when the eyes are kept open or closed, EEG is stationary for 25 seconds in wide sense, taking into account the mean, variance and power spectrum. Studies by McEwen and Anderson [2.1] show that the EEG records are stationary in the wide sense for 32 seconds with more than fifty percent probability and their gaussianity and stationarity together fall to less than ten percent. However records less than 4 seconds are both Gaussian and stationary with a probability of more than fifty percent. The occipital EEG activity shows better Gaussianity and stationarity than the frontal one. Similar results found by Cohen and Sances [2.2] have indicated that records of less than 12 seconds are stationary taking into account the mean value and the frequency structure. Based on the mean value alone, records of a length of 24 seconds are stationary with less than ten percent error. Also the assesment of the ergodicity of EEG has been made by the scatter of the smoothed power spectral estimates [2.3].

Researchers view is that neither ergodicity nor Gaussianity is important with a single realisation, but it is stationarity that is of crucial importance for analysis. It has been felt that a non-Gaussian but stationary model is adequate [2.4].

The fourth moment is rarely significant in the case of non-paroxysmal activity and the third moment has indicated patterns of second harmonics and has potential use in paroxysmal activity. The

nonstationarities like coupling between frequency bands in EEG has been explored [2.5]. Usually the underlying process that generates the EEG is assumed to be linear and any occurence of nonlinearity results in jumps and hysterisis.

It is clear from the above description of the EEG that spectral content of the background activity and characterstics of the transients adequately represent the EEG records and hence processing is concerned with the extraction of features of these two aspects. Specifically with respect to background activity, spectral estimation forms the major processing problem. The spectral estimation of the background activity forms the subject of the present study. It however does not include the clinical aspects of the EEG, classification of EEG records and detection of EEG transients.

The review of the EEG processing techniques that follows brings out the importance of different methods and substantiates the relevance of the problem chosen for the work.

2.3 EEG Signal Processing - a review

2.3.1 Introduction

Analysis procedures generally fall into two categories, i.e. time domain and frequency domain. In general, frequency domain approach is suitable for analysis of background activity and time domain for nonstationary transients or paroxysmals. However, time and frequency domain techniques are applied for both cases without much restrictions. In the review that follows various techniques that have been used for EEG analysis are discussed.

2.3.2 Time Domain Analysis

Time domain analysis include amplitude analysis, period analysis, amplitude period analysis and correlation analysis. Amplitude information is obtained by the measurement of the average peak to peak amplitude and also by envelope (boundaries of peak and trough) measurement. The average of the squared amplitude deviations (from the mean) provides the variance of the signal and its square root, the standard deviation. This measurement yields the amplitude distribution which provides a

better representation of the signal, which in turn cannot be obtained by the EEGer visually, since the latter considers only the amplitude greater than the average value of the signal. The amplitude distribution is found to be Gaussian [2.6 - 2.8], although asymmetrical distributions some time occur [2.1]. The envelope distribution function follows Rayleigh distribution [2.9]. Amplitude measurement does not take into account the shape of the waveform and frequency unless it is applied to a particular frequency. For this purpose, wave indices which specify the percentage of duration occupied by different activities have been used [2.10].

In period analysis of EEG, by counting the intervals at which the zero line is crossed in classes corresponding to different frequency bands, information about the frequency content is obtained. As superimposed higher frequency components with lower amplitudes are either not at all or inadequately detected, the first and second derivatives are also analysed. But as the signal to noise ratio reduces with differentiation and also as the signal to noise ratio is poor in the beta activity region, there will be practical difficulties and inaccuracies in measurements. Inspite of these problems, the period analysis has found wide applications particularly in psychopharmacology [2.11 - 2.12].

In order to get information about amplitude and frequency, frequency to voltage ratio technique [2.13] and amplitude period analysis have been used. Wave length amplitude profile analysis of clinical EEG by Carrie and Frost [2.14] has indicated high correlation with human EEGer in relation to some aspects of EEG evaluation and has also brought out some aspects of EEG which are not obvious to the EEGer. In general, the amplitude period analysis provides data reduction and much information about the primary EEG tracing. It has been found that, if the sequence of waves is retained it is possible to describe many features of the background and paroxysmal or transient EEG activity in the absence of noise [2.15].

Hjorth [2.16 - 2.18], has represented the EEG signal in time domain by three parameters, i.e., activity, mobility and complexity. Activity deals with variance of the amplitude fluctuations, mobility with the measure of mean frequency and complexity with the ratio of the mobility of the first derivative of the signal to the mobility of the signal itself. The relation between Hjorth's parameters and the signal spectra has been given by Saltzberg and Burch [2.19]. This has found many applications in

modeling and discrimination of different EEG recordings in normal children. Hjorth's time domain descriptors do not provide valid information when the signal contains more than one spectral peak, and also there are problems regarding computational and signal to noise ratio requirements [2.20]. Despite these limitations, it is an important approach to the problem of quantifying the EEG by a small number of parameters.

Correlation analysis is effective in demonstrating the periodic components within a signal or shared between two signals. Prior to the existence of the Fast Fourier Transform (FFT), the spectrum and cross spectrum were computed by transforming the auto and cross correlation functions [2.21]. Digital methods of computing the correlation functions by FFT are preferred and have been used in the study of delta activity in cerebral hypoxia. Correlation technique has been used in the removal of eye movement artefact from EEG and also in interhemispheric synchrony in EEG of full term new born babies. Reverse correlation technique which preserves all the interphase relationships and changes in the temporal patterns in the output has been applied in the study of slow posterior EEG rythm in adults. Though correlation analysis is used in many applications mentioned, it has been found that in many cases positive correlation may not be significant and may be due to a slow component, the finer details of the two signals may be still different [2.9]. Further, direct interpretation of correlation function is difficult. Hence with the avaliability of other methods, correlation technique has been considered as a special purpose method of EEG analysis in which direction and phase relations of periodic activities are of primary interest.

2.3.3 Frequency domain analysis

Frequency domain representation provides better insight into the generation of EEG signals, is more descriptive of pattern fluctuations, and enables valid comparisons. This is due to the fact that each spectral amplitude represents a time pattern fluctuation throughout the signal epoch, where as in time domain each amplitude is confined only to that instant in time. Further, the spectrum provides information about frequency components of small amplitudes, even in the presence of large amplitude components. Because of these advantages and also the disadvatages of time domain techniques men-

tioned above, frequency domain analysis has gained popularity over time domain representation.

Initially, analog techniques using band pass filters were used to estimate the spectrum of the signal. Their poor resolution, instability and sensitivity resulted in their failure in practical applications. Walter [2.22] introduced digital spectral analysis to EEG as a most promising quantification and analysis technique and this was possible only with large computer facility and computer time. Only with the advent of the FFT and the avaliability of low cost fast mini computers, the frequency domain or spectral analysis has become very popular in both experimental and clinical EEG due to reduction in computation time provided by the FFT algorithm. The use of FFT algorithms other than radix 2 provides further reduction in computation [2.23 - 2.24]. In this attempt, FFT with pruning facility which avoids multiplications for the padded zeros is of significance [2.25]. Spectral analysis in principle provides same information as the correlation analysis since they form a Fourier transform pair. However, spectral analysis has been found to have important statistical advantages over correlation analysis and also found to correspond to more conventional description of background EEG activity in terms of relative frequency content. Also, spectral analysis has been found to be a powerful analytical tool with well behaved statistical properties, as long as certain assumptions about the data are not grossly violated. If the data is stationary, spectral estimates do not depend upon the assumption of normality of amplitude distribution. In the non-Gaussian case however, they reflect only part of the information. With this in view, the EEG signal has been classified into different categories as shown below [2.26] :

1. Spontaneous non-paroxysmal activity

2. Spontaneous paroxysmal activity

3. Evoked activity

For real time applications, FFT poses problems due to its enormous computational requirements as it requires ($N \log_2 N$) complex multiplications and complex additions, where N is the length of the FFT. As an alternative to the Fourier transform, Walsh transform is used as it requires only real additions and no multiplications. However, Walsh transform based power spectrum was considered to be inferior in discriminating power for classification purposes. Recently, Larsen and Lai [2.27], have

examined both these transforms for their statistical properties and resolution. Application of both these transforms for classification of sleep EEG data using minimum distance cluster algorithm provides enough justification to take advantage of the computational superiority of the Walsh transform. According to Smith [2.28], the simplicity and speed of the Walsh transform can be used for EEG spectral monitoring without sacrificing performance.

The major problems associated with these transform methods of spectral estimation are :

(i) leakage effect due to high side lobe levels of the window function (spectrum) applied to the time signal and the resolution problem resulting in reducing the leakage effect [2.29]. Windows with better characterstics for spectral estimation have recently been reported [2.30 - 2.31].

(ii) also, the periodogram which is the squared magnitude of the Fourier transform of the signal is not a consistent estimate of the spectrum, as the stability does not improve with the increase in the number of samples [2.29]. A stable estimate is obtained by smoothing over the adjacent frequency bands by convolving the signal spectrum with a suitable window spectrum that is known as quadratic tapering, or by averaging the peridograms of the succesive segments of the signal [2.32]. Recently it has been found that linear tapering (windowing in time domain) is of great importance for the spectrum with large dynamic and only quadratic tapering would not be of use [2.33]. Further, when segmental averaging is done, equivalent quadratic window in spectral domain can be used to get equivalent leakage suppresion at substantially reduced computational cost [2.34]. For a given length of data, high stability (low variance) and high resolution are the conflicting requirements and a trade off is necessary. In addition, the stationarity of the EEG data also limits both stability and resolution.

Inspite of these problems, spectral analysis by FFT has been widely used. It has been found that the amplitude spectrum obtained by FFT accords more closely than the power spectrum with the visual analysis, when records are technically good. Bickford's [2.35] compressed spectral array based on FFT provides information of 30 to 40 minutes of EEG record in a single page which can be easily interpreted. Such an analysis that is economical and feasible on a microcomputer, provides information related to frequency, space and time is very helpful to the neurologist. The spectral density function computed by the Fourier transform does not provide information about whether a particular

frequency component is due to short burst of activity or it is due to one which occurs throughout the analysis epoch. Compressed spectral array which uses Berg's transform overcomes this [2.36].

Coherence studies have been carried out by computing cross spectrum using the FFT algorithm. Coherence function provides information about functional coupling between different parts of the brain. These include seizure discharge, EEG correlates of hemespheric function and study of behavioural feature attributable to disorganization of cerebral function.

Real time system at Langley Porter Clinic, PDP 12 computer based system at the Montreal Neurological Institute, Hybrid computer based system at the Medical School of Hannover and the PDP 15 computer based system at Shelgren Hospital in Gottenberg, Sweden are some examples which are having FFT based analysers and where FFT based multichannel EEG spectral analysis are being used both for experimental and and clinical applications.

2.3.4 Parametric Models for EEG Analysis

Even though spectral analysis by windowed periodograms provides spectral details of the EEG signal, it does not provide any substantial data reduction and the data is only in a different form. The large mass of spectral data has to be interpreted and evaluated. Hence for further processing, the spectral data has to be condensed and the several methods used for this purpose are listed as under:

Synoptic presentation :

Contour plot, Sequential spectral display (spectogram), Compressed spectral display, three dimensional plot (VOS)

Parameter extraction :

Simple parametrs - peak frequencies, peak intensities, half power bandwidth, peak area;

Spectral baseline slope, Phase slope, Spectral quotients, Resonance factor, Topographic parameter display

Statistical treatment - mean and standard deviation of peak frequencies, peak intensities etc.

Especially for classification of the EEG data by computer pattern recognition techniques, compact parametric representation is very much desired. Though parameters like bandwidth, centre frequency and fractional power content can be computed from the power density spectrum, it has been found that such estimates are not efficient and further their statistical uncertainities are not known [2.37]. This calls for direct representation of the EEG signal by parametric modeling. Zetterberg was the first to introduce the parametric representation of the EEG signal [2.38]. Generally, in parametric representation the signal is considered as the output of a system characterised by the numerator and denominator polynomials, with white noise as the input. If the numerator polynomial is a constant, the model is called an all pole model or Autoregressive (AR) model. Otherwise, the model is known as a pole-zero or Autoregressive Moving Average (ARMA) model. The parametric techniques model the data and extract its structure, and modeling can be applied either in time or in frequency domain. The AR model, because of its simplicity has been widely used in other fields like speech and seismology; EEG is no exception to this.

In AR modeling, the present data sample is estimated as a weighted linear combination of M previous data samples and the weighting coefficients are obtained by minimising the mean square error between the actual sample value and its estimate. This minimisation results in a system of linear equations, called the Yule-Walker normal equations which involve covariance or autocorrelation functions of the signal. Different methods of solving this system of equations are in practice, e.g. Cholesky's decomposition and the Levinson Robinson and Durbin algorithm, which is more economical in terms of computer time [2.39]. The studies of Rappelsberger and Petsche [2.40] indicate that the AR model provides better spectral estimates of the true spectrum than by FFT method and the length of data required is smaller than that required by the FFT method. To get the performance of a 15^{th} order AR model with 4 seconds length of EEG data, FFT method requires 180 seconds of data. The studies of Blinowska et.al. [2.41] also show that the AR model provides better resolution with much smaller statistical fluctuations than the FFT method. As the sample length of the data required is small, the AR model is very useful in detecting rapid short lasting (stationary over short durations) changes in EEG like epileptic siezures [2.42]. The AR coefficients obtained by this method have been

succesfully used in the classification of EEG records by computer pattern recognition technique in sleep staging and in the classification of physiological states of patients in need of intensive care [2.43].

AR spectral analysis has been used by Crowell et. al. [2.44], as an objective and quantifying technique in combination with the logistic discrimination algorithm for testing hypothesis about infant EEG developement. With other clinical indicators, the AR coefficients serve as bench marks of maturation with age and help in monitoring and early identification of infants who are at risk of mental retardation and other developemental disabilities.

Use of AR coefficients as input parameters in the discriminant analysis instead of arbitrary chosen frequency bands has brought a significant improvement in distinguishing the effects of medication. The percentage of correct classification for diazepam for F4-C4 and P4-O2 leads with AR coefficients are 84.5 and 75 and with FFT they are 72 and 68 respectively [2.41].

The difficulty in applying this method is that the autocorrelation matrix may not be positive definite due to the round off errors generated by the solution [2.39]. The studies of Jansen et. al. [2.45] indicate that 5% of models were unstable out of 8800 cases with the order of the model being 5. The optimal order of the model indicated by Akaike's Final Prediction Error Criterion (FPE) was less than 5, while the order required was 10 to get a realistic spectral fit to the FFT spectrum. With the optimal order of the model, the instability was 7%. For Yule-Walker's method, according to them, the order of the model given by FPE is too low.

Burg [2.46] introduced the concept of maximum entropy in order to achieve high spectral resolution even with a small number of data samples. In this approach no assumption is made about the data outside of the observation window. In the FFT method the data is assumed to be periodic where as in the Linear Prediction autocorrelation method it is assumed to be zero outside the observation interval. According to this, any spectrum which is consistent with the observed data and at the same time maximises the entropy function provides high resolution. It has been shown that the spectrum derived by the Maximum Entropy Method (MEM) is also AR model spectrum [2.47]. Burg [2.46] also proposed an algorithm to compute the prediction filter coefficients (AR) directly from the data values,

without explicitly computing the autocorrelation values. The reflection coefficient of the Mth order filter is found by minimising the average of the forward and backward prediction errors. The other coefficients are obtained by the Levinson recursion. The performance of the Burg algorithm has been found to be considerably superior to the Yule-Walker method both in terms of resolution and stability. The studies of Branwell [2.48] with speech data show that the MEM provides distortion free spectral estimate even with data lengths as small as 60 points, where as in case of the YWM it is not so. The studies of Jansen et. al. [2.49] with EEG data indicate that there was no unstable case out of 8800 with MEM (AR) method, using an optimal order, whereas YWM had 7% and required higher order models. The MEM scores over YWM even in classification of EEG records. Though MEM requires three times computer time than the FFT method it is preferred where accurate frequency estimation is required.

Another method of spectral estimation, the Maximum Likelihood Method, a minimum variance unbiased estimator of the spectrum, has also been applied for EEG signals by Childers et. al. [2.50] and is found to yield poorer resolution than YWM.

In view of the importance of the AR modelling in spectral analysis, attempts have been made to improve its performance. The performance of the AR model for signals in the presence of noise is often criticized because the model required is an ARMA model. However, since an ARMA model is represented by an AR model of infinite order, in practice a higher order AR model will provide better spectral estimation especially when the spectrum is a peaky one [2.52 - 2.55]. In general, the representation of an ARMA process by an AR process requires higher order and longer data lengths to get better fit in the valley regions of the spectrum. Otherwise the AR model will introduce a bias in the valley region. The spectral fit obtained by a finite order AR model to a stationary ARMA data will increase with the fourth power of the number of data points considered [2.56].

Though methods based on AR model of spectral estimation offer higher resolution, better spectral estimates for short data length, and do not distort the spectrum due to leakage effect of the window function as in the periodigram method, they have the problem of line splitting or introduction of spurious peaks in certain cases [2.57 - 2.58]. The minimization of the average of the forward and backward

prediction errors with respect to each coefficient of the prediction filter instead of only with respect to the reflection coefficient without the constraint of the Levinson recursion, overcomes this problem [2.59 - 2.60]. This algorithm is found to provide better spectral estimates with lower bias and variance and higher resolution than the Burg algorithm [2.61]. For this method, Marple [2.62] has proposed an algorithm that is computationally as efficient as Burg's algorithm.

Signals in general, as mentioned previously, have to be represented by an ARMA model for an accurate representation than by AR models. AR models can characterize the peaks better than the valleys. From this point of view, AR models are sufficient for frequency estimation. But to get accurate information about the bandwidth and percentage of power for the spectral peak in addition to peak frequency, as required in EEG analysis, ARMA model is necessary. ARMA model in general represents the signal with better accuracy by a smaller number of parameters than the AR model. The estimation of ARMA model parameters for a given signal is more complicated than that of AR as it involves solution of nonlinear equations. Hence, only limited attempts have been made in the use of ARMA models for EEG signal analysis.

Zetterberg [2.38] estimates the ARMA parameters by maximising the likelihood function expressed in terms of the autocorrelation function and this involves more number of iterations in the optimization algorithm. This method has been used in EEG data modeling. Their study with normal subject shows that an ARMA (5,5) model adequately represents such EEG data [2.63]. The analysis is based on the assumption that the EEG spectral density function is conceived of three types of components corresponding to :

(a) white noise characterised by its power

(b) first order lowpass signal (δ) characterized by its bandwidth and power

(c) bandpass signal (α or β or θ) characterized by its centre frequency, bandwidth and power

The spectral properties of the EEG signal are better described by the spectral components determined by their centre frequency, bandwidth and power; than by assuming arbitrary frequency ranges for α , β , δ and θ activities [2.37]. In most cases considered, one lowpass component corresponding to alpha and beta have been found. The physiological interpretation for these parameters are given

and the parameters obtained for the group of subjects considered are expressed in terms of mean values and standard deviations. Further, Zetterberg [2.64] has applied this method to heart patients with external pacemakers and the results indicate that, although the frequency parameters do not change within 10 to 20 seconds, the power parameters change greatly and this was particularly true for alpha activity and even for such cases the method was found to be satifactory.

ARMA modeling by Diekman [2.65] involves the identification and estimation of the model parameters, fitting the model to the EEG data, and evaluating the goodness of fit. Identification is based on the autocorrelation function (determines an approximate estimate of the order of the AR) and the partial correlation coefficients (used for determining the MA order). Fitting the model involves in the first step, estimation of the AR parameters and then the MA parameters (by an iterative algorithm) and in the second step, the estimated parameters are fitted to the EEG data by ML procedure. The study, aimed at analysing the changes in EEG due to change in blood gas levels, indicates that high levels of carbon dioxide reduces the dominant activity severely and this requires an ARMA (10,7) (i.e. 10 AR coefficients and 7 MA coefficients). Reduction in sampling rate to some extent may reduce the order. The ARMA model is found to be sufficient and provides objective description of the FFT spectrum of EEG with high degree of data reduction inspite of the higher computational effort and is helpful in scientific investigations.

ARMA model parameters have been used in the classification of sleep stages by Gersch et. al. [2.66]. The parameters are estimated by a two stage least square approach having the computational economy and statistical efficiency of the MLM, using the Akaike's criteria for order determination. The statistical properties of the estimates of the natural frequency and damping achieved by the ARMA models are found to be far superior to the estimates of those achieved by conventional spectral analysis. It is felt that though a 6th order AR model is highly sufficient for classification of sleep stages, a higher order AR or ARMA model with additional dominant spectral frequency feature is informative.

Bohlin [2.67] has compared the generalized least square (GL) AR parametric modeling of EEG data with that of ARMA model based on MLM which involves optimization techniques. The GL AR

is an AR model which uses a prefilter that suppreses the frequency components in the unexpected frequency region. The results of the GL AR model for EEG data are comparable to that of the more general ARMA model at the cost of only increasing the number of parameters, i.e., 10 to 17 for GL models compared to 10 to 14 (5,5 to 7,7) for ML ARMA. The computational effort for ML ARMA is two to ten times higher than that for GL AR and problems like selection of minimum from a set of local minima, round off errors and occurence of intermediate unstable models which result in higher computing time are severe for ML ARMA than for GL AR model. Even from the spectral analysis point of view, the GL AR is found to be superior to ML ARMA.

Recently parametric modeling algorithms have been evaluated for on line spectral analysis of EEG by Smith and Lager [2.68]. The algorithms chosen are simple in the sense, they are not iterative and work with fixed model order and data length. The two algorithms are i) the ARMA model based on the extended Yule-Walker equation [2.69] and ii) the AR model by autocorrelation LP [2.39]. The ARMA (M,N) produces unbiased estimates, while the AR (M) provides smaller standard deviation and is simpler in form (M=10, N=M-1). Inspite of the bias with AR model, the AR method has been recommended for on line EEG monitoring.

The study by Isaksson et. al. [2.37] shows that an ARMA (5,4) results in 12 spectral parameters, of which 10 parameters correspond to bandwidth, centre frequency and power of different activities, the other two are total absolute power and the model fit parameter. The spectral asymmetry power parameter and the model order fit parameter can be omitted if only the spectral parameters are of interest for further statistical processing, and this results in 9 parameters. The corresponding AR model order needed for this is more than 15. The spectral parameters of EEG have been found to be affected severely by the sampling frequency. It has been found that a sampling frequency less than 100 Hz. will especially affect the estimation of the beta activity parameters and also results in a high standard deviation of spectral parameters of the EEG. Hence sampling frequency of 100 Hz.has been recommended for accurate EEG analysis. With the introduction of the LRD algorithm, Isaksson et. al. are in favour of a fixed AR model for reasons like simplicity of the algorithm, modest amount of computations, automatic test facility for model validity and the order of the model.

2.3.5 Nonstationary EEG Analysis

The validity of the parametric and nonparametric methods is based on the assumption that EEG is stationary. It has already been pointed out in the previous section that EEG is stationary only over short durations. The deviations from stationarity are of different types. The unexpected nonstationarities cover transients and gradual changes. The expected one are due to stimulations like hyperventilation, flickering of light and mental arithmetic. The transient types are mainly paroxysmal phenomena like spikes and spike-and-waves encountered in interictal epileptic patients. The gradual nonstationarities are transitions in arousal level, variations in depth of anasthesia or conscious level of changes in background activity that occur prior to epileptic crisis. Even short duration EEGs will contain spontaneous nonstationarities and this is especially true in case of pathological cases and the nonstationarity property itself may have physiological significance. The severe measurement problems like eye movements result in disturbances which appear in EEG as large transients of low frequency. Analysis of nonstationary EEG has been made by several appraoches. The first approach divides the EEG data into approximately stationary segments and these stationary segments are analysed by methods described for stationary EEG. This has led to developement of efficient segmentation algorithms. The segmentation algorithms must provide

i) the estimation of the boundary with minimum delay

ii) precise estimation of the boundary (i.e. its bias and variance must be small)

iii) minimum number of false alarms (false boundary indications)

The last factor is of importance from the point of view of EEG data reduction. Initially single AR model methods were used for this purpose where the sequence of innovations was tested for its deviation from white noise nature [2.70]. This method has limitations in detecting wide range of abrupt jumps. The methods that overcame this limitation in principle use two windows (models), the fixed window for the refrence data and the moving window for the test data. The features corresponding to both are compared and a large deviation indicates the occurence of the segmentation boundary.

The gradual nonstationarities of the EEG have been analysed by direct methods (without segmentation). A statistical method which describes the statistical characterstics of nonstationary EEG

has been done by Kawabata [2.71]. The method involves estimation of nonstationary power spectrum defined as the ensemble average of the instantaneous power spectrum of a group of signals to which the given signal belongs. The instantaneous power spectrum is the derivative of the energy spectrum. This has been applied to evolution and decay of the alpha activity during closing and opening of eyes in human subjects. The validity of such a time varying spectrum is based on the assumption that the characterstics do not change from trial to trial on repetition. Vos [2.72] has pointed out that such a spectrum is not realistic for processing spontaneous EEG data and is limited to only stimulus response type of EEG. The method of spectral estimation based on segmentation and averaging the periodograms has been preferred to the time varying spectrum mentioned. This has been illustrated for the case of sleep state cycling data of infants of two hours duration.

Bohlin [2.73 - 2.74] introduced Kalman filtering for EEG analysis. Kalman filter algorithms suitable for processes with time varying AR and ARMA parameters are given by Isaksson et. al. [2.37]. Here control over the variability of the process is achieved by different methods. In one method, the parameter vector is assumed to be governed by a first order Markov process and in the other the loss function used in estimating the parameter vector is changed by giving additional weight to more recent observations [2.75]. The application of Kalman filter to different types of EEG signals has been illustrated by Issakson [2.76].

2.3.6 Transients in EEG and their Detection

The transient activities play an important role in EEG assesment, particularly in the case of epileptic patients. Though in some cases the spikes and sharp waves are clearly distinct because of their shape, there are many instances in which they are merged with the background activity. In addition to this the classification of different types of transient spikes is also of importance in the assesment ofa particular type of epilepsy. For this purpose many techniques have been developed.

Carrie [2.77] has proposed a method which detects the transient abnormalities in an EEG by comparing measurements from consecutive waves in the signal with a moving average of similar measurement from the preceding waves. The second derivative has been found to provide most

efficient discrimination for the sharp transients. Further the system developed is specifically suitable for the detection and quantification of the spike and wave paroxysmal discharges. Walter [2.78] has also developed a simple and inexpensive method of quantifying the transients and the method uses rectified second derivative of the EEG signal. Ktonas and Smith [2.79] have also used six parameters which characterise a well defined triangular spike.

2.3.7 Artefacts in EEG and their Elimination

The presence of external disturbance or noise affects the performance of different types of analyses considered, i.e. the time domain and frequency domain which includes parametric and non-parametric methods based on stationarity assumption and the algorithms for time varying signals. In EEG specifically, noise may be technical due to measurement, or physiological due to the subject himself and is known as artefact.

The measurement noise may be due to mains interference, improper contact between electrode and scalp surface, clips, plug and socket etc. The contact resistance may change due to perspiration which results in an undesired low frequency component which can be removed to a certain extent by decreasing the highpass filter time constant (0.3 to 0.03 secs.). Usually, proper precaution prior to EEG recording will help in removing the measurement artefacts. However, to take care of the sudden changes in the contact potential at the scalp-electrode interface, known as "pop artefact", Barlow [2.80] has proposed an analog technique. The pop artefact introduces a large magnitude low frequency component which obscures the low frequency components of the EEG in the compressed spectral array and the technique removes the unwanted low frequency component successfully.

The disturbances due to the subject are extracerebral and are usually due to the eye movement (occular artefact), ECG pulsation, ECG pickup and due to contraction of scalp and neck muscles. The extracerebral artefacts cannot be removed easily and their presence severely affects both the visual and computer EEG analysis. Hence every effort is made to either completely remove or to minimise these artefacts and this forms part of the analysis. The artefact removal was considered as a monumental problem in the last decade [2.81]. Attempts have been made to remove the artefacts as a whole

and also individually. Ktonas et. al. [2.82] have considered a general method of removing artefacts when the data to be processed is large (50 hrs.). This is based on the chisquare goodness fit test to Gaussian distribution. This test being very sensitive to nonstationarities in the EEG amplitude distribution, produces a large value for the chisquare coefficient when an artefact is present in the EEG epoch considered. Hence, any crossing of the preset threshold by the chisquare coefficient indicates the presence of an artefact. Barlow [2.83] has also proposed a general purpose multichannel electronic switch for artefact elimination.

The occular artefact is due to the vertical and horizontal eye movements and blinks. Removal of the eye movement artefact by spectral method has been done by Whitton et. al. [2.84].

The method involves calculation of the ratio of EEG to electrooculograph (EOG) which adequately controls the low frequency component in the EEG due to artefact and allows the removal of dominant peaks in the scalp EEG spectrum. This is based on the assumption that the low frequency components in EEG are mainly due to eye movement. In the method based on correlation by Jervis et.al. [2.85], the correction factor is calculated by the correlation between the EOG and the measured EEG. A fraction of the EOG thus computed is subtracted from the EEG considered. Further, a comparison of this method is made with an analog method where a constant fraction of the EOG is subtracted and the results are in favour of the correlation method both in terms of performance and ease. Blinovaska et. al. [2.86] have used a fast and simple moving integration method. The other methods are by Barlow and Remond [2.87], off line method of Gratton et. al. [2.88], and the biophysical approach of Elbert [2.89].

The ECG pulsation artefact appears as a saw tooth waveform and is prominent with pad electrodes than with stick on electrodes. This is due to mechanical movement or change in pressure at the electrode and can be reduced by moving the electrode properly.

The ECG pickup is significant with unipolar montages than with bipolar. The ECG pickup can be reduced, to some extent, by transverse rather than by antero posterior bipolar linkages depending on the orientation of the EEG field. This artefact is found in recordings which use ear and temporal leads [2.90]. Recently, a computer based real time subtraction method of minimising ECG pickup for

noncephelic reference has been proposed [2.91 - 2.92]. The ECG pickup affects the delta and theta regions of the EEG spectrum.

The removal of the muscle artefact which is comparitively difficult has been attempted by nonlinear filtering [2.93], by Kalman filtering [2.94], by time domain filtering [2.95] and by lowpass filtering [2.96]. The muscle artefact affects the beta component of the EEG more significantly than the alpha and delta components.

To summarise, the review has covered different aspects of the EEG signal which are of significance in the evaluation of the EEG record. Various techniques for the processing of stationary EEG, nonstationary EEG , detection of transients and minimising different types of artefacts are considered.

2.4 References

[2.1] McEwen,J.A., and Anderson,G.B., 1975, Modeling the stationarity and Gaussianity of spontaneous electroencephalographic activity, IEEE Trans. on Biomedical Engineering, 22, pp. 361-369.

[2.2] Cohen,B.A., and Sances,A., 1977, Stationarity of human electroencephelogram, Medical biological engineering and computing, 15, pp. 513-516.

[2.3] Craig,T., 1986, Statistical characterisation of the EEG : The use of power spectrum as a measure of ergodicity, Electroencephalography and clinical neurophysiology, 63, pp. 488-493.

[2.4] Gasser,T., 1977, General characterstics of the EEG as a signal, EEG Informatics, pp. 37-56.

[2.5] Dumermuth,G., Huber,P.J. and Kleiner,B., 1971, Analysis of interrelations between frequency bands of the EEG by bispectrum, Electroencephalography and clinical neurophysiology, 31, pp. 137-148. 31, pp. 137-148.

[2.6] Saunders,M.G., 1963, Amplitude probability density studies on alpha and alpha like patterns, Electroencephalography and clinical neurophysiology, 15, pp. 761-764.

[2.7] Saunders,M.G., 1965, Amplitude probability density studies of alpha activity in the electroencephalogram, In : Mathematics and Computer Science in Biology and Medicine, Proc. of MRC, 1964, Oxford Conf., London.

[2.8] Byford,G.H., 1975, The anatomy of alpha rythm, In Quantative analysis of the EEG, Ed. Matousek,M., and Schenk,G.K., AEG Telefunken, pp. 357-368.

[2.9] Cooper,R., Osselton,J.W., and Shaw,J.C., 1980, EEG Technology, Third Edition, Butterworth Publication, Chapter-9.

[2.10]Samson,D., and Goldberg,P., 1979, Electroencephalographic quantification by time domain analysis in normal 7 to 15 year old children, Electroencephalography and clinical neurophysiology, 46, pp. 147-149.

[2.11]Fink,M., 1975, Cerebral Electrometry - Quantative EEG applied to human psychopharmacology, In : CEAN, pp. 271-285.

[2.12]Itil,T.M., 1975, Digital computer period analysed EEG psychiatry and psychopharmacology, In : CEAN, pp. 289-308.

[2.13]Riehl,J.L., 1966, Analysis of the frequency voltage ratio of the EEG in intracamial diseases, Electroencephalography and clinical neurophysiology, 21, pp. 235-241.

[2.14]Carrie,J.R., and Frost,J.D., 1973, Wavelength amplitude profile analysis in clinical EEG, In : Automation of clinical EEG, pp. 65-74.

[2.15]Hamer,R.N., 1977, EEG analysis in time domain, In : EEG Informatics, pp. 57-72.

[2.16]Hjorth,B., 1970, EEG analysis based on time domain properties, Electroencephalography and clinical neurophysiology, 29, pp. 306-311.

[2.17]Hjorth,B., 1973, Physical significance of time domain descriptors in EEG analysis, Electroencephalography and clinical neurophysiology, 34, pp. 321-330.

[2.18]Hjorth,B., 1975, Time domain descriptors and their relation to a particular model for generation of EEG activity, Electroencephalography and clinical neurophysiology, 36, pp. 134-141.

[2.19]Saltzberg,B., and Burch,N.R., 1971, Periodic estimates of moments of the power spectrum : a simplified EEG time domain procedure, Electroencephalography and clinical neurophysiology, 30, pp. 568-571.

[2.20]Denoth,F., 1975, Some general remarks on Hjorth's parameters used in EEG analysis, In : CEAN Computerised EEG analysis, Ed. Dolce,G., and Kunkel,H., Stuttgart, Gustav-Fischer, pp. 9-18.

[2.21]Kunkel,H., 1977, Historical review of principle methods, EEG Informatics, pp. 9-26.

[2.22]Walter,D.O., 1973, Semiautomatic quantification of sharpness of EEG, IEEE Trans. on Biomedical Engineering, 29, pp. 53-55.

[2.23]Dumermuth,G., 1970, Numerical analysis of electroencephelographic data, IEEE Trans. on Audio and Electroacoustics, 18, pp. 404-411.

[2.24]Dumermuth,G., 1973, EEG spectral analysis by means of the Fast Fourier Transform, Automation of clinical EEG, pp. 145-160.

[2.25]Markel,J.D., 1971, FFT pruning, IEEE Trans. on Audio and Electroacoustics, 19, pp. 305-311.

[2.26]Dumermuth,G., 1977, Fundamentals of spectral analysis in electroencephalography, In : EEG Informatics , pp. 83-105

[2.27]Larsen,H., and Lai,D.C., 1980, Walsh spectral estimates with application to the classification of EEG signals, IEEE Trans. on Biomedical Engineering, 27, pp. 485-492.

[2.28]Smith,W.D., 1981, The simplicity and speed of Walsh Transform for EEG spectral monitoring without sacrificing the performance, IEEE Trans. on Biomedical Engineering, 28, pp. 790-793.

[2.29]Oppenheim,A.V., and Schafer,R.W., 1975, Digital Signal Processing, Prentice-Hall, Englewood Cliffs, N.J.

[2.30]Nuttal,A.H., 1981, Some windows with very good side lobe behaviour, IEEE Trans. on Acoustics, Speech and Signal Processing, 29, pp. 84-91.

[2.31]Tseng,F.I., Sarkar,T., and Weiner,O.D., 1981, A novel window for harmonic analysis, IEEE Trans. on Acoutics, Speech and Signal Processing, 29, pp. 177-188.

[2.32]Welch,P.D., 1967, The use of Fast Fourier Transform for estimation of power spectra : A method based on time averaging over short modified periodograms, IEEE Trans. on Audioelectro Acoustics, 15, pp. 70-73.

[2.33]Vanschooneveld,C., and Frijding,D.J., 1981, Spectral analysis : On the usefulness of linear tapering for leakage supression, IEEE Trans. on Acoustics, Speech and Signal Processing, 29, pp. 323-329.

[2.34]Mathews,V.J., and Youn,D.H., 1984, Spectral leakage supression properties of linear and quadratic windowing, IEEE Trans. on Acoustics, Speech and Signal Processing, 32, pp. 1092-1095.

[2.35]Bickford,R.G., 1973, Application of compressed spectral array in clinical EEG, Automation of clinical electroencephelography, Ed. Kellaway,P and Peterson,S, Reven Press, New York, pp. 55-64.

[2.36]Sciarretta,G., and Erculiani,P., 1975, The Berg Transform : A method of spectral evaluation of the dynamic properties of the EEG, In : Quantitative analysis of the EEG, Ed. Matousek,M. and Schenk,G.K., Konstanz, AEG Telefunken, pp. 487-496.

[2.37]Isaksson,A., Wennberg,A., and Zetterberg,L.H., 1981, Computer analysis of EEG signals with parametric models, Proceedings of the IEEE, 69, pp. 451-461.

[2.38]Zetterberg,L.H., 1969, Estimation of parameters for a linear difference equation with application to EEG analysis, Mathematical Biosciences, 5, pp. 227-255.

[2.39]Makhoul,J., 1975, Linear prediction : A tutoarial review, Proceedings of the IEEE, 63, pp. 561-580.

[2.40]Rappelsberger,P., and Petsche,H., 1975, Spectral analysis of the EEG by means of autoregression, In : CEAN , pp. 25-40.

[2.41]Blinowska,K.J., Czerwosz,L.T., and Drabik,W., 1981, EEG data reduction by autoregressive representation and discriminant analysis procedures, Electroencephelography and clinical neurophysiology, 51, pp. 650-658.

[2.42]Tharp,B.R., 1972, Autoregressive spectral analysis - A unique technique for human seizure activity, Computers and Biomedical Research, 5, pp. 26-31.

[2.43]Mathieu,M., Trisch,W., and Poppl,S.J., 1975, Multichannel online EEG analysis by means of an autoregressive model with applications. In : Quantitative analysis of EEG : Methods and Applications, pp. 475-486.

[2.44]Crowell,D.H., Jones,R.H., and Leung,P., 1977, Autoregressive representation of infant EEG for the purpose of hypothesis testing and classification, Electroencephelography and clinical neurophysiology, 43, pp. 317-324.

[2.45]Jansen,B.H., Bourne,J.R., and Ward,J.W., 1981, Autoregressive estimation of short segment spectra for computerised EEG analysis, IEEE Trans. on Biomedical Engineering, 28, pp.630-638.

[2.46]Burg,J.P., 1975, Maximum entropy spectral analysis, Ph.D Dissertation, Stanford University.

[2.47]Childer,D.G., 1978, Modern Spectral analysis, IEEE Press, New York.

[2.48]Branwell,J.P., 1980, Windowless techniques for LPC analysis, IEEE Trans. on Acoustics, Speech and Signal Processing, 28, pp. 421-427.

[2.49]Jansen,B.H., Ward,J.W., and Richards,R.S., 1982, Spectral estimation of EEG signals : a clinical study, Electroencephelography and clinical neurophysiology, 48, pp. 214-220.

[2.50]Childers,D.G., Aunon,J.I., and McGillem,C.D., 1981, Spectral analysis : prediction and extrapolation, Critical Reviews in Bioengineering, 6, CRC Press, pp. 133-175.

[2.51]Mattis,P.M., Scheffner,D., and Benninger,C., 1981, Spectral analysis of EEG : Comparison of various spectral parameters, Electroencephelography and clinical neurophysiology, 52, pp. 218-221.

[2.52]Kay,S., 1979, The effects of noise on the autoregressive spectral estimator, IEEE Trans. on Acoustics, Speech and Signal Processing, 27, pp. 478-484.

[2.53]Tierney,J., 1980, A study of LPC analysis of speech in additive noise, IEEE Trans. on Acoustics, Speech and Signal Processing, 28, pp. 389-397.

[2.54]Kay,S., 1980, Noise compensation for autoregressive spectral estimates, IEEE Trans. on Acoustics, Speech and Signal Processing, 28, pp. 292-303.

[2.55]Quirk,M.P., and Liu,B., 1983, Improving the resolution of autoregressive spectral estimator, IEEE Trans. on Acoustics, Speech and Signal Processing, 31, pp. 630-637.

[2.56]Gersch,W., and Sharpe,D.R., 1973, Estimation of power spectra with finite order autoregressive models, IEEE Trans. on Automatic Control, 13, pp. 367-369.

[2.57]Herring,R.W., 1980, The cause of line splitting in Burg's maximum entropy spectral analysis, IEEE Trans. on Acoustics, Speech and Signal Processing, 28, pp. 692-701.

[2.58]Kay,S., and Marple,L., 1979, Sources of and remedies for spectral line splitting in autoregressive spectrum analysis, Int. Conf. on Acoustics Speech and Signal Processing, pp. 151-154.

[2.59]Nuttal,A.H., 1976, Spectral analysis of univariate process with bad data points via maximum entropy and linear prediction techniques, Naval Underwater System Centre, New London, CT, Tech. Report, 5303, March 1976.

[2.60]Ulrych,T.J., and Clayton,R.W., 1976, Time series modeling and maximum entropy, Phys., Earth. and Plan. Int., 12, pp. 188-200.

[2.61]Lang,S.W., and McClellan,J.H., 1980, Frequency estimation with maximum entropy spectral estimators, IEEE Trans. on Acoustics, Speech and Signal Processing, 28, pp. 716-724.

[2.62]Marple,L., 1980, A new autoregressive spectral analysis, IEEE Trans. on Acoustics, Speech and Signal Processing, 28, pp. 441-445.

[2.63]Wennberg,A., and Zetterberg,L.H., 1971, Application of a computer based model for EEG analysis, Electroencephelography and clinical neurophysiology, pp. 457-468.

[2.64]Zetterberg,L.H., 1973, Interpretation of EEG parameters of heart patients, Electroencephelography and clinical neurophysiology, pp. 312-323.

[2.65]Diekman,V., 1975, EEG analysis by an autoregressive moving average model: Application to the study of EEG changes measured under various blood gas levels, In : Quantitative analysis of EEG, Methods and applications, pp. 369-378.

[2.66]Gersch,W., Yonemoto,J., and Naitoh,P., 1977, Automatic classification of multivariate EEGs using an amount of information measure and eigenvalues of parametric time series model features, Computers and Biomedical Research, pp. 297-317.

[2.67]Bohlin,T., 1973, Comparison of two methods of modeling stationary EEG signals, IBM Journal of Research and Developement, pp. 194-205.

[2.68]Smith,W.D., and Lager,D.L., 1986, Evaluation of simple algorithms for spectral parameter analysis of the electroencephelogram, IEEE Trans. on Biomedical Engineering, 33, pp. 352-358.

[2.69]Cadzow,J.A., 1982, Spectral estimation : An overdetermined rational model equation approach, Proceedings of the IEEE, 70, pp. 907-939.

[2.70]Segen,J., and Sanderson,A.C., 1980, Detecting changes in a time series, IEEE Trans. on Information Theory, 26, pp. 249-255.

[2.71]Kawabata,N., 1973, A nonstationary analysis of the Electroencephelogram, IEEE Trans. on Biomedical Engineering, 20, pp. 444-452.

[2.72]Vos,J.E., 1975, Representation in frequency domain of nonstationary EEGs. In CEAN, pp. 41-50.

[2.73]Bohlin,T., 1971, Comparison of two methods of modeling stationary EEG signals, IBM Journal of Research and Developement, pp. 194-205

[2.74]Bohlin,T., 1977, Analysis of EEG signals with changing spectra using a short-word Kalman estimator, Mathematical Biosciences, pp. 221-259.

[2.75]Zetterberg,L.H., and Herolf,M., 1975, Spectral analysis of EEG for on line computer implementation based on an adaptive linear model, In : Quantitative analysis of the EEG : Methods and Applications, pp. 461-473.

[2.76]Isaksson,A., 1975, On the time variable properties of EEG signals examined by means of a Kalman filter method, Tech. report-95, Examples of EEG signals with time varying spectra, Tech. report-96, Deptt. of Telecommunication Theory, Royal Institute of Technology, Stockholm, Sweden.

[2.77]Carrie,J.R.G., 1973, The detection and quantification of transient and paroxysmal EEG abnormalities, In : Automation of Clinical Electroencephelography, pp. 217-226.

[2.78]Walter,D.O., 1973, Semiautomatic quantification of sharpness of the EEG, IEEE Trans. on Biomedical Engineering, 29, pp. 53-55.

[2.79]Ktonas,P.Y., and Smith,J.R., 1974, Quantification of abnormal EEG spike characterstics, Computers in Biology and Medicine, 4, pp. 157-163.

[2.80]Barlow,J.S., 1986, Automatic elimination of electrode-pop artefact in EEGs, IEEE Trans. on Biomedical Engineering, 33, pp. 517-521.

[2.81]Bickford,R.G., 1977, Computer analysis of background activity, In EEG Informatics : A Didactic review of methods and applications of EEG data processing, Ed. Remond,A., Amsterdam, Elsevier/North Holland, pp. 215-232.

[2.82]Ktonas,P.Y., Osorio,P.L., and Everett,R.L., 1979, Automated detection of EEG artefacts during sleep : Preprocessing for all night spectral analysis, Electroencephelography and clinical neurophysiology, 46, pp. 382-388.

[2.83]Barlow,J.S., 1985, A general purpose automatic multichannel electronic switch for EEG artefact elimination, Electroencephelography and clinical neurophysiology, 60, pp. 174-176.

[2.84]Whitton,J.L., Lue,F., and Modofsky,H., 1978, A spectral method for removing eye movement artefact from EEG, Electroencephelography amd clinical neurophysilogy, 44, pp. 735-741.

[2.85]Jervis,B.W., Kiloh,R.S., and Persson,H., 1985, The assesment of two methods for removing eye artefact from the EEG, Electroencephelography and clinical neurophysiology, 61, pp. 444-452.

[2.86]Blinovaska,K,J., Czerwosz,L,T., Drabik,W., and Ekiert,H., 1981, EEG data reduction by autoregressive representation and discriminant analysis procedures,Electroencephelography and clinical neurophysiology, 51, pp. 650-658.

[2.87]Barlow,J.S., and Remond,A., 1981, Eyemovement artefact nulling in EEGs by multichannel on line EOG subtraction, Electroencephelography and clinical neurophysiology, 52, pp. 418-423.

[2.88]Gratton,G., Forgens,T., and Cooper,S., 1983, A new method for offline removal of occular artefact, Electroencephelography and clinical neurophysiology, 55, pp. 468-484.

[2.89]Elbert,T., 1985, Removal of occular artefact from EEG : A biophysical approach to EOG, Electroencephelography and clinical neurophysiology, 60, pp. 455-463.

[2.90]Kiloh,L.G., McComas,A.J., and Osselton,J.W., 1979, Clinical Electroencephelography, Butterworth Publications.

[2.91]Barlow,J.S., and Dubinsky,J., 1980, EKG artefact minimisation in referential EEG recording by computer subtraction, Electroencephelography and clinical neurophysiology, 48, pp. 470-472.

[2.92]Forgens,C., and DeBruin,M.P., 1983, Removal of eyemovement and ECG artefact from the noncephalic reference EEG, Electroencephelography and clinical neurophysiology, 56, pp. 90-96.

[2.93]Johnson,T.L., Wright,S.C., and Segall,A., 1979, Filtering of muscle artefact from the electroencephalogram, IEEE Trans. on Biomedical Engineering, 26, pp. 556-563.

[2.94]Bartoli,F., and Cerutti,S., 1983, An optimal linear filter for reduction of noise superimposed on the EEG signal, Journal of Biomedical Engineering, 5, pp. 274-280.

[2.95]Barlow,J.S., 1983, Muscle spike artefact minimisation by time domain filtering, Electroencephelography and clinical neurophysiology, 55, pp. 487-491.

[2.96]Barlow,J.S., 1984, EMG artefact minimisation during clinical EEG recordings by special analog filtering, Electroencephelography and clinical neurophysiology, 58, pp. 161-174.

CHAPTER 3

SOFTWARE SIMULATION OF THE EEG

3.1 Intoduction

Simulation tests form an important step in the evaluation of the performance of any signal processing technique. Sinusoidal and white noise data are commonly used for this purpose. However in practice, a simulated signal that is close to the actual signal for which the technique has to be applied is preferred. Since the parameters of the simulated signal are known, it helps in ascertaining the accuracy of the performance of the technique under study and also enables valid comparisons of the results of different methods. This is particularly true for EEG signals as there is a necessity to convince the neurologist about the utility and validity of the analysis techniques. In view of this, various methods of simulating EEG like the one based on autoregressive series [3.1] and analog techniques [3.2 - 3.5] have been reported. The autoregressive series method, simulates the EEG by filtering the white noise using an autoregressive filter having the desired characteristics. The analog techniques use electronic circuits, where independent white noise signals generated by zener diodes are filtered by active lowpass and bandpass filters having prescribed centre frequencies and bandwidths. Further, the filtered outputs are scaled and added to get the required analog EEG signal. For evaluating the digital signal processing techniques, the analog EEG signal must be converted to digital form and stored in the magnetic tape. Hence, it is desirable to generate the EEG data directly in digital form by a simple software technique using digital filters. This chapter deals with the implementation of such a technique which in principle is based on the technique of Zetterberg which assumes that the EEG spectrum is composed of spectral components.

In the sections that follow, the first one deals with the model on which the simulation is based, the second one with the implementation and the third one deals with the illustration of the simulation by examples and results.

3.2 The Basic Model

As previously mentioned, the EEG is regarded as a statistical occurence with two components : a stationary component and the transients (wave train, spikes and sharp waves) that occur sporadically. The present simulation is concerned with the stochastic component, the background activity.

The spectral properties of a stationary stochastic process can be represented by a model consisting of a filter driven by a white noise generator. The reason for using this model is that EEG signals are formed by an organic system which adds and filters the primary impulses. The technical reason is that filtering is a very flexible way of shaping the spectrum, and filter functions are well known and easy to describe in parametric form. It is important to note that the model does not imitate the complicated neurological process that generates the EEG, but represents rather a description of the EEG signal [3.6].

It has been assumed that the spectral density function (PSDF) of the EEG signal can be described by a rational function of the form [3.2]

$$\frac{B(f^2)}{A(f^2)} \tag{3.1}$$

where $A\ (f^2)$ and $B\ (f^2)$ are polynomials in f^2 of order M and N respectively.

The function in Eqn.(3.1) allows resonances to appear in the PSDF and it is possible to control the resonance frequency, bandwidth of resonance and the power content related to a certain peak. On partial fraction expansion of Eqn.(3.1), the PSDF can be expressed as a sum of several spectral components, each corresponding to one term in the partial fraction expansion. These terms are of two types, depending on where the poles or resonances are located. For type-I term, the poles are located on the negative real axis and for type-II, poles appear in the complex conjugate pairs with negative real part, in the S-plane $(\sigma + j\ \omega)$. That is the PSDF of the two functions are given by :

Type-I :

$$S_{Ii}(f) = \frac{C}{f^2 + \sigma_i^{\,2}} \tag{3.2}$$

and

Type-II :

$$S_{IIi}(f) = \frac{D f^2 + E}{(f_i^2 + \sigma_i^2 - f^2)^2} + (2f\sigma_i)^2 \tag{3.3}$$

The first function has a resonance at $f = 0\,Hz.$ and the second has a peak close to $+f_i$ when σ_i is much less than f_i . The parameter σ_i measures the bandwidth of the resonance peak for type-I and half the bandwidth for type-II. A weighted sum of these two will give the function in Eqn.(3.1). The correlation functions corresponding to Eqn.(3.2) and Eqn.(3.3) are given by [3.2] :

$$r_{Ii}(\tau) = G_i \exp[-2\pi\sigma_i |\tau|] \tag{3.4}$$

$$r_{IIi}(\tau) = [G_i \cos(2\pi f_i |\tau|) - H_i \sin(2\pi f_i |\tau|] \exp[-2\pi\sigma_i |\tau|] \tag{3.5}$$

The parameter G_i expresses the power contribution from each spectral component, whereas H_i gives a measure of asymmetry for the PSDF relative to the resonance frequency f_i . The spectral parameters are σ_i and f_i agree in two sets of expressions, whereas relations between G_i and H_i and D and E parameters are somewhat involved.

In effect, the spectral properties of the EEG registration are described by certain frequency and power parameters. Further, the EEG δ activity is described by type-I function and α , β and θ activities are described by type-II functions. In general, for a complete description of PSDF, one more type of function should be added which takes into account an activity that is due to constant spectral density within the frequency band of observation. The corresponding power is denoted by ε . This activity corresponds to white noise and results in a component of type-0. In summary, the model describing the EEG must have the following parameters [3.6] :

For Type-0 : Power parameter ε .

For Type-I : Frequency parameter σ_i and power parameter G_i

For Type-II : Frequency parameters σ_i and f_i , power parameters G_i and H_i .

3.3 Implementation

Based on the model described above, knowing the frequency and power parameters of different

activities involved, simulation can be carried out by the procedure described in this section.

As mentioned, the δ activity can be described by Type-I function and transfer function which can realise this is :

in analog domain,

$$T_\delta(s) = \frac{1}{s + 2\pi\sigma_\delta} \tag{3.6a}$$

in discrete domain,

$$T_\delta(z) = \frac{1}{1 - a_\delta z^{-1}} \tag{3.6b}$$

where,

$$a_\delta = \exp[-2\pi\sigma_\delta T_S]$$

σ_δ is the -3 dB cut off frequency in Hz. and $(1/T_S)$ is the sampling frequency.

The α , β and θ activities are described by Type-II function and the transfer function realising this are

$$T_i(s) = \frac{s + 2\pi\sigma_{zi}}{(s + 2\pi\sigma_i)^2 + (2\pi f_i)^2} \tag{3.7a}$$

and

$$T_i(z) = \frac{1 - b_{1i} z^{-1}}{1 - a_{1i} z^{-1} + a_{2i} z^{-2}} \tag{3.7b}$$

in analog and digital domain respectively, and where

$$b_{1i} = \exp[-2\pi\sigma_i T_S]\,[\cos(2\pi f_i T_S + \frac{\sigma_i - \sigma_{zi}}{f_i} \sin(2\pi f_i T_S)]$$

$$a_{1i} = 2\exp[-2\pi\sigma_i T_S]\cos(2\pi f_i T_S)$$

$$a_{2i} = \exp[-4\pi\sigma_i T_S]$$

σ_{zi} , σ_i and f_i are different for α , β and θ activities. σ_{zi} is the -3 dB zero frequency. Simulation of the EEG is carried out by filtering independent random number sequences by transfer functions corresponding to different activities and adding the filtered outputs with appropriate gain factors to get the required power distribution among individual activities. This is schematically shown in Fig.3.1.

Independent random number sequences having Gaussian distribution are generated by changing the seed value. For each activity, a random number sequence is filtered by the corresponding transfer function. This filtering is done by time domain convolution.

If $x_\delta(n)$ is the random number sequence used for the δ activity, the output $y_\delta(n)$ is given by :

$$y_\delta(n) = x_\delta(n) + a_\delta\, y_\delta(n-1) \tag{3.8a}$$

For α, β and θ activities, the output $y_i(n)$ is given by :

$$y_i(n) = x_i(n) - b_{1i}x_i(n-1) + a_{1i}y_i(n-1) - a_{2i}y_i(n-2) \tag{3.8b}$$

The sum of the squares of the filtered data for each activity i.e., $\sum_{k=1}^{L} y_i^{\,2}(k)$ is also found.

The required power distribution is done in the following way:

Let

$$\sum_{k=1}^{L} y_\alpha^{\,2}(k) = X \tag{3.9a}$$

$$\sum_{k=1}^{L} y_\beta^{\,2}(k) = Y \tag{3.9b}$$

and

$$\sum_{k=1}^{L} y_\delta^{\,2}(k) = Z \tag{3.9c}$$

(assuming that only α, β and δ activities are present).

thus if the percentage of power distribution of each activity in the process is p : q : r , then

$$p = \frac{G_1^{\,2}.X.100}{X' + Y' + Z'} \tag{3.10a}$$

$$q = \frac{G_2^{\,2}.Y.100}{X' + Y' + Z'} \tag{3.10b}$$

and

$$r = \frac{G_3^{\,2}.Z.100}{X' + Y' + Z'} \tag{3.10c}$$

where,

$$G_2^2 = (Z/Y) \cdot (q/r) \cdot G_3^2$$
$$G_1^2 = (Z/X) \cdot (p/r) \cdot G_3^2$$
$$X' = G_1^2 \cdot X$$
$$Y' = G_2^2 \cdot Y$$
$$Z' = G_3^2 \cdot Z$$

Assuming G_3^2 (say = 10) , G_1^2 and G_2^2 can be found and further G_1 , G_2 and G_3 which are the required gain factors to obtain the desired power distribution can also be found. The filtered sequences for α , β and δ activities are multiplied by G_1 , G_2 and G_3 respectively and then summed (corresponding samples) to get the required EEG data. This method has the advantage that it allows independent control over frequency and power parameters. But it has the limitation that all possible values of H_i cannot be realised with a second order transfer function. However in practice, it has been found that this is not a serious limitation.

Assuming G_3^2 (say = 10) , G_1^2 and G_2^2 can be found and further G_1 , G_2 and G_3 which are the required gain factors to obtain the desired power distribution can also be found. The filtered sequences for α , β and δ activities are multiplied by G_1 , G_2 and G_3 respectively and then summed (corresponding samples) to get the required EEG data. This method has the advantage that it allows independent control over frequency and power parameters. But it has the limitation that all possible values of H_i cannot be realised with a second order transfer function. However in practice, it has been found that this is not a serious limitation.

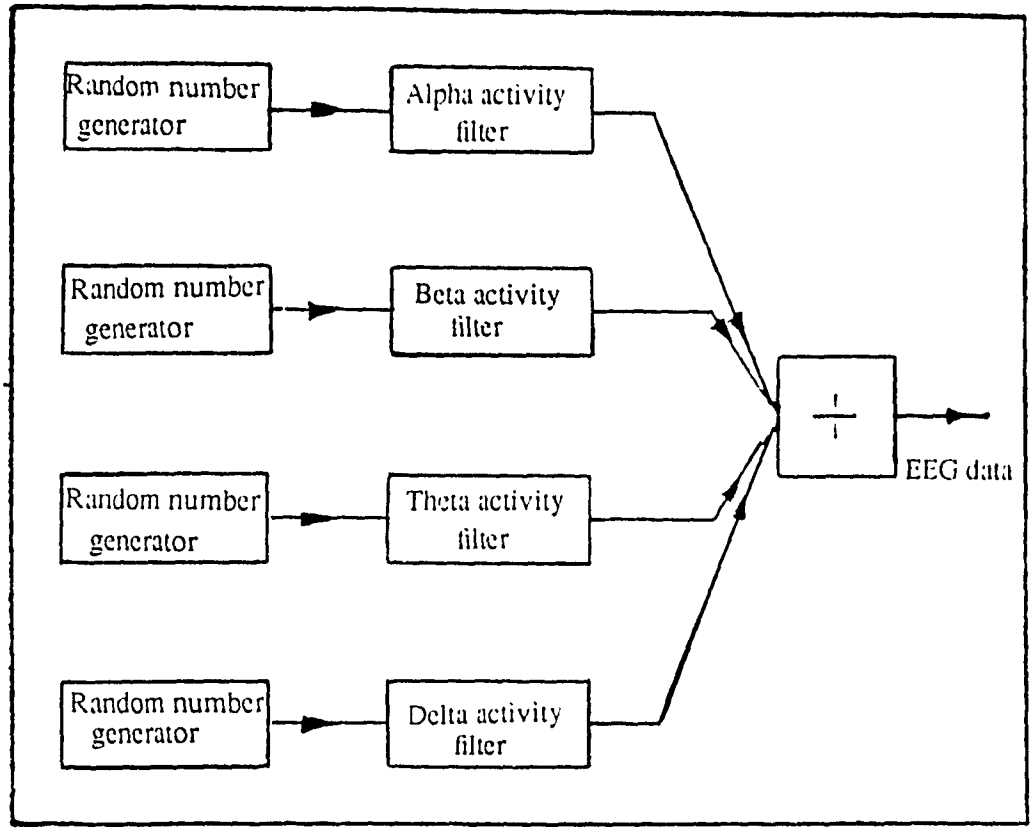

Fig.3.1 Schematic diagram of EEG simulator (Zetterberg, 1973)

3.4 Examples and Results

To illustrate the simulation and its performance, the parameters estimated by Zetterberg [3.2] are considered as shown in Table 3.1. The parameters H_i are considered to be small compared to G_i for α and β activities. The tolerance given indicate the deviations that one finds if data is analysed repeatedly for non-overlapping epochs. Using these values of σ_i and f_i for different activities, the coefficients of the filters are found using Eqns.(3.6b) and (3.7b). The parameters of the realised EEG filters are given in Table 3.2. The filtered outputs, for δ activity is obtained by Eqn.(3.8a) and for α and β activities by Eqn.(3.8b). The sampling frequency used is 100 Hz.

To determine the accuracy of the frequency parameters of the simulated data, the PSDF of each activity (α, β and δ*seperately*) and that of the EEG (α, β and δ together) are computed using Welch method. In computing the PSDF for α, β and δ and that for the EEG data, the length of the individual segments chosen is 256 samples. In each case, the data segments are windowed by a Hamming window and padded with zeros to a length of 1024. This provides a resolution of 0.1 Hz. (interpolated). Further, the spectral averaging is done over 25 segments. The frequency parameters of the simulated individual activities and that of the EEG data are given in Tables 3.3 and 3.4 respectively. The percentage of power distribution for α, β and δ activities is found by computing:

$$p_\alpha = \sum_{k=1}^{L} \frac{G_1^{\,2} y_\alpha^{\,2}(k)}{W}$$

$$p_\beta = \sum_{k=1}^{L} \frac{G_2^{\,2} y_\beta^{\,2}(k)}{W}$$

and

$$p_\delta = \sum_{k=1}^{L} \frac{G_3^{\,2} y_\delta^{\,2}(k)}{W}$$

where,

$$W = [G_1 y_\alpha(k) + G_2 y_\beta(k) + G_3 y_\delta(k)]^2$$

L is the total length of the signal considered. p_α, p_β and p_δ computed for the simulated data are 62.07%, 3.94% and 32.51%respectively. As the percentage of power distribution is calculated

directly, it is quite accurate. From Tables 3.2 and 3.4, it is evident that the centre frequency parameters are accurate than the bandwidth parameters. This is due to the fact that the Welch method of spectral estimation itself is not very accurate. The PSDF of individual activities are computed with the aim of testing whether the filtered outputs have the same charactersics as those of the respective filter frequency response (and the Welch method is adequate for this purpose).

It is important to note that in simulating the δ activity, the mean for the white noise must be removed over short segments. Otherwise, the filtered signal will not have the desired -3 dB cutoff frequency and also the percentage of power distribution will be erroneous.

To illustarte the performance of the method, simulation of different EEG signals whose parameters are given in Table 3.5 is carried out and the simulated EEG signals are shown in Fig.3.5. These parameters are the same as those considered by Zetterberg and Ahlin [3.3] and these were estimated by them from real EEG signals. The simulated EEG signals match quite well in their nature with real EEG signals.

The results indicate that the software method of simulation gives satisfactory results. The EEG signals simulated by this technique have been used in subsequent chapters wherever required.

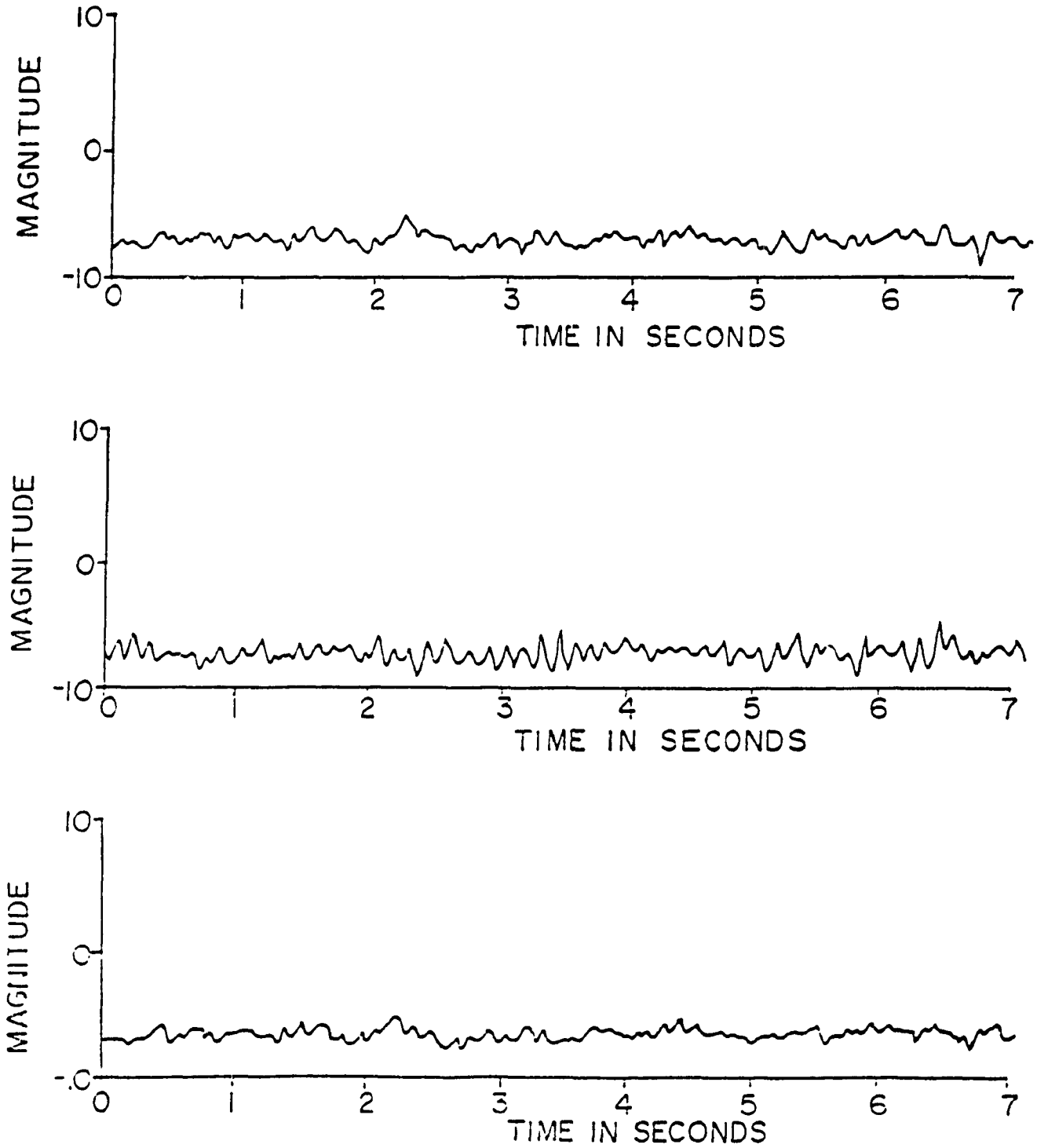

Fig.3.2 Simulated EEG signals for the set of parameters in Table 3.5

Table 3.1 Parameters of EEG registration.

Activity	σ_i (Hz.)	f_i (Hz.)	G_i (Hz.)
α	0.58 + 0.03	10.25 + 0.03	63 + 11
β	1.36 + 0.10	18.90 + 0.10	4 + 0.9
δ	1.27 + 0.07	0.0	33 + 6.0

Table 3.2 Parameters of realised EEG filters.

Activity	σ_i (Hz.) (Gain in dB)	f_i (Hz.)
α	0.586 (3.147)	10.352
	0.586 (2.875)	
β	1.367 (2.992)	19.043
	1.367 (3.053)	
δ	1.367 (2.981)	0.00
	1.269 (2.647)	

[**Note:** In the σ_i column, the first line corresponds to lower -3 dB and the second line corresponds to the upper -3 dB. This holds true for other tables as well.]

Table 3.3 The parameters of the individual EEG activities.

Activity	σ_i (Hz) (Gain in dB)	f_i (Hz.)
α	0.878 (2.696)	10.644
	0.488 (2.704)	
β	0.976 (2.800)	18.848
	0.977 (2.940)	
δ	1.367 (3.018)	0.0
	1.269 (2.600)	

Table 3.4 The parameters of the simulated EEG data.

Activity	σ_i (Hz) (Gain in dB)	f_i (Hz.)	G_i (%)
α	0.977 (3.182)	10.644	62.07
	0.488 (2.704)		
β	1.074 (2.762)	18.945	3.94
	1.562 (2.891)		
δ	1.367 (2.950)	0.0	32.51
	1.269 (2.558)		

Table 3.5 Parameters of the simulated EEG signal.

	δ - Activity		α - Activity			β - Activity		
No.	σ_δ (Hz)	G_δ (%)	σ_α (Hz.)	f_α (Hz.)	G_α (Hz.)	σ_β (Hz.)	f_β (Hz.)	G_β (%)
1	2.5	84	0.2	9.8	16	-	-	
2	1.8	52	1.8	7.5	48	-	-	
3	2.0	24	0.4	9.9	75	0.8	20.9	1
4	1.7	69	1.5	9.4	22	2.4	21.0	10
5	6.9	100	-	-	-	-	-	

3.5 References

[3.1] Fenwick,P.B., Mitchie,P., and Fenton,G.W., 1971, Mathematical simulation of electroencephalogram using an autoregressive series, Biomedical Computing, 2, pp. 281-307.

[3.2] Zetterberg,L.H., 1973, Experience with analysis and simulation of EEG signals with parametric description of spectra, in Automation of clinical electroencephalography, Ed. Kellaway,P., and Peterson,I., Raven Press, New York, pp. 161-201.

[3.3] Zetterberg,L.H., and Ahlin,K., 1975, Analog simulator of EEG signals based on spectral components, Medical and Biological Engineering, pp. 272-278.

[3.4] Issakson,A., and Wennberg,A., 1975, An EEG simulator - a means of objective clinical interpretation of EEG, Electroencephalography and clinical neurophysiology, 39, pp. 313-320.

[3.5] Shaw,J.C., 1967, Some comments on quantifying EEG records, Proceedings of the Electrophysiological Association, pp. 14-26.

[3.6] Wennberg,A., and Zetterberg,L.H., 1971, Application of computer based model for EEG analysis, Electroencephalography and clinical neurophysiology, 31, pp. 457-468.

CHAPTER 4

SPECTRAL ESTIMATION OF EEG SIGNALS

4.1 Introduction

The spectral information in an EEG record plays an important role in it's assesment and hence spectral estimation is very important in EEG processing. Among the many spectral estimation approaches, the parametric approach has become popular in the last decade. The parametric representation facilitates data reduction for storage or transmission and also makes the classification of EEG signals by pattern recognition methods effective [4.1]. In this approach, all pole or autoregressive (AR) modeling has been extensively used. Though an all pole model of higher order represents the signal with some accuracy, it poses some difficulties. In the signal spectrum, the spectral zero results in two effects: a dip in the spectrum and a 12 dB/octave rise. A higher all pole model can approximate the 12 dB/octave rise, but it is difficult to create the dip in the spectrum without disturbing the neighbourhood of the zero frequency [4.2]. The all pole approximation of a zero, hence, results in a shift in the location of spectral peaks near the zero and also merging of the closely spaced spectral peaks. Although the latter effect is not of significance as far as the EEG is concerned, the former affects to a considerable extent. Also, the number of poles required to approximate the effect of a zero increases the number of parameters. For these reasons, it is preferred to represent the EEG, speech etc. by pole-zero or autoregressive moving average (ARMA) model rather than by all pole model. In the review, different pole zero modeling methods used for EEG analysis were considered and some are in favor of the pole-zero model [4.3 - 4.6].

The popularity of the all pole and the pole-zero spectral modeling based on linear prediction technique in speech and seismology is due to the efficiency of linear prediction in extracting the structure of the signal and its computational efficiency compared to iterative methods. The linear prediction based methods require the signal to be either minimum or maximum phase. However real signals are neither minimum phase nor maximum phase, but are of a mixed phase nature. This limits the per-

formance of the all pole and pole-zero modeling methods based on linear prediction. However, the mixed phase signals can be converted to a linear prediction compatible form by homomorphic filtering [4.7]. Unlike linear prediction, the homomorphic filtering is applicable to all types of signals including the ones characterized by zeros. However, the absence of the underlying model makes this technique inefficient in extracting the structure of the signal. In order to have the advantages of both homomorphic filtering and linear prediction, their combination has been proposed. This combination that enjoys the generality and efficiency has been reported to yeild better results in processing of speech signals [4.7 - 4.8].

The present study deals with the application of two methods of pole-zero spectral modeling, both based on combinations of homomorphic filtering and linear prediction, for EEG spectral modeling and comparison of their performances. The first method is a direct combination which uses matching of autocorrelation coefficients of the signal with those of the model[4.8]. The second method is based on cepstral coefficient matching . The first method, often called homomorphic prediction, has been used for extracting the vocal tract features alleviating the problem of pitch synchronization in speech processing. Also this method has been used in ECG and PCG analysis [4.9]. However the second method based on pole zero decomposition has only been applied for speech analysis [4.10]. Speech, ECG and PCG signals are impulse excited type rather than white noise excited. The following sections deal with the theoretical aspects of the methods and their application to EEG.

4.2 Spectral Modeling by Homomorphic Prediction

In this method, the mixed phase signal is converted to linear prediction compatible form by Homomorphic filtering and then pole zero estimation is done by linear prediction.

(a) Homomorphic Deconvolution

Homomorphic deconvolution is a general method of seperating two signals which are non-additively combined like convolution and multiplication. If $x_1(n)$ and $x_2(n)$ are two signals combined by convolution (say) to give $x(n)$, then

$$x(n) = x_1(n) * x_2(n) \tag{4.1}$$

The homomorphic recovery of $x_1(n)$ and $x_2(n)$ from $x(n)$ is a three step process shown in Fig.4.1. The sequence $\hat{x}(n)$ is called the complex cepstrum of $x(n)$ and is defined by

$$\hat{X}(z) = D[X(z)] = Log[X(z)] \tag{4.2}$$

where $X(z)$ is the Z transform of $x(n)$ and the complex logarithm appropriately defined [4.11]. The fundamental property of a complex cepstrum is that if Eqn.(4.1) holds then,

$$\hat{x}(n) = \hat{x}_1(n) + \hat{x}_2(n) \tag{4.3}$$

so that the cepstra of convolved signals are related by ordinary addition. If $\hat{x}_1(n)$ and $\hat{x}_2(n)$ occupy disjoint time intervals ($\hat{X}_1(z)$ and $\hat{X}_2(z)$ occupy disjoint frequency bands) , then $x_1(n)$ and $x_2(n)$ can be recovered by making $L[]$ a time (frequency) domain window.

For the application of linear prediction techniques the following signal transformations by homomorphic filtering are of significance.

1) If $x(n)$ is the convolution of $x_{min}(n)$ and $x_{max}(n)$, where $x_{min}(n)$ and $x_{max}(n)$ are the minimum phase and maximum phase components of $x(n)$ respectively , then

$$\hat{x}(n) = \hat{x}_{min}(n) + \hat{x}_{max}(n) \tag{4.4}$$

Since $\hat{x}_{min}(n)$ is zero for $n<0$ and $\hat{x}_{max}(n)$ is zero for $n>0$, the complex cepstrum provides a means of factorizing the signal $x(n)$ into its minimum phase and maximum phase components and this is done by choosing a linear system $L[]$ in Fig.4.1 such that

$$\begin{aligned} \hat{y}(n) &= 0 , \quad \text{for } n<0 \\ \hat{y}(n) &= 0.5\,\hat{x}(0) , \quad \text{for } n=0 \\ \hat{y}(n) &= \hat{x}(n) , \quad \text{for } n>0 \end{aligned} \tag{4.5}$$

the output $y(n)$ will be equal to $x_{min}(n)$.

Alternatively, choosing the linear system such that

$$\begin{aligned} \hat{y}(n) &= \hat{x}(n) , \quad \text{for } n<0 \\ \hat{y}(n) &= 0.5\,\hat{x}(0) , \quad \text{for } n=0 \\ \hat{y}(n) &= 0 , \quad \text{for } n>0 \end{aligned} \tag{4.6}$$

will result in an output $y(n)$ equal to $x_{max}(n)$.

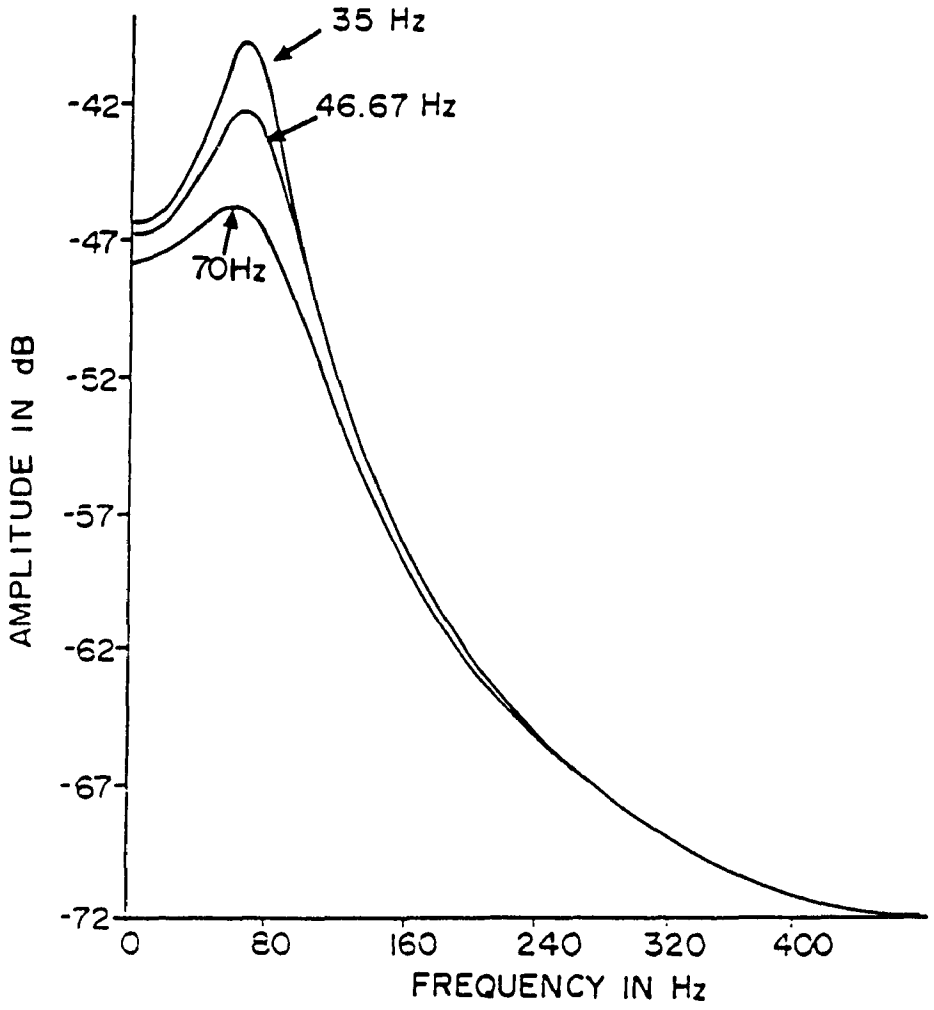

Fig.4.2 Negative derivative phase spectrum for all pole filters (Yegnarayana, 1981)

2) A mixed phase signal is converted to a minimum phase signal with the same spectral magnitude, $x_{mp}(n)$, called the minimum phase equivalent. This is done without the complex theoretical and computational issues of Eqn.(4.2), i.e. the phase unwrapping [4.11]. This implies

$$|X_{mp}(e^{j\omega})| = |X(e^{j\omega})|$$

and the phase of $X_{mp}(e^{j\omega})$ is related to $Log\,|X_{mp}(e^{j\omega})|$ by Hilbert transform. That is, $x(n)$ and $x_{mp}(n)$ have the same magnitude spectrum but different phase characterstics.

The advantage of minimum phase deconvolution is that $\hat{x}_{mp}(n)$ is a causal sequence and can be constructed from its even part. That is

$$\hat{x}_{mp}(n) = U(n)\,E\,V[\hat{x}_{mp}(n)] \tag{4.7}$$

where

$$U(n) = 0, \quad \text{for } n<0$$
$$U(n) = 1, \quad \text{for } n=0$$
$$U(n) = 2, \quad \text{for } n>0$$

Writing Eqn.(4.2) explicitly

$$\hat{X}(z) = Log[\,|X(e^{j\omega})|\,e^{j\theta(\omega)}]$$
$$\hat{X}(z) = Log[\,|X(e^{j\omega})|\,] + j\,\theta(\omega)$$

The even part of $\hat{x}(n)$, $EV[\hat{x}(n)]$ is obtained from the real part of $\hat{X}(z)$, i.e. $Log\,|X(e^{j\omega})|$.

The minimum phase component, maximum phase component and the minimum phase equivalent can be handeled by linear prediction techniques.

(b) Pole-Zero Estimation

Power spectrum estimation is done by modeling the signal by a rational transfer function $H(z)$ given by

$$H(z) = \frac{B(z)}{A(z)} \tag{4.8}$$

where

$$A(z) = 1 + \sum_{k=1}^{M} a_k\, z^{-k}$$

and

$$B(z) = \sum_{k=1}^{N} b_k z^{-k}$$

The problem is to choose the parameters a_k's and b_k's so that $h(n)$, the impulse response of $H(z)$, approximates the signal as closely as possible. That is if the error energy E is given by

$$E = \sum_{n=0}^{L} [x(n) - h(n)]^2 \tag{4.9}$$

then it is required that

$$\frac{\delta E}{\delta(A, B)} = 0$$

This is a nonlinear problem and not easy to solve. Many approaches have been used to solve a modified mean square error problem and the common ones are:

1) To treat the numerator as constant and this corresponds to the well known all pole modeling.

2) To assume that the $A(z)$ polynomial is fixed and it is required to estimate the numerator polynomial $B(z)$. If $A(z)$ is fixed as $A'(z)$ then the problem is linearised and leads to a system of equations given by

$$\frac{\delta}{\delta b_i} \sum_{n=0}^{L} [x(n) - \sum_{k=0}^{N} b_k f(n-k)]^2 = 0,$$

where $i = 0, 1, 2 \ldots\ldots N$

and where,

$$F(z) = \frac{1}{A'(z)}$$

This method of estimation of zeros is known as Shank's method [4.12].

3) Estimation of the poles and zeros simultaneously by solving the linear problem

$$\min_{A,B} \sum_{n=0}^{L} [A[x(n)] - B[\delta(n)]]^2$$

This is the Kalman filtering approach.

4) In this approach also, an initial estiamte of A, A' is obtained by some method to start with,

and then the next estimates are obtained by solving the linear problem $\min_{A,B} \sum_{n=0}^{L} [\frac{A[x(n)]}{A'} - \frac{B[\delta(n)]}{A}]^2$ and the new estimates of A and B are obtained by iteration and when the iteration converges then the succesive estimates of A are nearly equal [4.13].

The approach followed here is the second one [4.8]. In this, the poles and zeros are estimated in two steps. First, linear prediction is used to identify the poles, and zeros are located making use of the information about poles.

(a) Pole Identification

This is done by covariance linear prediction rather than by autocoorelation method. This is due to the fact that when the order of model is sufficiently high, the autocorrelation method approximates the whole spectrum including the effects of the zeros. Since the zeros have to be explicitly estimated, the covariance method is used in practice. The optimum coefficients a_k's are given by the following equations:

$$\sum_{k=1}^{M} a_k \, \phi_x(k, r) = -\phi_x(0, r), \qquad r = 1, 2, ...M \tag{4.10}$$

where,

$$\phi_x(t, u) = \sum_{n=T+1}^{\infty} x(n-t)\, x(n-u)$$

ϕ_x is a covariance like function of $x(n)$. T represents the initial segment of the signal which because of zeros of $X(z)$ is not predictable.

(b) Zero Identification

The zero identification is done by the above mentioned Shank's principle and this leads to the following equations :

$$\sum_{k=0}^{N} b_k \, \phi_{ff}(k, r) = \phi_{xf}(0, r), \qquad r = 0, 1, ...N \tag{4.11}$$

where,

$$\phi_{x_1 x_2}(t, u) = \sum_{n=0}^{\infty} x_1(n-t)\, x_2(n-u)$$

is a cross correlation function between $x_1(n)$ and $x_2(n)$.

The homomorphic prediction method considered in the present work involves the estimation of pole zero model of the minimum phase equivalent of the signal.

4.3 Spectral Modeling by Pole Zero Decomposition

This pole-zero modeling is based on cepstral coefficient matching and is achieved by pole-zero decomposition. This method is reported to provide better results than the one based on autocorrelation coefficient matching, since a large dynamic range frequency spectrum is represented better by log-magnitude spectrum than by the amplitude spectrum.

The basic principle involved is the splitting of the signal spectrum into an all pole and all zero spectrum and this is based on the properties of the negative derivative of the phase spectrum (DPS) of a minimum phase signal.

A minimum phase signal has its poles and zeros inside the unit circle in the Z plane. The properties of the minimum phase signal and that of the DPS have been described by Oppenheim [4.7] and Yegnarayana [4.10] respectively. The properties of the DPS are briefly presented,

If $A(z)$ is the minimum phase polynomial, then

$$A(\omega) = A(z)|_{z = e^{j\omega}}$$

and

$$A(\omega) = |A(\omega)|\, e^{-j\theta(\omega)}$$

while the negative derivative of phase spectrum is given by

$$\dot{\theta}(\omega) = \frac{d\theta(\omega)}{d\omega}$$

The polynomial $A(z)$ can be written as a cascade of first order polynomials with real roots and second order polynomials with complex conjugate roots. The negative derivative of phase spectra for the first and second order all pole filters are shown in Fig.4.2. The significant values of the negative derivative of the phase spectra for the first order pole are close to the origin and those for the second order pole are around the resonance frequency. Further, the negative derivative phase spectrum near

the resonance is approximately proportional to the squared magnitude response of the filter. The negative derivative of the phase spectrum of the overall all pole filter, $\frac{1}{A(z)}$ is a summation of the individual negative derivative of phase spectra responses of the first and second order filters. The effect of individual negative derivative of phase spectrum of real or complex poles over one another is negligible. The negative derivative phase spectra for the zeros are same as that of the poles except for the difference in sign. The negative derivative of phase spectra for real and complex poles is positive and for real and complex zeros it is negative. These properties enable the pole zero decomposition.

(a) Relationship between magnitude spectrum and phase derivative

Since $x_{mp}(n)$ represents a minimum phase sampled signal, $x_{mp}(\omega)$ is periodic in ω with a period of 2π. Also as $x_{mp}(n)$ is a minimum phase signal, its cepstrum $\hat{x}(n)$ is also a minimum phase signal and hence

$$Log\,[X(\omega)] = 0.5\,\hat{x}(0) + \sum_{n=1}^{\infty} \hat{x}(n)\, e^{-j\omega n}$$

i.e.

$$Log\,[X(\omega)] = 0.5\,\hat{x}(0) + \sum_{n=1}^{\infty} \hat{x}(n)\cos(n\omega) - j \sum_{n=1}^{\infty} \hat{x}(n)\sin(n\omega)$$

Also,

$$Log\,[X(\omega)] = Log\,|X(\omega)| - j\,\theta(\omega)$$

Comparing the real and imaginary parts,

$$Log\,|X(\omega)| = 0.5\,\hat{x}(0) + \sum_{n=1}^{\infty} \hat{x}(n)\cos(n\omega)$$

and

$$\theta(\omega) + 2\pi i = \sum_{n=1}^{\infty} \hat{x}(n)\sin(n\omega)$$

where i is an integer.

Therefore,

$$\theta'(\omega) = \sum_{n=1}^{\infty} n\, \hat{x}(n) \cos(n\omega)$$

where $\theta'(\omega)$ is the negative derivative of phase spectrum of the signal $x_{mp}(n)$. The logmagnitude spectrum and the negative derivative of phase spectrum are related by the cepstral coefficients.

(b) Pole Zero Decomposition

The decomposition of the pole and zero components of the spectrum is obtained by seperating the positive and negative parts of the negative derivative of the phase spectra.

$$\theta'(\omega) = [\theta'(\omega)]^{+} + \theta'(\omega)]^{-}$$

where,

$$[\theta'(\omega)]^{+} = \theta'(\omega) \quad \text{for } \theta'(\omega) > 0 \quad (\textit{pole part})$$
$$[\theta'(\omega)]^{+} = 0 \quad \text{for } \theta'(\omega) < 0$$

and

$$[\theta'(\omega)]^{-} = \theta'(\omega) \quad \text{for } \theta'(\omega) < 0 \quad (\textit{zero part})$$
$$[\theta'(\omega)]^{-} = 0 \quad \text{for } \theta'(\omega) > 0$$

The shape of the derivative phase spectrum curve in the positive portion of $\theta'(\omega)$, i.e. of $[\theta'(\omega)]^{+}$ is mainly due to poles only and the shape of the negative portion of $\theta'(\omega)$, i.e. of $[\theta'(\omega)]^{-}$ is mainly due to zeros only.

The cepstral coefficients for the pole part, $\hat{x}^{+}(n)$ and for the zero part, $\hat{x}^{-}(n)$ are related to $[\theta'(\omega)]^{+}$ and $[\theta'(\omega)]^{-}$ respectively by the following relations:

$$[\theta'(\omega)]^{+} = C + \sum_{n=1}^{\infty} n\hat{x}^{+}(n) \cos(n\omega)$$

and

$$[\theta'(\omega)]^{-} = -C + \sum_{n=1}^{\infty} n\hat{x}^{-}(n) \cos(n\omega)$$

where C is the average value which does not contribute to the shape of the spectrum. From $\hat{x}^{+}(n)$ and $\hat{x}^{-}(n)$ the pole spectrum and the zero spectrum can be computed through Fourier cosine transform and

exponentiation.

The first few cepstral coefficients determine the log spectrum as they are its Fourier coefficients. A truncated cepstral series results in a smooth spectrum, called cepstrally smooth spectrum. The value of $\hat{x}(0)$ does not determine the shape of the spectrum. On similar lines, cepstrally smooth spectrum for the poles and zeros seperately can be obtained by only considering the first few cepstral coefficients in $\hat{x}^{+}(n)$ and $\hat{x}^{-}(n)$ respectively. Further, the linear prediction coefficients for the pole spectrum and the zero spectrum are obtained from the respective cepstral coefficients by the following recursive relations:

For pole coefficients:

$$a_1 = -\hat{x}^{+}(1)$$

$$ia_i = -i\hat{x}^{+}(i) - \sum_{k=1}^{i-1} k\,\hat{x}^{+}(k)\,a_{i-k}$$

for $i = 2, 3, \ldots\ldots, M$.

For zero coefficients:

$$b_1 = \hat{x}^{-}(1)$$

$$ib_i = i\hat{x}^{-}(i) + \sum_{k=1}^{i-1} k\,\hat{x}^{-}(k)\,b_{i-k}$$

for $i = 2, 3, \ldots\ldots, M$.

The gain of the overall transfer function G , is given by $LogG = 0.5\,\hat{x}(0)$.

For a given model of order M , since the model parameters are determined so that the first $M + 1$ cepstral coefficients of the model are equal to the first $M + 1$ cepstral coefficients of the signal, the method has been interpreted as pole zero modeling by cepstral matching.

4.4 Results

For the purpose of illustrating the two methods discussed in the present chapter simulation studies were carried out on real EEG signal obtained from the Montreal Neurological Institute. The real EEG data segment considered is from a female subject aged 34 years. The data is recorded from o1-

o2 electrodes pair in 10-20 electrode placement system.

Studies were carried out on this EEG signal using the homomorphic prediction method for spectral modeling. Different model orders were explored to find which one fits the desired EEG signal the best and the results are presented in Table 4.1 and the corresponding spectra are plotted in Fig 4.3. Similarly, for the case of the pole zero decomposition method spectral modeling was attempted using different numbers of parameters and the results obtained are presented in Table 4.2 and the corresponding spectra are presented in Fig.4.4. The results obtained are quite satisfactory.

In order to ensure the applicability of these methods, they have been applied to six real EEG data segments, two each from three subjects (Fig.4.5). Spectral estimation is carried out for each signal and it is evident from the pole and zero spectrum for the real EEG signal (Fig.4.6) and it is only the zero spectral estimate that gets affected by direct estimation and not the pole spectrum. This is obvious since for a stable signal all the poles lie within the unit circle and hence poles satisfy the assumptions of the linear prediction technique. On the other hand, for zeros no such restriction exists and they can lie anywhere in the Z-plane. Infact the zeros which lie inside the unit circle do not get affected. However, the zeros which lie outside the unit circle will not satisfy the assumptions of linear prediction.

In order to investigate more about the zeros of the EEG signal, the spectral zero locations for each signal have been found by determining the roots of the numerator polynomial estimated by direct pole zero modeling and by homomorphic prediction (Table 4.3). Among the real EEG signals only for certain signals, some of the zeros estimated by the direct method are inside the unit circle and these contribute to excess phase. The evidence of these zeros atleast in some cases indicates that in general EEG is not a minimum phase signal.

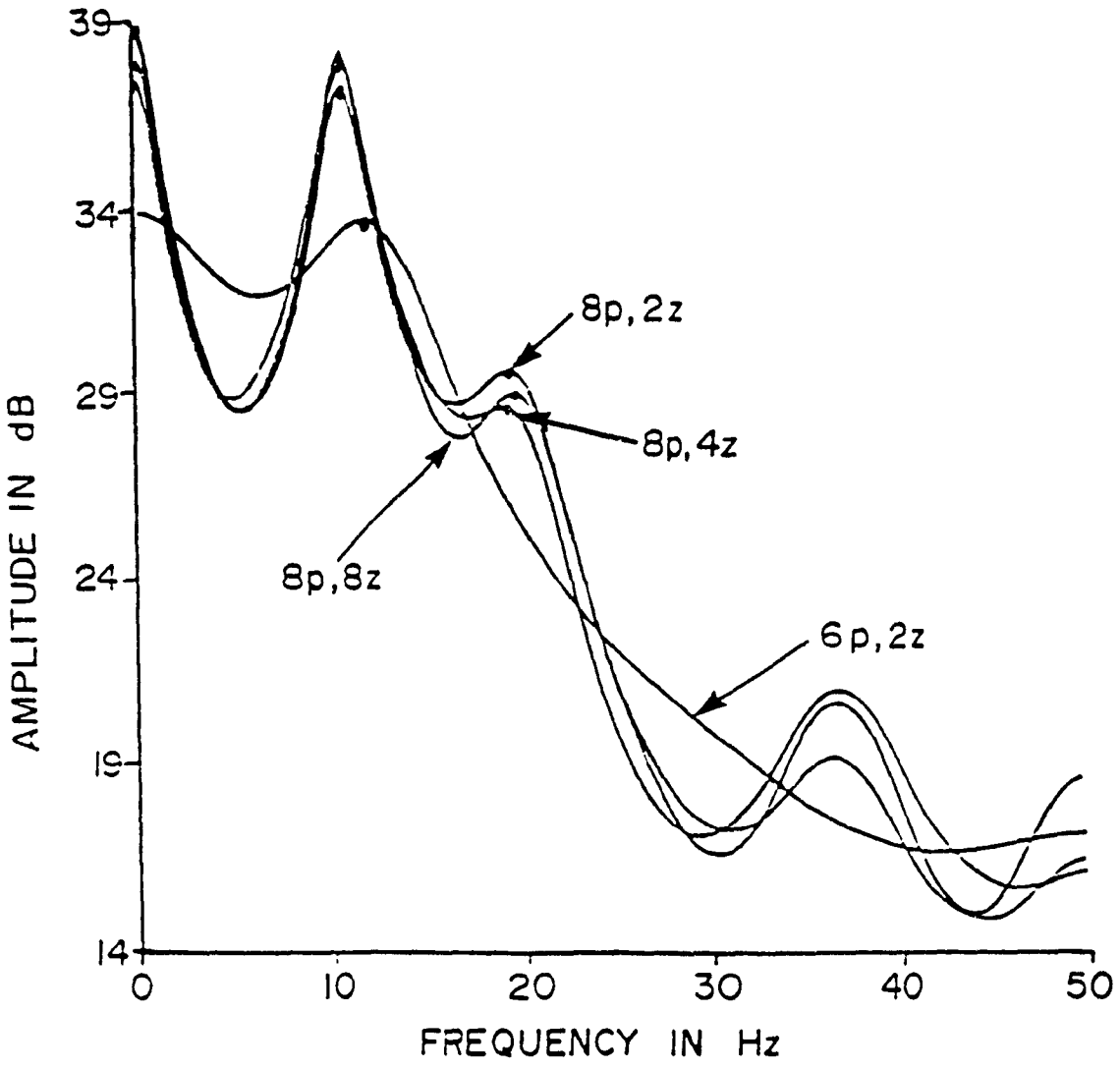

Fig.4.3 Comparison of spectrum of simulated EEG estimated by homomorphic prediction for different model orders

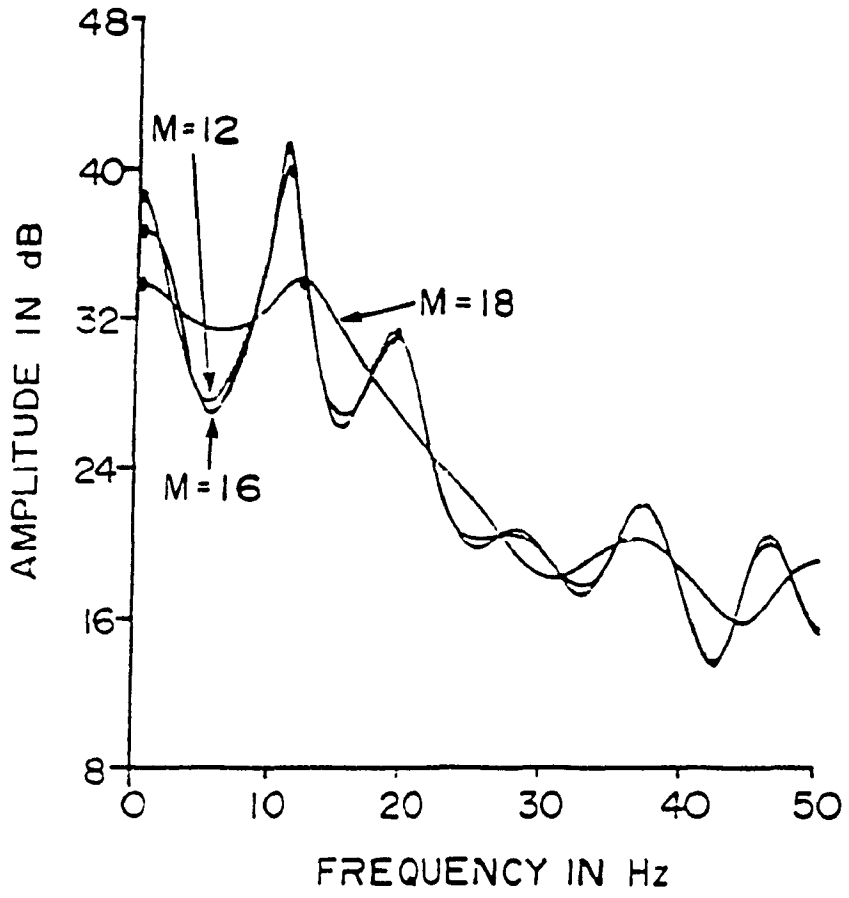

Fig.4.4 Estimated pole - zero spectrum for EEG signal for different number of parameters

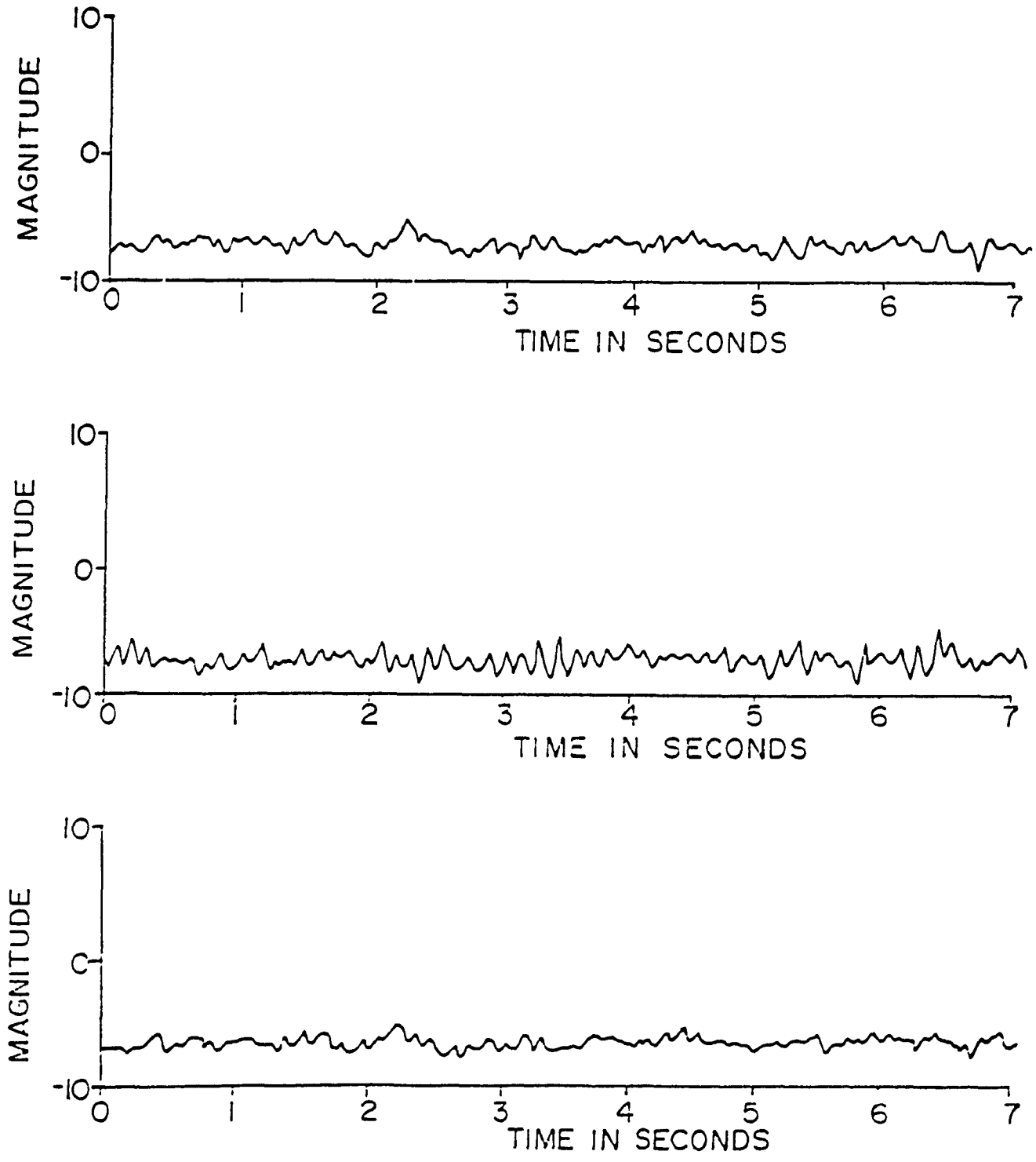

Fig.4.5 Real EEG signals recorded from different pairs of electrodes for three subjects (Montreal Neurological Institute, 1990)

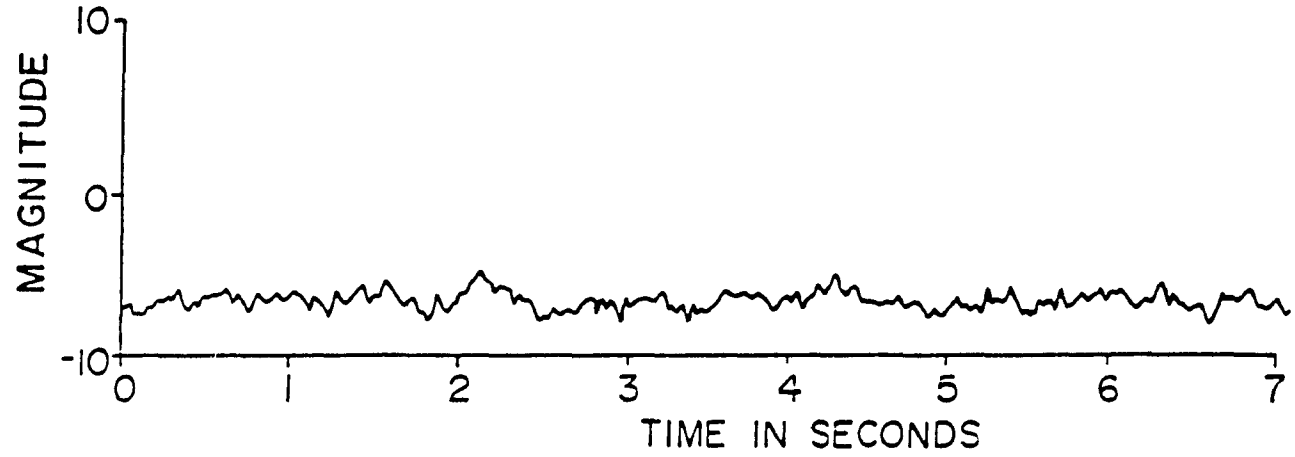
10
0
-10
MAGNITUDE
0
1
2
3
4
5
6
7
TIME IN SECONDS

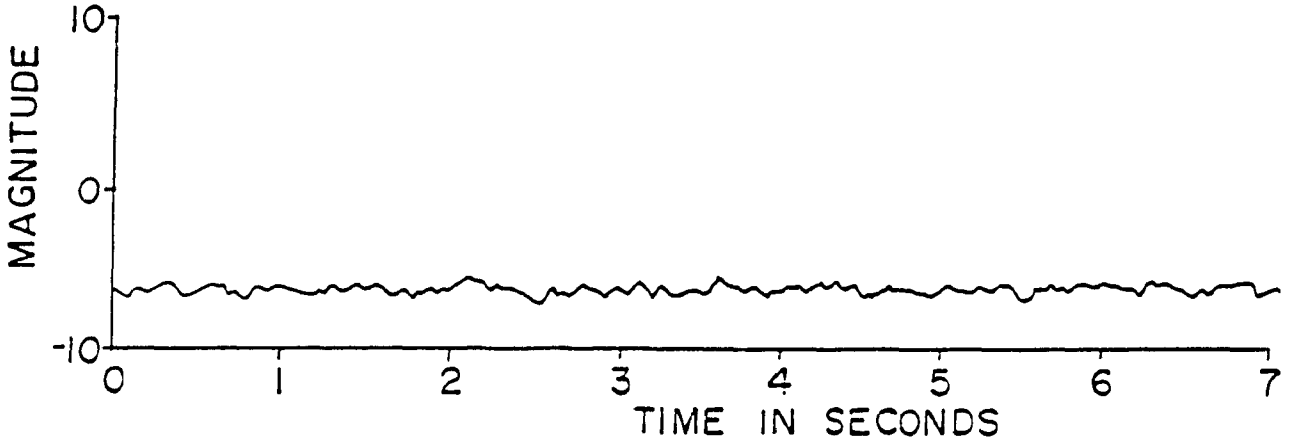
10
0
-10
MAGNITUDE
0
1
2
3
4
5
6
7
TIME IN SECONDS

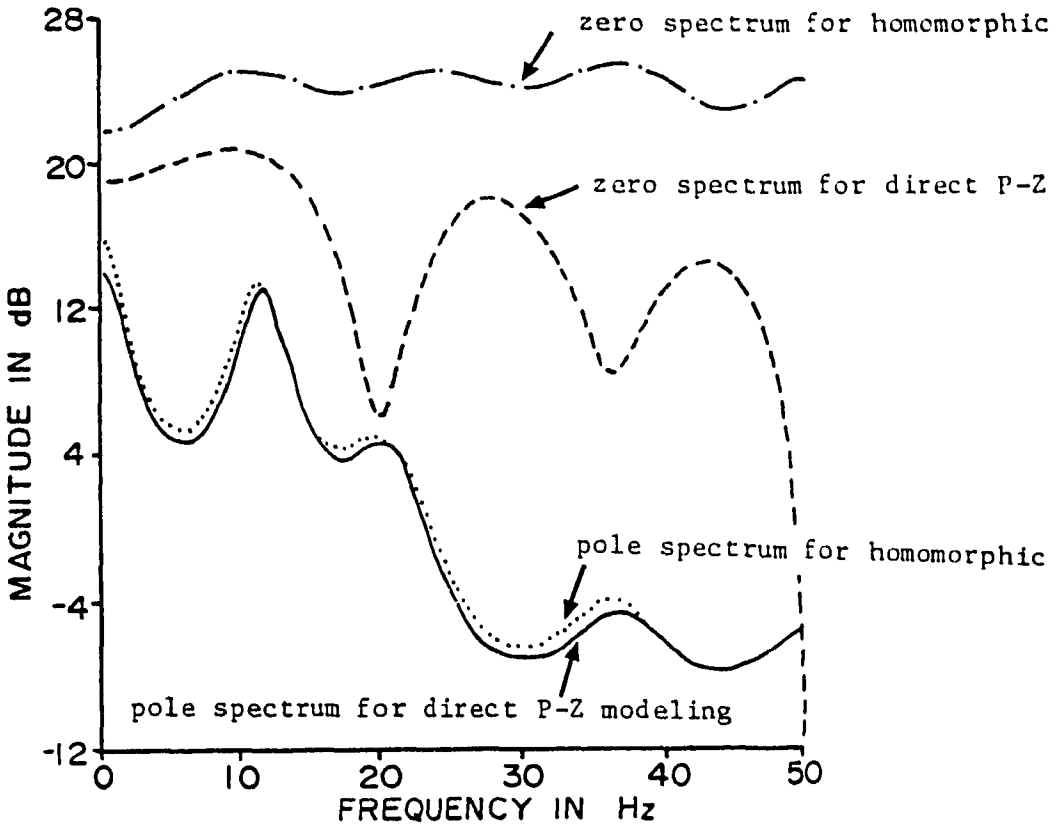

Fig.4.6 Component spectrum for real EEG by direct pole zero modeling and homomorphic prediction.

Table 4.1 Different model orders to fit simulated EEG signal spectrum by homomorphic prediction method.

Signal Spectrum	Activity	f_i (Hz.)	σ_i (Hz.)	G_i (%)
(8p, 8z)				
Spectrum 1	α	9.3	1.7	62.07
	β	17.9	2.2	3.94
	δ	0.5	1.2	32.51
(8p, 4z)				
Spectrum 2	α	9.3	1.6	62.18
	β	17.5	2.5	3.81
	δ	0.6	0.9	32.42
(8p, 2z)				
Spectrum 3	α	9.2	1.6	62.09
	β	17.4	2.3	3.89
	δ	0.6	0.9	32.48
(6p, 2z)				
Spectrum 4	α	13.6	2.3	62.14
	β	-	-	3.82
	δ	0.5	1.6	32.51

Table 4.2 Different number of parameters used to fit simulated EEG signal spectrum by pole-zero decomposition method.

Signal Spectrum	Activity	f_i (Hz.)	δ_i (Hz.)	G_i (%)
Original Spectrum				
		9.3	1.7	62.07
		17.9	2.2	3.94
		0.5	1.2	32.51
Spectrum 1 (M=16)				
	α	9.6	1.3	62.21
	β	19.1	2.7	3.72
	δ	0.7	1.4	32.48
Spectrum 2 (M=12)				
	α	9.8	1.6	62.13
	β	19.8	2.5	3.89
	δ	0.8	1.1	32.41
Spectrum 3 (M=8)				
	α	9.5	1.9	62.15
	β	21.1	2.9	3.92
	δ	0.6	1.9	32.39

Table 4.3 Estimated zeros by direct pole-zero modelling and by homomorphic prediction method for real EEG signal for subject-1, (8 poles, 4 zeros).

	By direct method		By homomorphic prediction	
No.	Zero location in z-plane	Distance of zero from the origin	Zero location in z-plane	Distance of zero from the origin
1	(0.9848, 0.0000)	0.9848	(1.3833, 0.0000)	1.3833
2	(-1.3249, 0.0000)	1.3249	(-1.2648, 0.0000)	1.2648
3	(0.5476, -1.2081)	1.2364	(0.5159, -1.4099)	1.5013
4	(0.5476, 1.2081)	1.2364	(0.5159, 1.4099)	1.5013

Table 4.3 Estimated zeros by direct pole-zero modelling and by homomorphic prediction method for real EEG signal for subject-1, (8 poles, 4 zeros).

	By direct method		By homomorphic prediction	
No.	Zero location in z-plane	Distance of zero from the origin	Zero location in z-plane	Distance of zero from the origin
1	(1.4947, 0.0000)	1.4947	(1.4102, 0.0000)	1.4102
2	(0.4930, 0.8554)	0.9872	(-1.1963, 0.0000)	1.1963
3	(0.4930, -0.8554)	0.9872	(0.3173, -1.2504)	1.2900
4	(-1.1104, 0.0000)	1.1104	(0.3173, 1.2504)	1.2900

Table 4.3 Estimated zeros by direct pole-zero modelling and by homomorphic prediction method for real EEG signal for subject-2, (8 poles, 4 zeros).

	By direct method		By homomorphic prediction	
No.	Zero location in z-plane	Distance of zero from the origin	Zero location in z-plane	Distance of zero from the origin
1	(0.8324, 0.0000)	0.8324	(1.3163, -0.9663)	1.6329
2	(1.0611, -1.1163)	1.5401	(1.3163, 0.9663)	1.6329
3	(1.0611, 1.1163)	1.5401	(-0.4709, -1.5942)	1.6623
4	(-5.0526, 0.0000)	5.0526	(-0.4709, 1.5912)	1.6623

Table 4.3 Estimated zeros by direct pole-zero modelling and by homomorphic prediction method for real EEG signal for subject-2, (8 poles, 4 zeros).

	By direct method		By homomorphic prediction	
No.	Zero location in z-plane	Distance of zero from the origin	Zero location in z-plane	Distance of zero from the origin
1	(0.8845, -0.5680)	1.0512	(-2.0962, 0.0000)	2.0962
2	(0.8845, 0.5680)	1.0512	(3.3601, 0.0000)	3.3601
3	(-59.8568, 0.0000)	59.857	(1.0044, 1.4379)	1.7540
4	(59.8568, 0.0000)	59.857	(1.0044, 1.4379)	1.7540

Table 4.3 Estimated poles and zeros by direct pole-zero modelling and homomorphic prediction method for simulated EEG signal. (8 poles, 8 zeros).

	By direct method		By homomorphic prediction	
	Location in z-plane	Distance from the origin	Location in z-plane	Distance from the origin
Poles	(1.0840, 0.0000)	1.0840	(1.0725, 0.0000)	1.0725
	(0.8321, -0.6977)	1.0858	(0.3477, -1.1179)	1.1707
	(0.8321, -0.6977)	1.0858	(0.3477, 1.1179)	1.1707
	(-1.2903, 0.0000)	1.2903	(-1.3143, 0.0000)	1.3143
	(-0.8077, -0.9567)	1.2521	(0.8425, -0.6930)	1.0909
	(-0.8077, 0.9567)	1.2521	(0.8425, 0.6930)	1.0909
	(0.3207, -1.1294)	1.1741	(-0.8495, -0.9540)	1.2774
	(0.3207, 1.1294)	1.1741	(-0.8495, 0.9540)	1.2774
zeros	(-0.1778, 0.0000)	0.1788	(0.7158, 1.2606)	1.4497
	(1.8242, 0.0000)	1.8242	(0.7158, -1.2606)	1.4497
	(0.9904, 0.0000)	0.9904	(2.3680, 0.0000)	2.3680
	(0.5511, 0.0000)	0.5511	(-1.2325, -0.5217)	1.4484
	(-0.5494, -0.6835)	0.8769	(-1.2325, 0.5217)	1.4484
	(-0.5494, 0.6835)	0.8769	(1.4214, 0.0000)	1.4214
	(0.3581, -1.0203)	1.0814	(-0.4178, -1.3577)	1.4205
	(0.3581, 1.0203)	1.0814	(-0.4178, 1.3577)	1.4205

Table 4.3 Estimated poles and zeros by direct pole-zero modelling and homomorphic prediction method for real EEG signal for subject-1 from 01-02 electrode pair. (8 poles, 8 zeros).

	By direct method		By homomorphic prediction	
	Location in z-plane	Distance from the origin	Location in z-plane	Distance from the origin
Poles	(1.2222, 0.0000)	1.2222	(1.1929, 0.0000)	1.1929
	(0.8022, -0.6507)	1.0329	(0.8053, -0.6646)	1.0441
	(0.8022, 0.6507)	1.0329	(0.8053, 0.6646)	1.0441
	(-1.1334, 0.0000)	1.1334	(-1.2352, 0.0000)	1.2352
	(-0.6423, -1.0689)	1.2470	(-0.6885, -0.9911)	1.2068
	(-0.6423, 1.0689)	1.2470	(-0.6885, 0.9911)	1.2068
	(0.2814, -1.1542)	1.1880	(0.2267, -1.1748)	1.1964
	(0.2814, 1.1542)	1.1880	(0.2267, 1.1748)	1.1964
zeros	(1.5359, 0.0000)	1.5359	(1.3110, 0.0000)	1.3110
	(0.8767, -0.5416)	1.0305	(-1.5606, 0.0000)	1.5606
	(0.8767, 0.5416)	1.0305	(1.1526, 1.2609)	1.7083
	(-1.0807, 0.0000)	1.0807	(1.1526, 1.2609)	1.7083
	(-0.6320, -1.0150)	1.1957	(-0.7205, -1.0916)	1.3079
	(-0.6320, 1.0150)	1.1957	(-0.7205, 1.0916)	1.3079
	(0.2540, -1.1443)	1.1722	(0.0317, -1.5662)	1.5665
	(0.2540, 1.1443)	1.1722	(0.0317, 1.5662)	1.5665

4.5 References

[4.1] Blinowska,K.J. and Drabik,W., 1981, EEG data reduction by autoregressive representation and discriminant analysis procedures, Electroencephalography and clinical neurophysiology, 51, pp. 650-658.

[4.2] Atal,B.S., and Schroder,M.R., 1978, Linear prediction analysis of speech based on pole zero representation, Journal of Acoustical Society of America, 64(5), pp. 1310-1318.

[4.3] Diekmann,V., 1975, EEG analysis by an autoregressive moving average model: Application to the study of EEG changes measured under various blood gas levels, In : Quantitative analysis of the EEG, Ed. Matejcek,M., and Schenk,G.K., pp. 369-378.

[4.4] Gersch,W., and Yonemoto,J., 1977, Automatic classification of multivariate EEGs using an amount of information measure and the eigenvalues of the parametric time series model features, Computers and Biomedical Research, 10, pp. 297-318.

[4.5] Smith,W.D., and Lager,D.L., 1986, Evaluation of simple algorithms for spectral parameter analysis of the electroencephalogram, IEEE Trans. on Biomedical Engineering, 33, pp. 352-358.

[4.6] Isaksson,A., Wennberg,A., and Zetterberg,L.H., 1981, Computer analysis of EEG signals with parametric models, Proceedings of the IEEE, 69, pp. 451-461.

[4.7] Oppenheim,A.V., Kopec,G., and Tribolet,J,M., 1976, Signal analysis by homomorphic prediction, IEEE Trans. on Acoustics, Speech and Signal Processing, 24, pp. 327-332.

[4.8] Kopec,G., Oppenheim,A,V., and Tribolet,J,M., 1977, Speech analysis by homomorphic prediction, IEEE Trans. on Acoustics, Speech and Signal Processing, 25. pp. 40-49.

[4.9] Rangaraj,M.R., 1979, Digital analysis of ECG, PCG and EMG signals, Ph.D Thesis, Deptt. of Electrical Engineering, Indian Institute of Science, Banglore, India.

[4.10]Yegnarayana,B., 1981, Speech analysis by pole zero decomposition of short time spectra, Signal Processing, 3, pp. 5-17.

[4.11]Schafer,R,W., 1968, Echo removal by discrete generalised linear filtering, Ph.D. Thesis, Deptt. of Electrical Engg., MIT.

[4.12]Shanks,J,L., 1967, Recursion filters for digital processing, Geophysics, 32, pp. 33-51.

[4.13]Steiglitz,K., 1977, On the simultaneous estimation of poles and zeros in speech analysis, IEEE Trans. on Acoustics, Speech and Signal Processing, 25, pp. 229-234.

[4.14]Zetterberg,L,H., 1973, Experience with analysis and simulation of EEG signals with parametric description of spectra, In : Automation of clinical electroencephalography, Ed. Kellaway,P., and Peterson,I., Raven Press, New York, pp. 161-201.

CHAPTER 5

MUSCLE ARTEFACT CANCELLATION FROM EEG SIGNALS

5.1 Introduction

Generally an EEG record is contaminated with extracerebral signals called artefacts and these may be due to muscle activity, ECG pickup, eye movement, improper electrode contact etc. These extracerebral signals play the role of noise for EEG background activity. Though in visual analysis, these artefacts are detected and EEG is interpreted with some difficulty, they pose a major problem for the automation of EEG, particularly at the EEG representation stage.

Of the many artefacts mentioned, the muscle artefact is very common and is many times larger in magnitude than the EEG signal. This artefact is due to the contraction of neck and scalp muscles. In a tense subject, the scalp activity is wide spread though it is maximal in the temporal regions. Artefacts in general and the muscle artefact in particular affect both the time domain analysis, such as correlation, slope descriptors, as they are very sensitive to noise [5.1], and the frequency domain analysis, i.e. spectral analysis, by changing the spectral parametrs like bandwidth, percentage of power distribution [5.2]. The muscle activity is found to affect considerably the EEG spectrum above 14 Hz. [5.3] i.e the beta activity. Even with visual analysis, the EEGers effort to reduce this artefact by decreasing the higher cut off frequency of the recording amplifier results in a distorted signal that can not be distinguished from the beta activity [5.4]. Hence in general and in particular for the automation of clinical EEG, removal of muscle artefact is mandatory. For this purpose, techniques such as analog filtering [5.5], nonlinear filtering [5.6] and Kalman filtering [5.7] have been reported. Also the most common least mean square gradient adaptive algorithm that has been extensively used for noise cancellation in the feild of speech and ECG has also been applied to muscle artefact cancellation from EEG and this forms the topic of study in this chapter.

This chapter deals with the simulation of muscle artefact and its filtering from EEG background activity by a hybrid method, which uses a least mean square gradient adaptive linear predictive filter

in combination with a lowpass filter. Also the effect of the muscle artefact on the parametric representation of the EEG and the performance of the filter to this end are considered.

5.2 Simulation of Muscle Artefact

The simulation of the muscle artefact is based on the model used by Johnson [5.6]. The muscle spike is assumed to be an impulse response of a second order linear system given by transfer function in the analog domain,

$$T_i(s) = \frac{1}{[(s + 2\pi\sigma_i)^2 + (2\pi f_i)^2]} \tag{5.1a}$$

where σ_i is the half bandwidth and f_i is the peak frequency and in the digital domain

$$H_i(z) = \frac{b_{1i}}{[1 - a_{1i}z^{-1} + a_{2i}z^{-2}]} \tag{5.1b}$$

where

$$b_{1i} = (\frac{1}{2\pi f_i}) \exp(-2\pi\sigma_i T) \sin(2\pi f_i T)$$

$$a_{1i} = 2\exp(-2\pi\sigma_i T) \cos(2\pi f_i T)$$

$$a_{2i} = \exp(-4\pi\sigma_i T)$$

where, $(\frac{1}{T})$ is the sampling frequency.

In the muscle artefact, the amplitude and the duration of the spike vary much more than the shape of the spike. The impluse response of a second order system with a peak frequency of 70 Hz. and a bandwidth of 70 Hz. represents a typical muscle spike. Muscle spikes of different durations can be achieved by having similar spikes but whose duarations are one and a half times and twice that of the one considered. The different type of spikes occur with equal probability. The linear system corresponding to each spike is driven by an independent Poisson noise process.

Simulation of the muscle artefact is carried out by filtering the Poisson random numbers by transfer functions corresponding to differet types of spikes and adding the filter outputs with appropriate gain factors to get the required amplitude variability of the spikes.

In the simulation here, three types of spikes, each characterized by a transfer function of the type given by Eqn.(5.1) and having bandwidths of 70 Hz., 46.67 Hz. and 35 Hz. and centre frequency of 70 Hz. are considered. Their corresponding frequency responses are shown in Fig.5.1. The sampling rate used is 1 KHz.

To generate each spike train, independent Poisson random number sequences are generated by changing the seed value in the random number generator. To get an inter-spike interval of 20 msec., the spike rate for each random number sequence chosen is 15 spikes per second. For each type of spike train, the filtering of the Poisson random number sequence by corresponding filter transfer function is done by time domain infinite impulse response filtering.

If $x_i(n)$ is the poisson random number sequence, then the output $y_i(n)$ is given by

$$y_i(n) = b_{1i}\, x_i(n-1) + a_{1i}\, y_i(n-1) - a_{2i}\, y_i(n-2) \tag{5.2}$$

Each filtered sequence corresponding to different types of spikes thus produced are multiplied by proper gain factors to get required amplitude variation and then summed point to point to get the desired muscle artefact data. In estimating the spectral density function, the length of the data chosen is 0.1 seconds in order to get a resolution of 10 Hz. Further, the data is Hamming windowed, padded with zeros to a length of 1024 points, and the number of spectra averaged is 25.

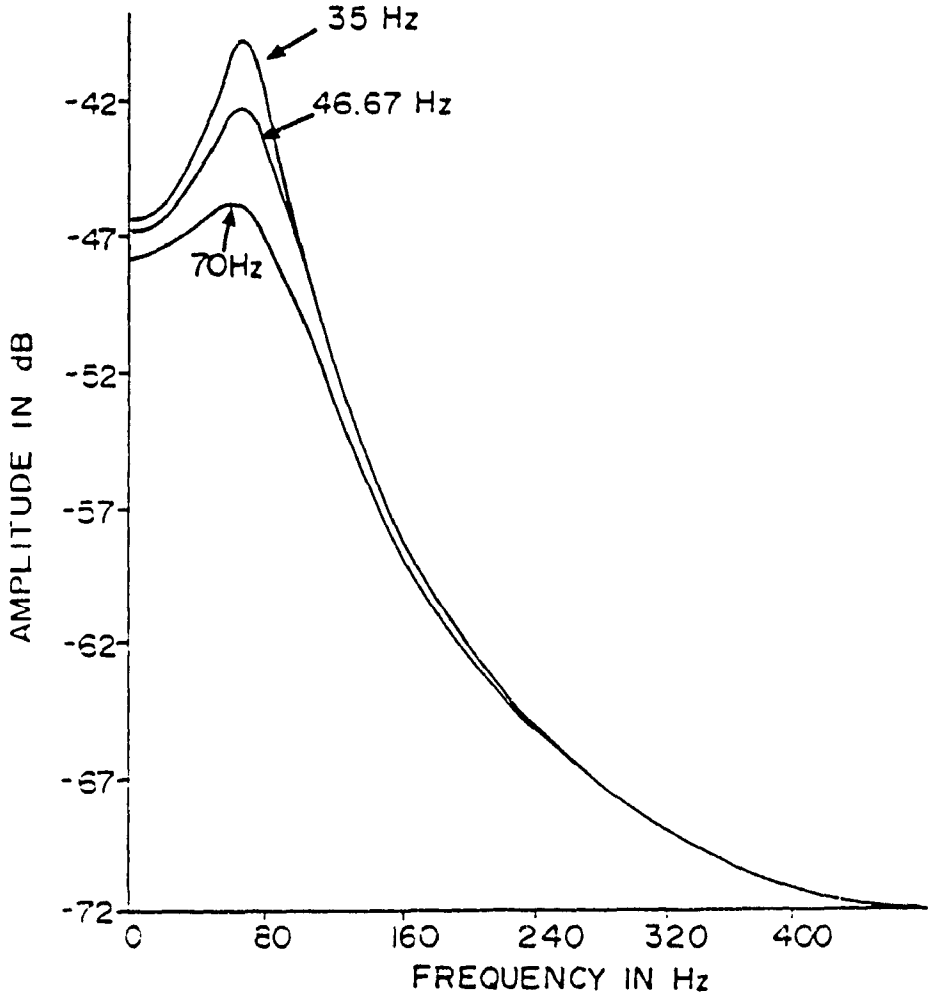

Fig.5.1 Logmagnitude spectrum of the impulse response of filters generating muscle spikes with required bandwidths.

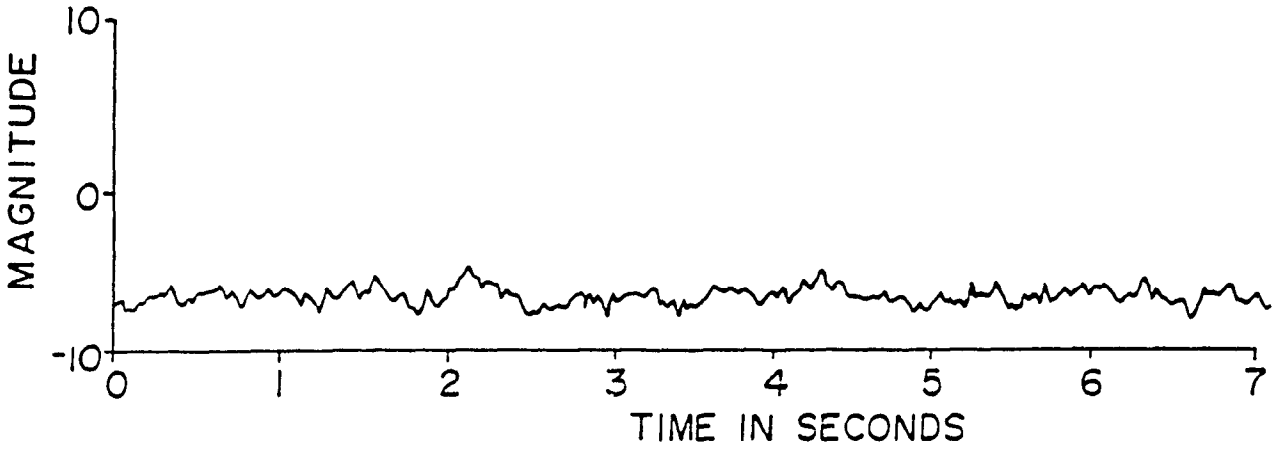

Fig.5.2 Simulated muscle noise sampled at 200 Hz.

5.3 Filtering of Muscle Artefact from EEG

The muscle artefact and the EEG spectra are overlaping and the range of the overlap is about 30 Hz. Hence the muscle artefact can be considered to be made up of two components :

1) the out of band component (outside the EEG frequency band)

2) the inband component (within the EEG frequency band)

In the present method of filtering of the muscle artefact, the out of band component is removed by a lowpass filter and subsequently the inband component is supressed by an adaptive filter.

The out of band component is removed by a fourth order Butterworth lowpass filter having a cutoff frequency of 35 Hz. This is based on the fact that the EEG spectrum is confined to 30 Hz. This lowpass filter is having a fairly linear phase characterstic atleast within the EEG band of interest. In this simulation study, an equivalent digital infinite impulse response filter [5.8] is considered. In practice, a fourth order Butterworth active lowpass filter can be used as an antialiazing filter. Further, any phase distortion introduced by it due to small amount of nonlinearity in its phase characterstic can be compensated by an equaliser [5.9].

After lowpass filtering, the inband component is removed by an adaptive noise cancellation technique based on least mean square filtering. This type of cancellation is effective when an external reference of noise (interference) which is uncorrelated with the signal and highly correlated with the noise is avaliable. In the absence of such a reference, it is still possible to cancel the noise using predictive filtering approach, provided the signal bandwidth is significantly less than the bandwidth of the additive noise [5.10]. The inband component of the muscle artefact plays the role of a wide band noise and the EEG plays the role of a narrow band signal. The muscle noise contaminated EEG signal is shown in Fig.5.2. The linear prediction filter coefficients are chosen such that the power of the error signal $\varepsilon(n)$ between the predictor output (estimate) $\hat{x}(n)$ and the actual signal $x(n)$ is minimised. The delay D represents the prediction distance of the filter. The noise suppresion is due to the fact that the decorrelation time for broad band noise is much smaller than that of a narrow band signal. This enables us to choose the value of D which will effectively decorrelate the broad band noise and also prevents the noise appearing in the predictor output. An adaptive version of the linear prediction

filter has been succesfully used for processing noisy speech [5.10]. In the present study, a LMS-TDL adaptive predictor is applied for muscle artefact removal. A brief description of the predictor from the point of view of noise cancellation is given below.

The Fig.5.3 itself forms the schematic of an LMS-TDL predictor. The estimate $\hat{x}(n)$ of the present input sample $x(n)$ is based on the M previous input samples which are D samples away from the present instant [5.11 - 5.12]. That is

$$\hat{x}(n) = \sum_{k=1}^{M} a_k \, x(n-k-D+1) \tag{5.3}$$

By the LMS gradient adaptation rule,

$$a_k(n) = a_k(n-1) + 2\,\mu\,\varepsilon(n-1)\,x(n-k-D)\ , \quad k = 1, 2, 3, \ldots\ldots\ldots\ldots M \tag{5.4}$$

where,

$$\varepsilon(n) = x(n) - \hat{x}(n)$$

and

$$\mu = \frac{\nu}{M\ E_x(n)}\ , \quad 0 < \nu < 1\ ,$$

and

$$E_x(n) = \upsilon\, E_x(n-1) + x^2(n)\ , \quad 0 < \upsilon < 1\ ,$$

where υ is the forgetting factor.

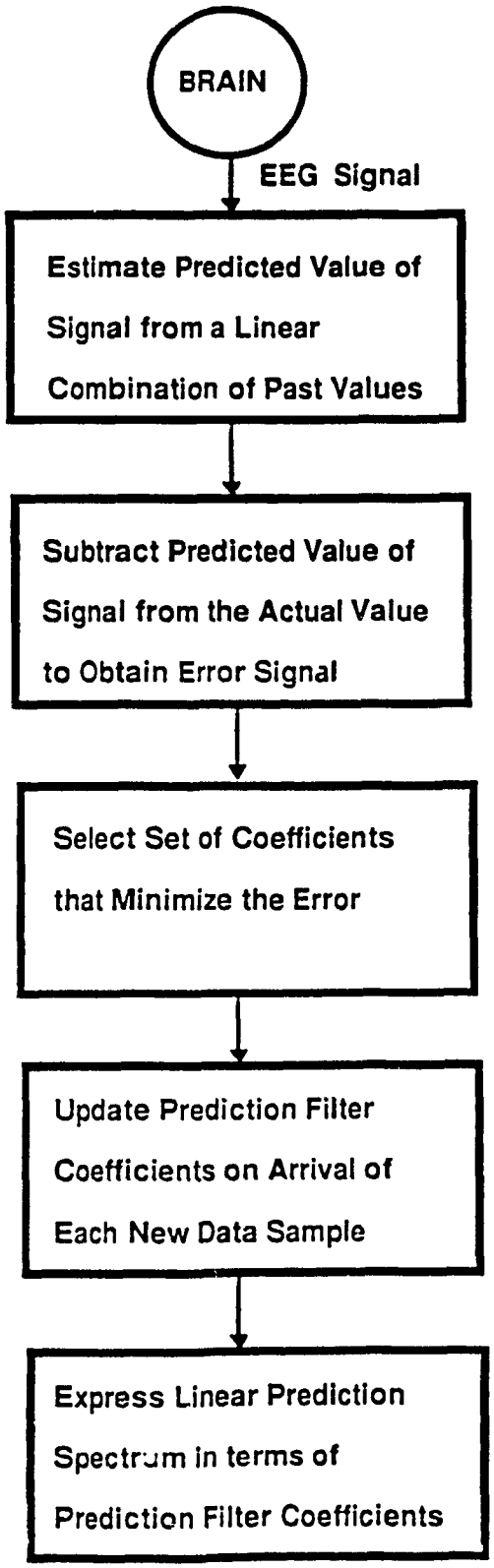

Fig.5.3 The LMS-TDL predictor with decorrelation delay.

5.4 Studies with Simulated Data

For the purpose of illustrating the removal of muscle noise, the EEG signal having specifications given in Table 5.1 sampled at 200 Hz. is considered. Also, the muscle noise is sampled at 200 Hz. and added to the EEG data. The choice of the sampling frequency is based on the studies carried out by Bartoli and Cerutti [5.7]. The EEG to muscle artefact power ratio is -1.78 dB. The original EEG signal itself is filtered by the Butterworth lowpass filter in order to asses its effect on the signal. The muscle artefact contaminated EEG is filtered by the lowpass filter. The lowpass filtered signal is only free from the out of band EEG muscle noise component but not completely free from the muscle artefact, and the remaining noise is due to inband component. By subjecting the lowpass filtered output to adaptive filtering, the remaining noise is removed. The order of the adapative filter M used is 10 and the decorrelation delay D is 20. The values of ν and υ used are 0.2 and 0.92 respectively.

In order to find the effect of the muscle artefact on the parametric representation of the EEG and the improvement achieved by the predictive filtering, the original EEG , the muscle artefact contaminated EEG, the lowpass filtered signal and the adaptive filtered outputs are subjected to Burg's spectral estimation method. For this purpose a 15th order prediction filter has been used.

Fig.5.4 shows the respective Burg's spectra. It is seen that for the muscle artefact contaminated EEG signal, the Burg's spectrum does not indicate the peak corresponding to the beta activity at all. For the lowpass filtered signal, though there is a peak in the spectrum corresponding to the beta activity, the peak is alomost at the same level as the noise peak. But after subsequent adaptive filtering, all the peaks are clearly brought out by Burg's method and the beta activity is much above the noise level. This indicates that Burg's parametric representation gets severely affected by the muscle noise and the predictive filtering method alleviates this problem.

Table 5.1 Parameters of EEG registration.

Activity	σ_i (Hz.)	f_i (Hz.)	G_i (Hz.)
α	0.58 + 0.03	10.25 + 0.03	63 + 11
β	1.36 + 0.10	18.90 + 0.10	4 + 0.9
δ	1.27 + 0.07	0.0	33 + 6.0

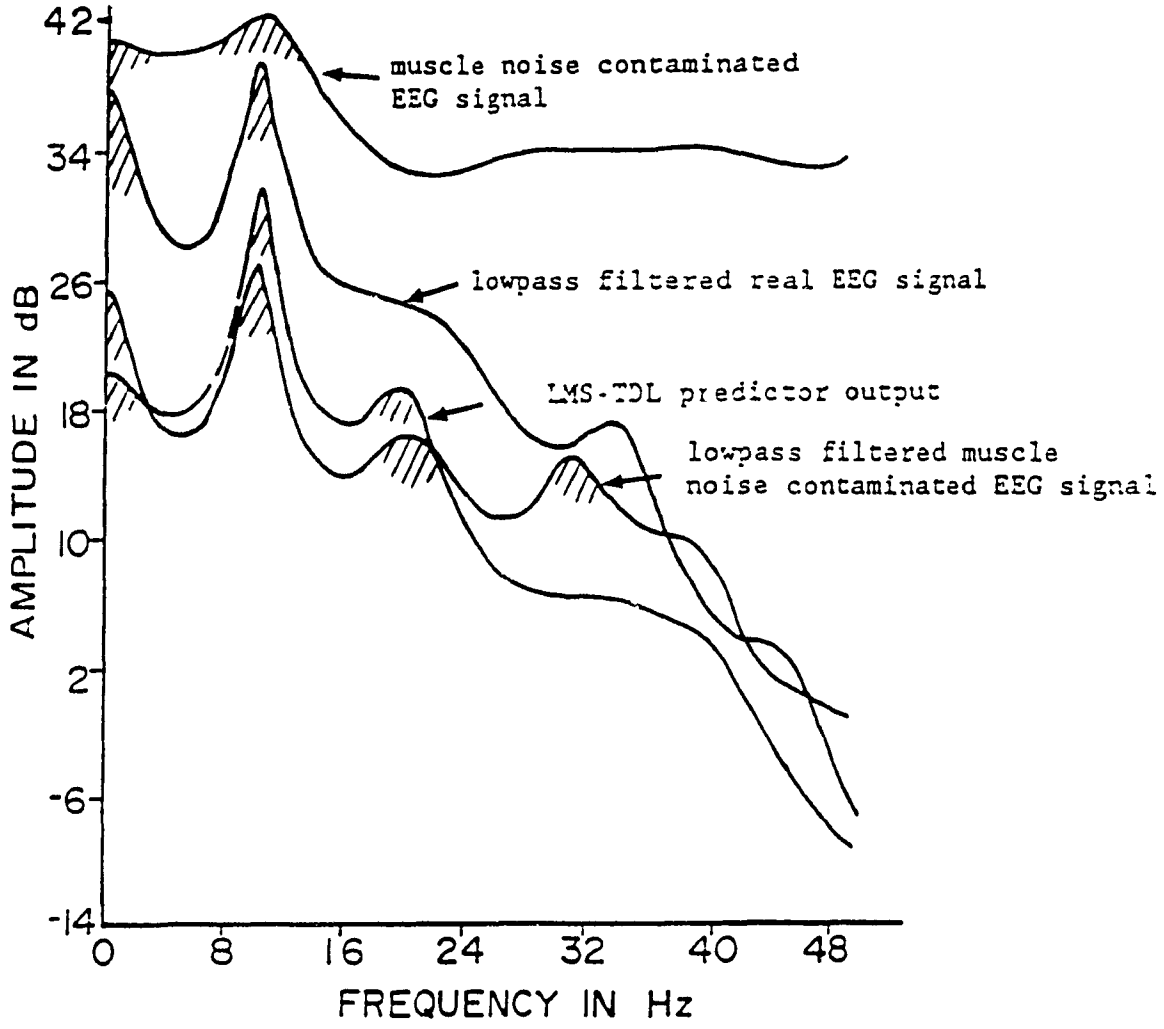

Fig.5.4 Burg spectrum for different stages of filtering of the muscle noise contaminated EEG signal

The frequencies estimated by Burg's method at different stages of filtering are listed in Table 5.2. The accuracy of peak frequency estimation of alpha and beta activity peaks is approximately the same for low pass filtered output and for both the predictor outputs. However prior to any filtering, Burg's spectral estimation does not indicate the beta activity peak and so neither its frequency.

In the above illustration, Burg's spectrum of the lowpass filtered EEG signal is taken as reference instead of the Burg's spectrum of the original EEG. This is due to the fact that the Burg spectrum for filtered EEG signal and for the original EEG signal will be different as the method is very sensitive to noise. The original EEG signal which is simulated by filtering the noise by filters occupying different frequency bands of the EEG spectrum will have some noise upto the folding frequency. But in the lowpass filtered signal this noise is removed. This reference for comparison is valid as the lowpass filtered EEG and the original EEG are identical within the EEG band.

The effect of higher decorrelation delay D on the performance of the adaptive predictor has also been assessed. A higher delay will result in a decrease in the magnitude of the beta activity peak in the spectrum of the adaptive filtered signal. This has been verified for a delay of 30 sample points with a 15th order prediction filter. The adaptive predictors though bring out the β activity peak well above the noise level, they seem to slightly decrease the δ activity peak magnitude (Fig.5.5).

Table 5.2 Frequencies estimated by Burg's method at various stages of filtering for simulated EEG signal.

	Signals	α - Activity peak frequency (Hz.)
1) EEG (original)	10.742	20.122
2) EEG + Muscle noise	10.552	-
3) Lowpass filtered signal (EEG + Muscle noise)	10.172	20.419
4) LMS - TDL predictor output	10.359	19.817
5) LMS - lattice predictor output	10.769	19.982

5.5 Studies with Real Data

The real EEG data is recorded for three subjects. The recording and digitization details are the same as mentioned in Chapter 3 except for the sampling rate which is 200 Hz. in the present case.

For the purpose of illustration, the data segment of an alcoholic patient of fifty-three years recorded from Fp1-Fp2 electrode pair with a high frequency cutoff at 120 Hz on the EEG machine is considered. This case is particularly chosen with an intention that the EEG activity will contain predominantly the beta activity and it is this activity that gets affected by the muscle noise to a greater extent than the alpha and delta activities.

Fig.5.6 shows the real EEG signal for which the mean is removed. This is filtered by a 4th order Butterworth lowpass filter and the filtered signal is shown in Fig.5.6b. The outputs of the adaptive filters are shown in Figs.5.6c and 5.6d, when the lowpass filter output is fed as input to them. The adaptive filters have the same parameters as in the simulation study.

It is seen that the adaptive filters are very effective in removing the muscle noise and the lowpass filter alone is not sufficient. Also for the muscle artefact contaminated EEG, in the Burg spectrum, the beta activity peak is not brought out clearly and it is almost at the noise level and the peak occurs at 22.65 Hz. With lowpass filtering, though the beta activity is brought out, it is associated with additional peaks of approxiametely the same magnitude and are due to inband muscle noise. These peaks occur at 19.53 Hz, 26.76 Hz. and 36.32 Hz. But for the adaptive filtered signals, the beta activity is brought out clearly and the additional peaks due to inband muscle noise are reduced significantly and only one peak is detected by the peak picking algorithm. The peak occurs at 20.31 and 19.14 Hz. for the LMS-TDL and LMS-lattice respectively.

The general applicability of the method is ascertained by considering other EEG data segments of different subjects and the results obtained are shown in Table 5.3. These results are in agreement with the above illustration of real EEG data and there is noticeable noise reduction after adaptive filtering in each case.

It is important to note that with real EEG signals, there is no appreciable decrease in delta activity due to adaptive filtering unlike with simulated EEG.

This study clearly indicates that even in the case of real data, the parametric estimation gets affected by the muscle noise (by both EEG out of band and EEG inband) and the proposed method minimises the muscle noise significantly and enables Burg's parametric estimation to provide valid results. Generally, the results obtained with real data are consistent with those of simulated data at different stages of filtering.

The present study has only aimed at exploring the possibility of applying the LMS predictive filtering for muscle noise cancellation. However, no efforts have been made to evaluate the comparitive performance of this method in removing the muscle noise with the existing ones such as Kalman filtering and non-linear filtering. The study indicates that the proposed filtering provides satisfactory results from the point of view of parametric spectral estimation and is computationally efficient compared to other methods mentioned. In particular, it is quite satisfactory in bringing out the beta activity spectral peak above the noise level in the Burg's spectrum. This is of significance, since it is the beta activity that gets affected by the muscle noise to the maximum extent. The LMS-TDL and LMS-lattice provide almost same performance. Of the two, LMS-TDL is computationally simpler and hence can be preffered to lattice.

The performance of the existing methods of muscle noise cancellation from EEG have not been assessed from the point of view of parametric spectral modeling. The present study establishes that the proposed filtering provides valid results even from the point of view of parametric representation of EEG and this provides additional information about the utility of sequential adaptive algorithms for muscle noise cancellation. Further the study emphasises that mere lowpass filtering is not sufficient and some type of adaptive filtering is essential to remove the muscle noise component within the EEG frequency band.

Barlow has used lowpass filters alone for muscle noise cancellation and the lowpass filter has a cutoff frequency at 12.5 Hz. This cutoff frequency is too low, since the EEG frequency band is upto 30 Hz. and infact, the frequency band of alpha activity is from 8 to 14 Hz. However, the simulation results in the present study indicate that the muscle noise can be minimised and even the beta activity can be recovered by a combination of a 4th order Butterworth lowpass filter with a cutoff frequency of

35 Hz and an adaptive predictive filter. This method of removing the noise component whose frequency band overlaps the signal frequency band is not a new one in the field of communication engineering.

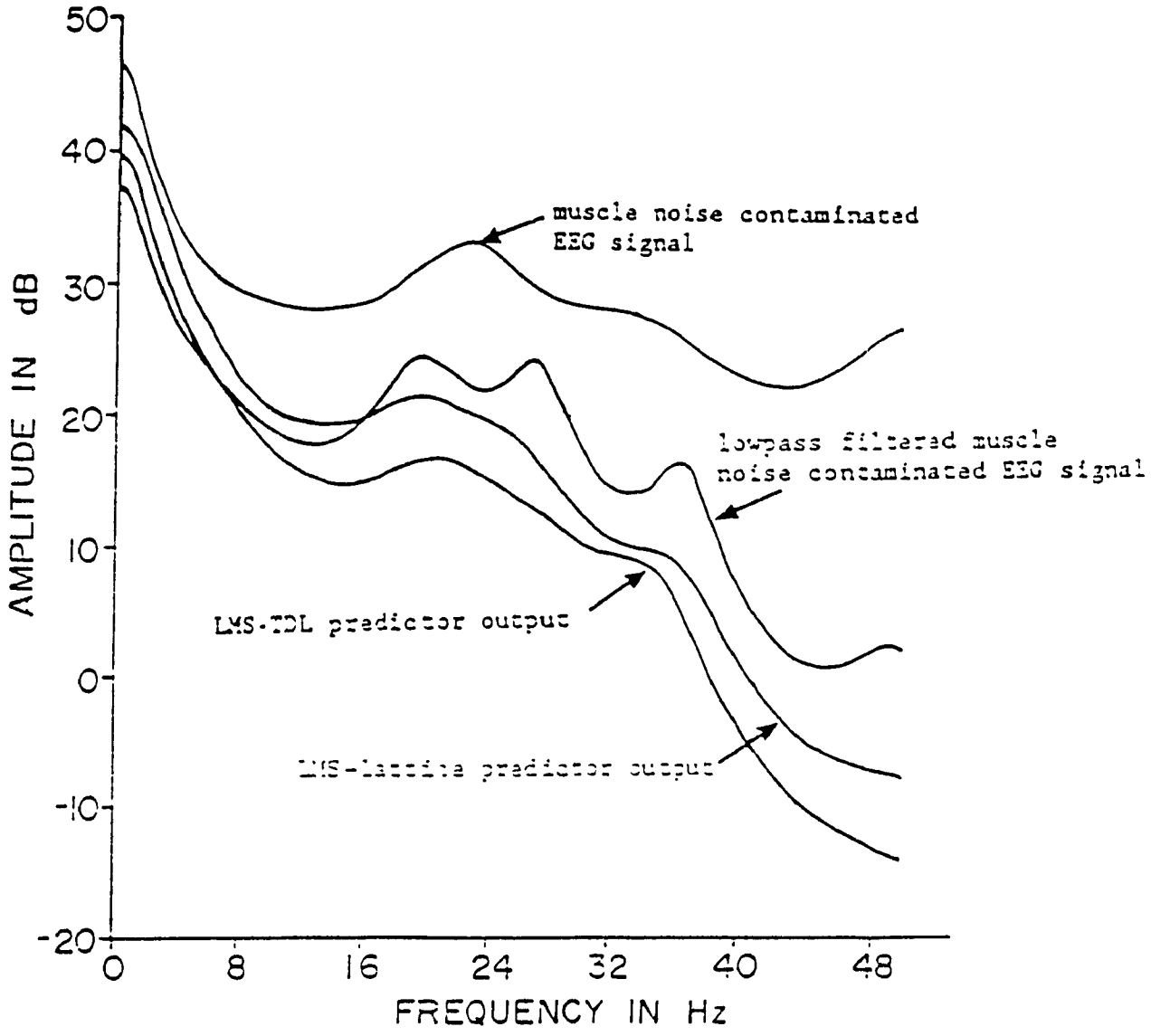

Fig.5.5 Burg spectrum for different stages of filtering of the muscle noise contaminated real EEG

Table 5.3 Frequencies estimated by Burg's method at various stages of filtering for real EEG signals.

	Signals	α - Activity peak frequency (Hz.)
Signal 1		
1) EEG + Muscle noise	9.87	-
2) Lowpass filtered signal (EEG + Muscle noise)	9.32	19.37
3) LMS - TDL predictor output	9.61	19.83
4) LMS - lattice predictor output	9.73	19.87
Signal 2		
1) EEG + Muscle noise	11.25	-
2) Lowpass filtered signal (EEG + Muscle noise)	10.98	21.62
3) LMS - TDL predictor output	11.14	20.39
4) LMS - lattice predictor output	11.18	20.47

5.6 References

[5.1] Isaksson,A., Wennberg,A. and Zetterberg,L.H., 1981, Computer analysis of EEG signals with parametric models, Proceedings of the IEEE, 69, pp. 451-461.

[5.2] Isaksson,A., and Wennberg,A., 1975, Visual evaluation and computer analysis of the EEG - a comparison, Electroencephalography and clinical neurophysiology, 38, pp. 79-86.

[5.3] O'Donnell,R,D., Berkhout,J., and Adey,W,R., 1974, Contamination of scalp EEG spectrum during contraction of carnio-facial muscles, Electroencephalography and Clinical Neurophysiology, 37, pp. 145-151.

[5.4] Kiloh,L.G., McComas,A,J., and Osselton,J,W., 1979, Clinical Electroencephalography, Chapter-3, pp. 46-49, Butterworth Publications.

[5.5] Barlow,J.S., 1984, EMG artefact minimisation during clinical recordings by special analog filters, Electroencephalography and Clinical Neurophysiology, 58, pp. 161-174.

[5.6] Johnson,T,L., Wright,S,C., and Segall,A., 1979, Filtering of the muscle artefact from the electroencephalogram, IEEE Trans. on Biomedical Engineering, 26, pp. 556-563.

[5.7] Bartoli,F., and Cerutti,S., 1983, An optimal linear filter for the reduction of muscle noise superimposed on the EEG signal, Journal of Biomedical Engineering, 5, pp. 274-280.

[5.8] Oppenheim,A.V., and Schafer,R.W., 1975, Digital signal processing, Prentice Hall.

[5.9] Budak,A., 1974, Passive and active network analysis and synthesis, Houghton Mifflin Company, Boston, Chapter-22, pp. 647-651.

[5.10]Satorius,E.H., and Alexender,S.T., 1979, Noise cancellation via linear prediction filtering, International Conference on Acoustics Speech and Signal Processing, pp. 937-940.

[5.11]Sambur,M.R., Adaptive noise cancelling for speech signals, IEEE Trans. on Acoustics, Speech and Signal Processing, 26, pp. 419-423.

[5.12]Griffiths,L.J., 1977, A continuosly adaptive lattice filter implemented as a lattice structure, IEEE Conference on Acoustics Speech and Signal Processing, pp. 683-686.

CHAPTER 6

ADAPTIVE SPECTRAL ESTIMATION OF EEG SIGNALS

6.1 Introduction

The estimation of the prarameters of the EEG signal by block data methods yield satisfactory results when the signal is stationary. However, they require complete data block to be processed in advance and the parameters are valid only for the block of the EEG data considered. That is, the parameters of the filter are fixed for a particular block of data. In another type of estimation, the Sequential Adaptive Eetimation (SA) , the coefficients of the filter are adjusted automatically by built-in parameter adjustment algorithm which optimises the filter in some sense. The main advantage of this type of filtering is that it does not require entire block of data in advance, since the adaptation is done on a sample to sample basis, and improved parameter estimation is often achieved when the signal is nonstationary [6.1].

The SA approach is appealing due to its ability to process unbroken flow of data. Unlike in the sequential adaptive approach, the block data approach involves repetition of the whole method for each block of data and further, some of the methods involve computation of correlation coefficients and solution of a system of equations. Hence from the point of view of implementation, sequential adaptive algorithms have an edge over block data methods and have gained importance because of microprocessors and VLSI circuitry. For EEG signal analysis, sequential adaptive algorithms form yet another approach of processing. In this direction, Kalman filtering and its variations have been used for EEG analysis [6.2 - 6.3].

Among the sequential adaptive algorithms [6.4 - 6.5], the most simple and common one is the Least Mean Square gradient (LMS) adaptive algorithm, implemented as a Transversal or Tapped Delay Line (TDL) filter of Widrow [6.6]. This algorithm has found many applications like Antenna Array Processing [6.7], Channel Equalization [6.8], Adaptive Noise Cancelling [6.9], and Time Delay Estimation [6.10]. The major problems with the LMS-TDL filter are slow convergence rate and high

convergence error. The rate of convergence depends on the spread in eigenvalues of the autocorrelation matrix of the input signal [6.6]. The slow convergence problem has been solved to some extent by resorting to a lattice structure (LMS-lattice). The interstage decoupling nature of the lattice structure results in a rate of convergence that is less sensitive to spread in eigenvalues of the autocorrelation matrix [6.9]. The lattice structure in addition to having superior rate of convergence, is known for its advantages like stability [6.11], lower sensitivity to finite word length effects [6.12] and design flexibilty compared to the TDL structure.

Recently, an attempt has been made by Walach and Widrow [6.13] to reduce the convergence error by proposing a generalised version of the LMS algorithm called the least mean 2Kth power algorithm. In particular the algorithm with $K=2$, called the Least Mean Fourth (LMF) power gradient algorithm, has been considered in detail.

The study here deals with the application of various kinds of adaptive algorithms as spectral estimators in the quantification of both the simulated and real EEG signals.

In the following sections, a brief description of the LMS, LMF and LMS-lattice algorithms is presented. In further sections, the derivation of the LMF-lattice algorithm and the application of LMF adaptive algorithm to EEG signals is presented.

6.2 LMS Gradient Adaptive Algorithm

The basic form of the transversal (TDL) linear prediction filter is shown in Fig.6.1a. Let $s\,(n)$ be the signal and $N\,(n)$ be the associated zero mean noise; $x\,(n)$ represents the sum of the signal and the noise. It is assumed that the signal $s(n)$ and noise $N(n)$ are independent of each other. The prediction of $s(n)$ at time n, represented by $\hat{x}\,(n)$ is formed by the linear combination of the M previous values of $x(n)$ i.e. $x(n-1)\,, x(n-2)\,, \ldots\ldots\ x(n-M)$. Thus

$$\hat{x}\,(n) = \sum_{k=1}^{M} a_k(n)\, x(n-k) \qquad (6.1)$$

where a_k is the kth prediction filter coefficient at the nth instant of time. The predicted value $\hat{x}(n)$ is subtracted from the actual input $x(n)$ to obtain the error $\varepsilon(n)$. That is, the error at the nth instant is

given by

$$\varepsilon(n) = x(n) - \hat{x}(n)$$

In the linear prediction approach [6.11], the set of coefficients $a_1(n)$, $a_2(n)$, ... $a_M(n)$, are chosen which produce a minimum mean square error $E[\varepsilon^2(n)]$ and is expressed in the matrix form as

$$A^* = R^{-1} P \tag{6.2}$$

where

$$A^{*T} = [a^*_1(n) \, . \, a^*_2(n) \, . \quad \ldots\ldots\ldots\ldots \, a^*_M(n)]$$
$$P^T = [r(1)\, r(2) \quad \ldots\ldots\ldots\ldots \quad r(M)]$$

$$R = \begin{bmatrix} R(0,0) & R(1,1) & \ldots & R(p,p) \\ R(-1,-1) & R(0,0) & \ldots & R(p-1,p-1) \\ . & . & \ldots & . \\ . & . & \ldots & . \\ R(-p,-p) & R(-p+1,-p+1) & \ldots & R(0,0) \end{bmatrix}$$

R is the correlation matrix and T denotes the transpose operation.

The linear prediction spectrum $S(\omega)$ is expressed in terms of the optimum filter coefficients and is given by

$$S(\omega) = \frac{r(0) - \sum_{k=1}^{M} a_k^* \, r(k)}{[1 - \sum_{k=1}^{M} a_k^* \, e^{(-j\omega k)^2}} \tag{6.3}$$

The numerator is the mean square value of the output signal $\varepsilon(n)$ in Fig.6.1a. When the filter coefficients are found by using Eqn.(6.2), the optimal solution using minimum mean square error criterion, the numerator is the mean square value of the output.

The direct solution of Eqn.(6.2) requires the knowledge of autocorrelation values $r(0)$, $r(1)$, $r(2)$, ... $r(M)$. Usually, the autocorrelation coefficients have to be updated over a certain interval of time and the computation of these autocorrelation coefficients involves a major por-

Table 6.1 Frequency estimated by Burg's method and different adaptive algorithms for real EEG signals.

Signal No.	SNR (dB)	Freq. (Hz.) (Burg's method)	Freq. (Hz.) (LMS-TDL method)
		9.67	11.03
1	31.20		
		19.34	21.31
		10.64	10.49
2	30.95		
		19.92	21.38
		10.35	10.55
3	30.98		
		21.09	21.48
		32.36	20.21
4	31.30		
		43.12	31.45
		3.81	3.61
5	31.14		
		-	16.31
		11.47	10.93
6	32.06		
		21.19	22.07
		10.93	10.74
7	30.77		
		20.81	21.68

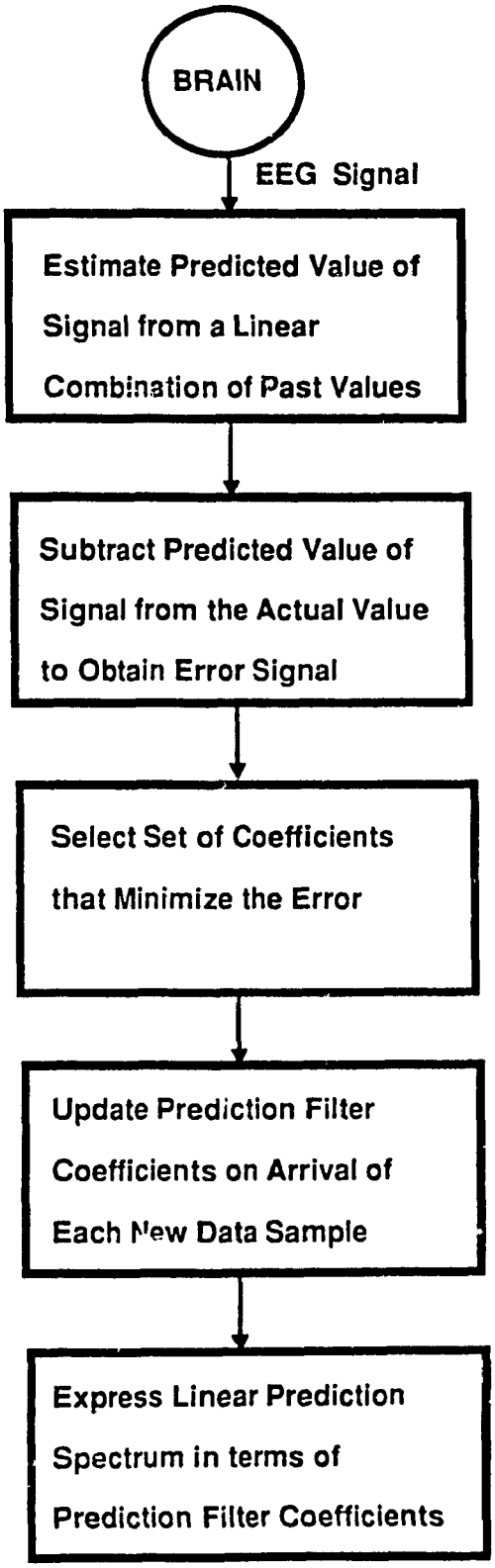

Fig.6.1a The LMS - TDL prediction filter.

In the LMS algorithm, the prediction filter coefficients are updated on the arrival of each new data sample. This is a single step procedure and does not involve computation of autocorrelation coefficients and solution of normal equations.

The solution of normal Eqns.(6.2) results in a set of filter coefficients which minimizes the mean square error $E[\varepsilon^2(n)]$. For stationary input statistics, the expected value of the error is given by

$$\begin{aligned} E[\varepsilon^2(n)] &= E[(x(n)-\hat{x}(n))^2] \\ E[\varepsilon^2(n)] &= E[(x(n)-x^T(n)A)^2] \\ E[\varepsilon^2(n)] &= r(0)-2P^T A + A^T R A \end{aligned} \tag{6.4}$$

where

$$X^T(n) = [x(n-1)\,x(n-2)\,.....x(n-M)]$$

and

$$\hat{x}(n) = X^T(n)\,A(n)$$

Since this equation is a quadratic function of the filter coefficients A and has a unique minimum value achieved by A^* (by virtue of solution of Eqn.(6.2)), gradient methods are used to obtain an iterative algorithm which converges to A^*. In the steepest descent method, the coeffiecients are iterated in the negative direction of the gradient of ther error surface [6.6], [6.9]. The gradient is given by

$$\nabla E[\varepsilon^2(n)] = -2\,[P - R\,A]$$

And the adaptation rule for coefficient vector $A(n)$ is given by

$$A(n+1) = A(n) + 2\,\mu\,[P - R\,A(n)] \tag{6.5}$$

where μ is the scalar proportionality constant that regulates the iteration step size. Repetitive application of Eqn.(6.5) using an initial value $A(0)$ results in a coefficient error vector $V(n)$ given by

$$\begin{aligned} V(n) &= A(n) - A^* \\ V(n) &= [1 - 2\,\mu\,R]^n\,V(0) \end{aligned} \tag{6.6}$$

The coefficient vector $A(n)$ obtained by succesive iterations converges to optimum value A^* provided the term in the square bracket converges to zero, and for a positive definite R, the convergence is guaranteed if,

$$0 < \mu < \frac{1}{\lambda_{max}} \tag{6.7}$$

where, λ_{max} is the maximum eigenvalue of R .

The gradient algorithm of Widrow [6.6] is obtained by replacing the average values by their corresponding instantaneous values in Eqn.(6.5) and the LMS adaptive algorithm is given by

$$\begin{aligned} A(n+1) &= A(n) + 2\mu\,[x(n) - \hat{x}(n)]\,X(n) \\ A(n+1) &= A(n) + 2\mu\,\varepsilon(n)\,X(n) \end{aligned} \tag{6.8}$$

6.3 The LMS-Lattice Adaptive Algorithm

The basic lattice structure is shown in Fig.6.1(b). Here also, $x(n)$ stands for the sum of the signals $s(n)$ and noise $N(n)$. $f(n)$ and $b(n)$ are the forward and backward errors at stage m . The lattice relations are

$$\begin{aligned} f_0(n) &= b_0(n) = x(n) \\ f_m(n) &= f_{m-1}(n) + K_m(n)\, b_{m-1}(n-1) \\ b_m(n) &= b_{m-1}(n) + K_m(n) f_{m-1}(n) \\ |K_m(n)| &< 1, \quad 1 < m < M \end{aligned} \tag{6.9}$$

where M is the order of the filter and $K_m(n)$ is the reflection coefficient.

For the lattice algorithm, the gradient is evaluated by differentiating the average of the forward and backward square errors with respect to the reflection coefficient $K_m(n)$ [6.14 - 6.15].

If

$$E^{LMS} = \frac{[f^2{}_m(n) + b^2{}_m(n)]}{2}$$

then

$$\frac{\partial E^{LMS}}{\partial K_m(n)} = f_{m-1}(n)\, b_m(n) + b_{m-1}(n-1) f_m(n)$$

Hence the rule for adpating the reflection coefficients $K_m(n)$ is

$$K_m(n+1) = K_m(n) - \mu_m\,(n+1)\,\frac{\partial E^{LMS}}{\partial K_m(n)} \tag{6.10a}$$

$$\mu_m(n+1) = \frac{\beta}{M\, E_{m-1}(n)}, \quad 0 < \beta < 1 \tag{6.10b}$$

$$E_m(n) = \gamma E_m(n-1) + [f^2{}_m(n) + b^2{}_m(n-1)], \quad 0 < \gamma < 1 \tag{6.10c}$$

where γ is called the forgetting factor. The smaller the value of γ, faster will be the adaptation. In Eqn.(6.10b), $\mu_m(n)$ is the step size adaptation $E_m(n)$ is the power of the signal plus noise at stage m and at time n.

6.4 The LMF-Lattice Adaptive Algorithm

For the LMF-lattice algorithm, the gradient is derived by LMF algorithm. That is the gradient is obtained by differentiating the average of the forward and backward fourth power errors with respect to the reflection coefficient $K_m(n)$. If

$$E^{LMF} = \frac{[(f^4)_m(n) + (b^4)_m(n)]}{2}$$

then

$$\frac{\partial E^{LMF}}{\partial K_m(n)} = 2\,[K^3{}_m(n)\,(A^2 - 2B^2) + 6B^2 K_m(n) + B\,A\,(3K^2{}_m(n) + 1)]$$

where

$$A = f^2{}_{m-1}(n-1) + b^2{}_{m-1}(n-1)$$

and

$$B = f_{m-1}(n)\, b_{m-1}(n-1)$$

Hence the rule for adapting the reflecting coefficients $K_m(n)$ is

$$K_m(n+1) = K_m(n) - \mu_m(n+1)\frac{\partial E^{LMS}}{\partial K_m(n)} \tag{6.11a}$$

where

$$\mu_m(n+1) = \frac{\beta}{6M\, E_{m-1}(n)\, E_N(n+1)}, \quad 0 < \beta < 1 \tag{6.11b}$$

$$E_m(n) = \gamma E_m(n-1) + [f^2{}_m(n) + b^2{}_m(n-1)]$$

and

$$E_N(n) = \gamma E_N(n-1) + N^2(n) \ , \ 0 < \gamma < 1 \qquad (6.11c)$$

In the expression for $\mu_m(n+1)$ in Eqn.(6.11b), $E_m(n)$ is same as in the case of LMS gradient lattice. But the term $E_m(n+1)$ does not exist for LMS-lattice. $E_N(n)$ is the noise power and is independent of m , the order of the stage of the lattice. This is due to tha fact that the lattice filter models only the correlated data.

6.5 Simulation Results

The simulated EEG signal whose parameters are shown in Table 6.1 is considered here. The EEG signal is filtered by a 4th order Butterworth lowpass filter (infinite impulse response) having a cutoff frequency of 35 Hz. to remove the noise above the EEG frequency band. (The signal simulated with a sampling frequency of 200 Hz. is filtered by a 4th order Butterworth filter and this filtered signal is down sampled to 100 Hz. This is due to the fact that the 4th order Butterworth filter for data sampled at 200 Hz. provides better attenuation in the stopband than for the data sampled at 100 Hz.) Poisson noise is added to this EEG signal and simulations are carried out at SNRs of 33.60 dB and 21.40 dB.

The spectra estimated by the different adaptive methods in comparison to Burg's Block data method are shown in Fig. 6.2 and the frequency estimated in the case of different SNRs are tabulated in Table 6.2. The accuracy of the peak frequency estimation by all algorithms is approximately the same. However, the peak picking algorithm could not estimate the frequency of the β activity peak properly at SNR of 33.60 dB whereas it does estimate it at SNR of 21.40 dB. This may be due to the critical formation of the β activity peak and variance of the LMF-TDL spectral estimator.

A real EEG signal is considered. In this case, the signal and its associated noise are together considered as signal since it is not possible to identify the signal and noise seperately. The SNR is quite high, as the signal is subjected to a first order lowpass filter to remove the high frequncy noise while recording. To this signal a Poisson noise is added to get a SNR of 31.20 dB.

The accuracy of the peak frequency estimation by all adaptive algorithms is almost the same as that for simulated EEG (Table 6.3, signal-1). The LMF-lattice provides a slightly better accuracy than the LMS adaptation considering Burg's frequency estimation as the reference.

In order to ascertain the general applicability of different adaptive algorithms , they have been applied to six real EEG signals obtained from the Montreal Neurological Institute. These signals are numbered from 2 to 7 for the purpose of nomenclature. The spectra estimated by the adaptive algorithms for these signals are identified in terms of the estimated peak frequencies in each case which are listed in Table-6.3. As expected, the results obtained for these signals are almost similar to those for signal-1. That is, the spectral fit to the BBD spectrum obtained by LMF adaptation is superior to that obtained by LMS adaptation and the LMF-TDL in this respect scores over the LMF-lattice. Further, the accuracy of the peak frequency estimation is approximately the same for all the adaptive algorithms.

Generally, the real EEG signals will be subjected to additional lowpass filtering prior to analog to digital conversion and this will further enhance the signal to noise ratio. But the signals considered here have not been subjected to such a filtering.

In all the examples (simulated EEG and real EEG) , the spectra corresponding to the 200th sample are considered and convergence is reached much prior to this instant.

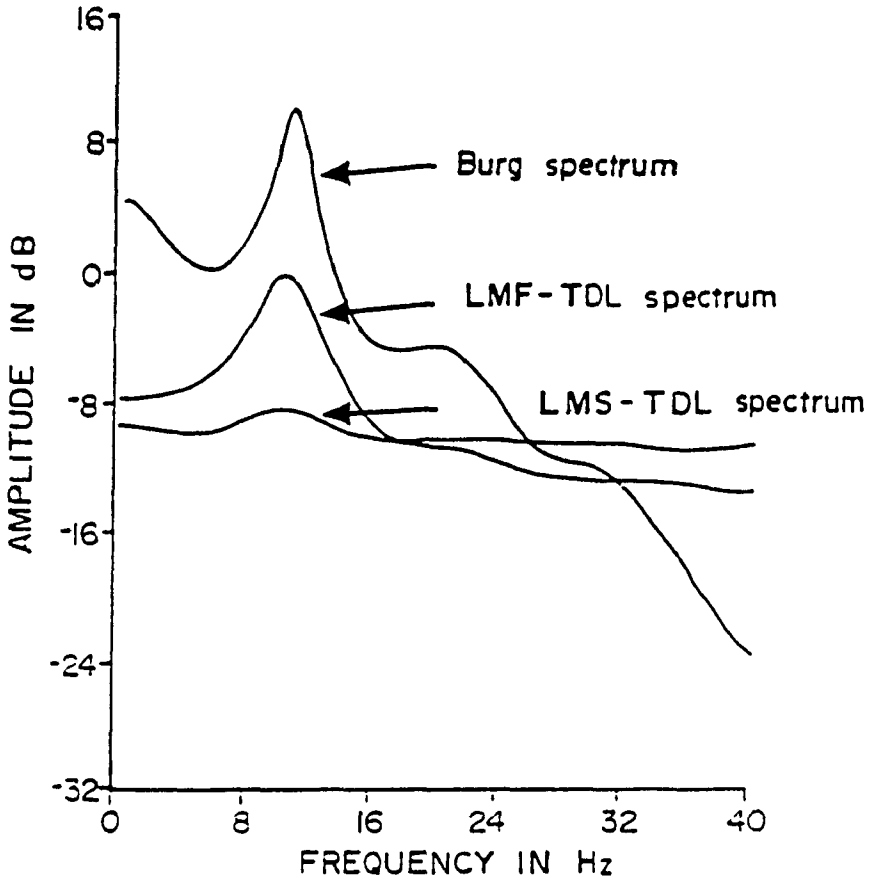

Fig.6.2 Computed spectrum from prediction filter coefficients for the simulated EEG signal

Table 6.1 Parameters of EEG registration.

Activity	σ_i (Hz.)	f_i (Hz.)	G_i (Hz.)
α	0.58 + 0.03	10.25 + 0.03	63 + 11
β	1.36 + 0.10	18.90 + 0.10	4 + 0.9
δ	1.27 + 0.07	0.0	33 + 6.0

Table 6.2 Frequency estimated by Burg's method and different adaptive algorithms for simulated EEG signal.

SNR (dB)	Freq. (Hz.)	Freq. (Hz.) (Burg's method)	Freq. (Hz.) (LMS-TDL method)
33.60	10.25	10.44	10.25
	18.90	20.42	21.57
21.40	10.25	10.46	10.27
	18.9	20.21	21.48

Table 6.3 Frequency estimated by Burg's method and different adaptive algorithms for real EEG signals.

Signal No.	SNR (dB)	Freq. (Hz.) (Burg's method)	Freq. (Hz.) (LMS-TDL method)
1	31.20	9.67	11.03
		19.34	21.31
2	30.95	10.64	10.49
		19.92	21.38
3	30.98	10.35	10.55
		21.09	21.48
4	31.30	32.36	20.21
		43.12	31.45
5	31.14	3.81	3.61
		-	16.31
6	32.06	11.47	10.93
		21.19	22.07
7	30.77	10.93	10.74
		20.81	21.68

6.6 Conclusions

Simulation results indicate that the LMF-TDL performs better than the LMF-lattice for EEG signals. In this work, a LMF-lattice algorithm has been implemented. The results indicate that the LMF adaptation performs better than the LMS adaptation in all cases. Further, for EEG signals, the LMF-TDL provides a better spectral fit to Burg's block data spectrum than the LMF-lattice. The decrease in spectral error measure, obtained by LMF-TDL for simulated and real EEG, is 3.29 and 3.0 dB respectively.

In all cases, the performance of adaptive algorithms as expected are found to be inferior to Burg's Block data method, since the sequential gradient adaptive algorithms cannnot approach the block data performance due to gradient noise. However, because of the advantages of sequential adaptive algorithms mentioned, they are well suited for processing nonstationary signals.

6.7 References

[6.1] Clark,G,A., 1981, Block adaptive filtering and it's application to seismic event detection, Ph.D. thesis, University of Califomia, Santa Barbara, U.S.A.

[6.2] Zetterberg,L.H., and Herolf,M., Spectral analysis of EEG for on line computer implementation based on adaptive linear model, In : Quantitative analysis of the EEG, Ed. Matejcek,M., and Schenk,G,K., Jongny sur Vevey, May 1975.

[6.3] Isaksson,A., Wennberg,A., and Zetterberg,L.H., 1981, Computer analysis of EEG signals with parametric models, Proceedings of the IEEE, 69, pp. 451-460.

[6.4] Freidlander,B., 1982, Lattice filters for adaptive processing, Proceedings of the IEEE, 70, pp. 829-837.

[6.5] Hodgkiss,W,S., and Presetey,J,A., 1981, Adaptive tracking of multiple sinusoids whose power levels are widely seperated, IEEE Trans. on Acoustics Speech and Signal Processing, 29, pp. 710-721.

[6.6] Widrow,B., Glover,J.R., and Goodlin,R.C., 1975, Adaptive noise cancelling : Principles and Applications, Proceedings of the IEEE, 63, pp. 1692-1716.

[6.7] Griffiths,L.J., 1969, A simple real time processing of antenna arrays, Proceedings of the IEEE, 57, pp. 1696-1704.

[6.8] Satorius,E,H., and Alexander,S.T., 1979, Channel equalisation using adaptive lattice algorithm, IEEE Trans. on Communications, 27, pp. 899-905.

[6.9] Griffiths,L.J., 1978, An adaptive lattice structure for noise cancelling applications, IEEE International Conference on Acoustics, Speech and Signal Processing, pp. 87-90.

[6.10]Etter,D.M., and Stearns,S.D., 1981, Adaptive estimation of time delay in sample data systems, IEEE Trans. on Acoustics, Speech and Signal Processing, 29, pp. 582-587.

[6.11]Makhoul,J., 1977, Stable and efficient lattice methods for linear prediction, IEEE Trans. on Acoustics, Speech and Signal Processing, 25, pp. 304-314.

[6.12]Chu,P.L., and Messrschmitt,D.G., 1983, Zero sensitivity properties of the digital lattice filters, IEEE Trans. on Acoustics, Speech and Signal Processing, 31, pp. 685-688.

[6.13]Walach,E., and Widrow,B., 1984, The least mean fourth (LMF) adaptive algorithm and it's family, IEEE Trans. on Information Theory, 30, pp. 275-283.

[6.14]Griffiths,L.J., 1978, An adaptive lattice structure for noise cancelling applications, IEEE International Conference on Acoustics Speech and Signal Processing, pp. 87-90.

[6.15]Honig,M.L., and Messerschmitt,D.G., 1981, Convergence properties of adaptive lattice filter, IEEE Trans. on Acoustics, Speech and Signal Processing, 29, pp. 642-653.

CHAPTER 7

BISPECTRUM ESTIMATION

7.1 Introduction

The power spectrum of a random process does not provide a complete description unless it is Gaussian or is generated in a linear fashion. The reasons are:

(1) The power spectrum is the Fourier Transform of the autocovariance sequence. For a zero mean Gaussian process, the autocovariance sequence contains all the required information. For non-Gaussian processes however, one can obtain some more information from higher order moments.

(2) In many cases of practical interest, due to nonlinear effects there are interactions among various harmonic components of a process giving rise to new components at other frequencies. These interactions involve the phase relationship among the harmonic components. Since the power spectrum does not reveal such phase relations, it does not provide information about nonlinearities.

Higher order spectra defined in terms of the higher order moments or in terms of higher order cumulants of a process serve as useful tools in investigating non-Gaussianness and nonlinearities. In particular, the bispectrum which is defined as the Fourier transform of the third moment sequence provides information about

1) Deviations from normality (Gaussian assumptions) :

The bispectrum of a zero mean Gaussian process is identically zero. Thus a non-zero bispectrum indicates that the process being dealt with is non-Gaussian.

2) Second order (quadratic) nonlinearity :

The output of a quadratic system contains power contributions at frequencies that are sums and differences of pairs of input frequencies. This phenomenon which is referred to as quadratic phase coupling can be detected by means of the bispectrum.

3) The phase of the signal in noise :

Unlike the power spectrum, the bispectrum retains some phase information which can be recorded from it.

Bispectral analysis has been applied in various fields to obtain the kind of information mentioned above. Hasselmann [7.1] has presented an application of bispectral analysis to an oceanographic problem. A number of interesting phenomena such as surf beats, wave breaking and energy transfer between components can be explained only by nonlinearity of wave motion. An important part of the analysis of fluctuations in nonlinear media is to discriminate between nonlinearly coupled waves and spontaneously excited waves and to measure the extent of nonlinear coupling. Kim and Powers [7.2] show successful application of bicoherence (a normalized bispectrum) measurement to plasma density fluctuation data to achieve such discrimination. Godfrey [7.3] uses bispectrum measurements on economic time series. Other applications of bispectral analysis include those of Hinich and Clay [7.4] to geophysical data, Huber et.al. [7.5] to EEG data and Lii et. al. to fluid mechanics [7.6]. Bispectrum estimation has also been applied for seismic deconvolution by Lii and Rosenblatt [7.7], and Matsuoka and Ulrych [7.8]. In all these cases, the bispectrum was estimated by using DFTs of data records.

Parametric methods based on the autoregressive model for bispectrum estimation have also been developed. Specifically, the parametric methods for power spectrum estimation are useful because:

(a) In terms of resolution, parametric methods perform better than conventional methods. The latter are bound by resolution limits imposed by certain properties of the Fourier transform.

(b) The process under consideration may indeed be parametric. Ignoring this aspect amounts to discarding useful information and the consequence will be estimates of poor spectral fidelity.

Spectrum estimation methods based on autoregressive (AR) and autoregressive moving average(ARMA) models of time series have been found to be suitable for use in such situations. Thus it is reasonable to expect that in such cases, parametric bispectrum estimation methods based on such models would provide better resolution and bispectral fidelity than conventional methods.

7.2 Bispectrum Estimation - a review

7.2.1 Introduction

The bispectrum is a special type of spectrum belonging to the general class of higher order cumulant spectra. Section 2 provides an account of cumulants and higher order spectra. In section 3, the bispectrum of a third order, stationary random process is defined and its properties are listed. The principal bispectrum estimation methods that are to be found in literature are described in section 4. Section 5 presents the most important uses of the bispectrum in signal processing.

7.2.2 Cumulants and Higher order spectra

Given a set of random variables $Y_1, Y_2, \ldots\ldots, Y_N$, their joint cumulant is defined as

$$k_{1..n}(Y_1,...,Y_n) = c[Y_1,...,Y_n] = (-j)^n \frac{\partial^n \ln\phi_{1,2,...,n}}{\partial u_1 \cdots \partial u_n} \quad ; \quad u_1=...=u_n=0 \tag{7.1}$$

where $\phi_{1,\ldots,n}(u_1,\ldots\ldots,u_n)$ is their joint characterstic function. $k_{1,\ldots,n}$ can be expressed in terms of the joint moments of the random variables. For example [7.1],

$$\begin{aligned} k_1 &= m_1 \\ k_{12} &= m_{12} - m_1 m_2 \\ k_{123} &= m_{123} - m_{12}m_3 - m_{13}m_2 - m_{23}m_1 + 2m_1 m_2 m_3 \end{aligned} \tag{7.2}$$

and so on.

The cumulant has the following important properties [7.1], [7.2],

(i) For $n \geq 3$, $k_{1,\ldots,n} = 0$ if the random variables are Gaussian

(ii) If the random variables can be divided into two statistically independent sets then again $k_{1,\ldots\ldots,n}=0$.

For a stationary random process $x(k)$, the nth order cumulant function is defined as

$$c[x(k),x(k+\tau_1),\ldots\ldots,x(k+\tau_{n-1})] = c_n(\tau_1,\ldots\ldots\ldots,\tau_{n-1}) \tag{7.3}$$

The nth order cumulant spectrum is defined as the nth order Fourier Transform of the cumulant

function i.e.

$$C(\omega_1,\ldots,\omega_n) = \sum_{l_1=-\infty}^{\infty} \cdots \sum_{l_n=-\infty}^{\infty} c_n(l_1,\ldots,l_n)\, exp\,[-j(\omega_1 l_1+\ldots+\omega_n l_n)] \tag{7.4}$$

where $C(\omega_1,\ldots,\omega_n)$ is the nth order cumulant spectrum. The above is called the $(n-1)^{th}$ order polyspectrum [7.1].

Higher order spectra are defined in terms of cumulants rather than moments because higher order ergodicity requirements are more easily met by the former. Also since moments of order greater than two do not provide any additional information for Gaussiuan processes, it is better to have a function that shows this fact explicitly. The cumulant function does so since third and higher order cumulants are zero for a normal process.

7.2.3 Bispectrum : Definition and Properties

A zero mean stationary process $x(n)$ has the spectral representation [7.3]

$$x(n) = \frac{1}{2\pi} \int_{-\pi}^{\pi} e^{jn\lambda}\, dz(\lambda) \tag{7.5}$$

where $E[z(\lambda)] = 0$

The process $z(\lambda)$ is one of orthogonal increments i.e.

$$E[dz(\lambda_1)\, dz^*(\lambda_2)] = 0, \qquad \text{for } \lambda_1 - \lambda_2 \neq 0 \tag{7.6}$$

In the case of a Gaussian process this property amounts to independence of these increments. For a skewed distribution when a Fourier-Stieltjes representation of its third moment sequence exists it can further be shown that

$$E[dz(\lambda_1)\, dz(\lambda_2)\, dz^*(\lambda_3)] = 0 \qquad \text{for } \lambda_1 + \lambda_2 - \lambda_3 \neq 0 \tag{7.7}$$

Defining

$$dG(\lambda_1, \lambda_2) = E[dz(\lambda_1)\, dz(\lambda_2)\, d^* z(\lambda_1 + \lambda_2)] \tag{7.8}$$

We have using Eqn.(7.5) and Eqn.(7.8),

$$R(m, n) = \frac{1}{(2\pi)^2} \int_{-\pi}^{\pi}\int_{-\pi}^{\pi} exp\,[-j(m\lambda_1+n\lambda_2)]\, dG(\lambda_1, \lambda_2) \tag{7.9}$$

where $R(m\ ,n)$ is the third moment sequence.

The function $G(\lambda_1\ ,\lambda_2)$ is the complex valued bispectral distribution. The bispectral density when it exists is defined as

$$B(\omega_1\ ,\omega_2) = \frac{\partial^2 G(\omega_1\ ,\omega_2)}{\partial\omega_1\,\partial\omega_2} \tag{7.10}$$

Alternatively, the bispectral density can be defined as the Fourier Transform of the third moment sequence. If $R(m\ ,n)$ denotes the third moment sequence then

$$B(\omega_1\ ,\omega_2) = \sum_{m=-\infty}^{\infty}\ \sum_{n=-\infty}^{\infty} R(m\ ,n)\exp[-j(\omega_1 m + \omega_2 n)] \tag{7.11}$$

Absolute summability of the third moment sequence $R(m\ ,n)$ is a sufficient condition for the existence of the bispectrum. Since the third order moment and cumulant are identical the bispectrum is a third order cumulant spectrum or a second order polyspectrum.

The bispectrum of a real process is in general complex and satisfies the following symmetries:

$$B(\omega_1\ ,\omega_2) = B(\omega_2\ ,\omega_1) = B^{*}(-\omega_2\ ,-\omega_1) = B(-\omega_1-\omega_2\ ,\omega_2) = B(\omega_1\ ,-\omega_1-\omega_2) \tag{7.12}$$

Also from the definition in Eqn.(7.11) it is seen that $B(\omega_1\ ,\omega_2)$ is periodic in ω_1 and ω_2 with a period 2π. Thus knowing the bispectrum on the triangle bounded by the lines $\omega_2 = 0\ ,\ \omega_1 = \omega_2$ and $\omega_1 + \omega_2 = \pi$, we can determine it's value over the entire $(\omega_1 - \omega_2)$ plane

7.2.4 Bispectrum estimation procedures

The problem met with in practice is one of estimating the bispectrum of a process when a finite realization is given. Rosenblatt and Van Ness [7.4] discuss the situation where a continuous time record $x_t\ ,0\le t\le N$ is avaliable. They consider estimation of the weighted and unweighted bispectral density based on third moment estimates. An estimate $r(\tau_1\ ,\tau_2)$ of the third moment function of the process can be made as

$$r(\tau_1\ ,\tau_2) = \frac{1}{N}\int_D x_t\, x_{t+\tau_1}\, x_{t+\tau_2}\, dt \tag{7.13}$$

where none of $|\tau_1|$, $|\tau_2|$ and $|\tau_1 - \tau_2|$ is greater than N and

$D = [-\min[0, \tau_1, \tau_2,],\ N - \max[0, \tau_1, \tau_2]]$.

Defining

$$\hat{g}_N(\omega_1,\omega_2) = \frac{1}{(2\pi)^2} \int_{-N}^{N} \int_{-N}^{N} exp\,[-j(\omega_1\tau_1+\omega_2\tau_2)]\, r(\tau_1,\tau_2)\, d\tau_1 d\tau_2 \tag{7.14}$$

the weighted bispectrum is estimated as

$$g_N(\omega_1,\omega_2) = \int_{-\infty}^{\infty} \int_{-\infty}^{\infty} W_N(\mu_1-\omega_1,\mu_2-\omega_2)\, \hat{g}_N(\mu_1,\mu_2)\, d\mu_1 d\mu_2 \tag{7.15}$$

where $\omega(\mu_1, \mu_2)$ is a sequence of weight functions chosen such that the bispectrum estimate in Eqn.(7.15) is consistent. The paper addresses key issues such as existence of consistent estimates of the third moment function and the bispectrum. However the proposed method is not applied to any experimental or synthetic data. In other papers, Brillinger and Rosenblatt [7.5], [7.6] deal with the computation of higher order spectra in the case of discrete processes. In most cases of bispectrum measurements reported in literature the estimation is done by methods similar to the periodogram approach of power spectrum estimation. These methods are described in what follows. The review of the methods presented here is drawn from the paper by Huber et al. [7.3]. There are three approaches to the estimation problem. These are:

(i) Averaging in the frequency domain

(ii) Averaging over successive records

(iii) Complex demodulation and averaging in the time domain

A detailed description of these approaches follws:

Assume that the bispectrum is to be estimated for frequencies between 0 and $\frac{\omega_0}{2}$ with a spacing of Δ_0 between them. It is assumed that all frequencies above $\frac{\omega_0}{2}$ are removed by prefiltering. Suppose that there are K records each of length N where N is a power of 2 and a multiple of $M = 2L + 1$, an odd integer. The total number of data points is $N_{tot} = KN$. The bispectrum has to be estimated only over the triangular region mentioned earlier.

The first three steps below are common to all approaches. The records are numbered $j = 1, 2, \ldots\ldots, K$. For each of them the following operations are performed:

1) Subtract the average and remove a linear trend if necessary.

2) Window the record and add zeros if necessary to make N a power of 2. Number the operations from 0 to $N-1$ as $x_0, x_1, \ldots, x_{N-1}$.

3) Perform a fast Fourier transform yielding

$$Y_q = \frac{1}{N}\sum_{t=0}^{N-1} x_t \, e^{-2\pi j(qt/N)}, \quad 0 \le q \le N/2 \tag{7.16}$$

4) Estimate the bispectral density $b(\omega_1, \omega_2)$ at

$$(\omega_1, \omega_2) = (q_1 \frac{\omega_0}{N}, q_2 \frac{\omega_0}{N})$$

for the three approaches as follows:

(i) Averaging in the frequency domain

Average triple products of Y_q over

(a) a quadratic window:

$$\hat{b_j}(\omega_1,\omega_2)\Delta_0^2 = \sum_{k_1=-L}^{L}\sum_{k_2=-L}^{L} Y_{q_1+k_1} Y_{q_2+k_2} Y^*_{q_1+q_2+k_1+k_2} \qquad j=1,\ldots,K \tag{7.17a}$$

or

(b) a hexagonal window

$$\hat{b_j}(\omega_1,\omega_2)\Delta_0^2 = \frac{4M^2}{3M^2+1}\sum_{|k_1|\le L,\ |k_2|\le L,\ |k_1+k_2|\le L} Y_{q_1+k_1} Y_{q_2+k_2} Y^*_{q_1+q_2+k_1+k_2} \qquad j=1,\ldots,K \tag{7.17b}$$

Form the final estimate by averaging over the K pieces:

$$\hat{b}(\omega_1, \omega_2) = \frac{1}{K}\sum_{j=1}^{K} \hat{b_j}(\omega_1, \omega_2) \tag{7.18}$$

(ii) Averaging over records

Take $L = 0$ in Eqn.(7.17) with a corresponding increase of K so that N_{tot} remains the same. Form the final estimate as in Eqn.(7.18).

(iii) Complex demodulation

(a) Put

$$Y_k(q) = Y_{q+k} \qquad \text{for } |k| \le L \tag{7.19a}$$

$$Y_k(q) = 0 \qquad \textit{otherwise}$$

$$\hat{Y}_k(q) = Y_{q+k} \qquad \text{for } |k| \le 2L \tag{7.19b}$$

$$\hat{Y}_k(q) = 0 \qquad \textit{otherwise}$$

In other words, a narrow bandpass filter is applied and the frequencies are shifted to zero.

(b) Transform back into the time domain i.e. obtain

$$Z_s(q) = \sum_k Y_k(q) \exp\left(\frac{2\pi jsk}{n}\right) \tag{7.20a}$$

$$Z_s(q) = \sum_k Y_k(q) \exp\left(\frac{2\pi jsk}{n}\right) \tag{7.20b}$$

(c) Average triple products of the complex demodulates so obtained in the time domain

$$\hat{b_j}(\omega_1,\omega_2)\Delta_0^2 = \frac{1}{n}\sum_{s=0}^{n-1} Z_s(q_1)\, Z_s(q_2)\, Z_s^*(q_1+q_2) \tag{7.21a}$$

or

$$\hat{b_j}(\omega_1,\omega_2)\Delta_0^2 = \frac{4M^2}{3M^2+1}\,\frac{1}{n}\sum_{s=0}^{n-1} Z_s(q_1)\, Z_s(q_2)\, Z_s^*(q_1+q_2) \tag{7.21b}$$

Finally, average over records as in Eqn.(7.18). The above procedures bear a great resemblance to conventional methods of power spectrum estimation and so are referred to as conventional bispectrum estimators. It can be shown that conventional estimators are unbiased and consistent [7.3].

7.2.5 Use of Bispectrum in Signal Processing

As mentioned in the previous section, the third order cumulant (which happens to be the third order moment too) is identically zero for a zero mean Gaussian process. Consequently it's bispectrum is also zero for all frequency pairs. A nonzero bispectrum thus indicates a deviation of the process

from normality.

Another important use of the bispectrum is in the detection of quadratic phase coupling. There arise situations where becuase of the interaction between two harmonic components of a process, there is contribution to the power at a frequency which is equal to the sum of or the difference between the interacting frequencies. Such a phenomenon could occur due to second order nonlinearities and is referred to as quadratic phase coupling. A common example is amplitude modulation where because of interaction between the modulating and carrier frequencies, there is contribution to power at their sum and difference frequencies. Any three frequencies are said to be at harmonically related positions if one of them is the sum of the other two. A special case is when we have two components with one being at twice the frequency of the other. Thus quadratic phase coupling can arise only among harmonically related frequency components of a process. In certain applications, it is necessary to find out if harmonically related peaks in the power spectrum are in fact phase coupled. The power spectrum suppresses all phase phase relations among the frequency components and so can not provide the answer.

Let us consider an example to illustrate this use of the bispectrum.

Consider the process.....

$$X_1(n) = \sum_{i=1}^{3} \cos(\lambda_i n + \phi_i) \tag{7.22}$$

where $\lambda_1 = \lambda_2 + \lambda_3$. ϕ_1, ϕ_2 are independent and uniformly distributed on $[0, 2\pi]$ and $\phi_3 = \phi_1 + \phi_2$. Thus the power at λ_3 is solely due to quadratic phase coupling between λ_1 and λ_2. The power spectrum has inipulses at λ_1, λ_2 and λ_3 The third moment sequence of $X_1(n)$ is

$$\begin{aligned} R_1(k,l) = 0.25\,[&\cos(\lambda_2 k + \lambda_1 l) + \cos(\lambda_3 k - \lambda_1 l) + \cos(\lambda_1 k + \lambda_2 l) \\ &+ \cos(\lambda_3 k - \lambda_2 l) + \cos(\lambda_1 k - \lambda_3 l) + \cos(\lambda_2 k - \lambda_3 l)] \end{aligned} \tag{7.23}$$

Thus the bispectrum magnitude evaluated over the triangle mentioned in section 3 has an impulse at (λ_1, λ_2). This impulse indicates coupling between the components at the frequencies λ_1 and λ_2.

Now consider the process

$$X_2(n) = \sum_{i=1}^{3} \cos(\lambda_i n + \phi_i) \tag{7.24}$$

which is the same as $X_1(n)$ in all respects but one, namely that the phases ϕ_1 , ϕ_2 and ϕ_3 in this case are all independent and uniformly distributed on $(0, 2\pi)$. Since ϕ_3 is statistically independent of ϕ_1 and ϕ_2 , the contribution to the power at λ_3 is from an independent harmonic component. This then is a case where there is no quadratic phase coupling. The power spectrum of $X_2(n)$ is the same as that of $X_1(n)$ and has impulses at the harmonically related frequencies λ_1 , λ_2 and λ_3 . The third moment sequence of this process, $R_2(k, l)$ is zero everywhere and hence the bispectrum is identically zero. A vanishing bispectrum is an indicator of nonexistence of phase coupling. This shows that since the power spectrum is identical in both the coupled and uncoupled cases, it does not help in the detection of quadratic phase coupling. On the other hand the bispectrum is well suited for this purpose. For a process where some of the components are quadratically coupled but others are not, only the coupled components contribute to it's third moment sequence.

One of the earliest examples of the application of the bispectrum for detection of quadratic phase coupling was to an Oceanographic problem. Hasselmann et al [7.7] investigated the phenomenon of peaking of shallow water wave crests. Bispectral measurements of fluctuating water depth showed that phase coupling of a dominant spectral component with itself and with other components caused the peaking. The measured bispectral values concurred with theoretical predictions. The approach involved narrow band pass filtering. Godfrey [7.8] shows application of bispectral analysis to two time series; one being the transaction prices on the New York stock exchange for a company for a particular month and the other a series of monthly observations of one of the monetary variables of the U.S. Federal Reserve System. The purpose of the analysis on the first series was to see if a log-linear model was better suited to the observations than a simple linear model and in the second series it was to test the adequacy of a linear model. Here complex demodulates were used for obtaining estimates of the bispectrum. Brillinger and Rosenblatt [7.6] show applications of the bispectrum and trispectrum (the fourth order cumulant spectrum) to sunspot numbers. Kim and Powers [7.9] have applied bispectrum estimation to the study of plasma fluctuation associated with the evolution of drift-wave turbulence. The purpose of the study was to detect presence of nonlinear wave-wave interaction. The bispectrum measurements were made by segmenting the experimental data into

records and then forming average triple products of the Fast Fourier Transforms of the (windowed) records. The measurements were made in both frequency and wave number domains. The results showed that in the multimode regime of the experiment there were significant wave-wave interactions while in the turbulent phase, wave-wave interaction was negligible. An application to fluid mechanics is given by Lii et al [7.10]. Bispectral analysis was carried out on the velocity derivative of turbulent atmosphere data collected by hot wire anemometer measurements. The method adopted for bispectrum estimation involved averaging in the frequency domain. The measurements suggested that contributions of wave- number triplets to spectral transfer and the rate of vorticity production were non-local in wavenumber space and comparable over a wide range of wavenumbers. Huber et al [7.3] obtained spectral measurements of EEG signals and found interaction between the alpha rhythm and it's higher harmonics. Some other papers that deal with phase coupling applications and computation of bispectra are those of Haubrich [7.11], Hinich and Clay [7.12], McComas and Briscoe [7.13], Zadro and Caputo [7.14], and Korein et al [7.15].

The fact that the third moment sequence retains phase information unlike the autocorrelation also makes the bispectrum useful in distinguishing between minimum phase and non-minimum phase sequences. Consider for example the processes

$$Y_1(n) = W(n) - (a+b)\ W(n-1) + a\,b\ W(n-2) \tag{7.25}$$

and

$$Y_2(n) = a\,W(n) - (1+a\,b)\,W(n-1) + b\,W(n-2) \tag{7.26}$$

where $0 < a < 1$, $0 < b < 1$, and $W(n)$ s are i.i.d with $E[W(n)] = 0$, $E[W^2(n)] = 1$ and $E[W^3(n)] = 1$.

Then

$$H_1(z) = \frac{Y_1(z)}{W(z)} = (1 - a\,z^{-1})(1 - b\,z^{-1}) \tag{7.27}$$

$$H_2(z) = \frac{Y_2(z)}{W(z)} = (a - z^{-1})(1 - b\,z^{-1}) \tag{7.28}$$

$H_1(z)$ is minimum phase since all it's zeros are inside the unit circle while $H_2(z)$ has a zero at $1/a$ which is outside the unit circle. $Y_1(n)$ and $Y_2(n)$ have the same power spectra but their bispectra are

different. When we are given samples of either of these processes, it is impossible with spectral measurements to distinguish between the minimum phase sequence from the non-minimum phase sequence. Bispectral measurements provide a way of making correct identification. This has important implications for seismic deconvolution.

A seismic reflection signal is commonly modelled as [7.16]

$$Y_n = \sum_{m=0}^{M} w_m r_{n-m} \tag{7.29}$$

where $w = (w_0, w_1, \ldots\ldots w_M)$ is the seismic wavelet due to a surface disturbance and r_n s are the reflection coefficients of the various layers of the earth. Usually only measurements of Y_n are available and it is required to find r_n. Thus we have a deconvolution problem. The r_n are assumed to form a white sequence. Since even the w_m s are unknown, a common restriction imposed on the wavelet is that it be minimum phase. But actual results indicate it is not necessarily so. By making bispectral maesurements on Y_n , the true phase of the seismic wavelet can be estimated (upto a linear phase factor) from the bispectral phase. Algorithms for this purpose have been developed by Brillinger [7.17], Li and Rosenblatt [7.18], and Matsuoka and Ulrych [7.16]. Some of the theory behind this type of application was developed by Rosenblatt [7.19]. Huzii [7.20] dicusses similar application of higher order moments in discriminating between poles of an AR filter that are inside the unit circle and those that are outside of it.

Lohmann and Wirnitzer [7.21] in an interesting paper describe applications of third moments and the bispectrum to the study of laser pulse shapes, sound quality, mobility of bacteria etc.. However analog methods were used in all these cases. Sato and Sasaki [7.22] discuss application of the bispectrum to holography.

7.3 Bispectrum Estimation based on Parametric Model

7.3.1 Introduction

For processes that are of parametric nature, using bispectrum estimation methods based on parametric models may provide estimates of higher fidelity. Another reason concerns the use of bispectrum estimation for detecting quadratic phase coupling among sinusoidal signals. In certain situations it may be necessary to resolve two closely spaced peaks in the bispectrum magnitude or detect presence or absence of phase coupling at frequency pairs that are very close to one another It is well known in power spectrum estimation that parametric techniques based on AR and ARMA models [7.23] possess higher resolution capabilities. This property has been used in the bispectrum domain as well by Raghuveer and Nikias [7.24].

7.3.2 AR Model for Bispectrum Estimation

From the definition of the bispectrum in the previous section, it follows that a parametric bispectrum estimation method should involve a model for the third moment sequence of a process. In this model proposed by Raghuveer and Nikias [7.24], only real discrete processes have been considered. The third moment sequence $R(m, n)$ of a process has the following symmetries

$$R(m,n) = R(n,m) = R(-m, n-m) = R(m-n, -n) \tag{7.30}$$

Thus the knowledge of $R(m,n)$ over the infinite wedge bounded by the lines $n = 0$ and $m = n$ for $m, n \geq 0$ suffices for a complete description of it (Fig.7.1). Also as mentioned in the previous section, for a real discrete process, it is enough to evaluate the bispectrum over the region $\omega_2 \geq 0$, $\omega_1 \geq \omega_2$ and $\omega_1 + \omega_2 \leq \pi$ (Fig.7.2).

Consider the p-th order AR process $X(n)$ given by

$$X(n) + \sum_{i=1}^{p} a_i X(n-i) = W(n) \tag{7.31}$$

where $W(n)$ s are i.i.d. with $E[W(n)] = 0$, $E[W^3(n)] = \beta \neq 0$ and $X(m)$ is independent of $W(n)$ for $m < n$. Note that $W(n)$ is non - Gaussian.

Since $W(n)$ is third order stationary, it follows that $X(n)$ is also third order stationary assuming it is a stable AR model. For the above model we have

$$R(-k,-l) + \sum_{i=1}^{p} a_i R(i-k, i-l) = \beta \delta(k,l) ; \qquad k, l \geq 0 \tag{7.32}$$

which is the same as $X_1(n)$ in all respects but one, namely that the phases ϕ_1 , ϕ_2 and ϕ_3 in this case are all independent and uniformly distributed on $(0, 2\pi)$. Since ϕ_3 is statistically independent of ϕ_1 and ϕ_2 , the contribution to the power at λ_3 is from an independent harmonic component. This then is a case where there is no quadratic phase coupling. The power spectrum of $X_2(n)$ is the same as that of $X_1(n)$ and has impulses at the harmonically related frequencies λ_1 , λ_2 and λ_3 . The third moment sequence of this process, $R_2(k, l)$ is zero everywhere and hence the bispectrum is identically zero. A vanishing bispectrum is an indicator of nonexistence of phase coupling. This shows that since the power spectrum is identical in both the coupled and uncoupled cases, it does not help in the detection of quadratic phase coupling. On the other hand the bispectrum is well suited for this purpose. For a process where some of the components are quadratically coupled but others are not, only the coupled components contribute to it's third moment sequence.

One of the earliest examples of the application of the bispectrum for detection of quadratic phase coupling was to an Oceanographic problem. Hasselmann et al [7.7] investigated the phenomenon of peaking of shallow water wave crests. Bispectral measurements of fluctuating water depth showed that phase coupling of a dominant spectral component with itself and with other components caused the peaking. The measured bispectral values concurred with theoretical predictions. The approach involved narrow band pass filtering. Godfrey [7.8] shows application of bispectral analysis to two time series; one being the transaction prices on the New York stock exchange for a company for a particular month and the other a series of monthly observations of one of the monetary variables of the U.S. Federal Reserve System. The purpose of the analysis on the first series was to see if a log-linear model was better suited to the observations than a simple linear model and in the second series it was to test the adequacy of a linear model. Here complex demodulates were used for obtaining estimates of the bispectrum. Brillinger and Rosenblatt [7.6] show applications of the bispectrum and trispectrum (the fourth order cumulant spectrum) to sunspot numbers. Kim and Powers [7.9] have applied bispectrum estimation to the study of plasma fluctuation associated with the evolution of drift-wave turbulence. The purpose of the study was to detect presence of nonlinear wave-wave interaction. The bispectrum measurements were made by segmenting the experimental data into

where $R(m,n)$ is the third moment sequence of the AR process and $\delta(k,l)$ is the 2-d unit impulse. From Eqn.(32), which has been refered to as the third order recursion [7.24], it follows that $2p+1$ third moment values on the $m=n$ line satisfy the matrix equation

$$R\,a = b \tag{7.33}$$

where

$$R = \begin{bmatrix} R(0,0) & R(1,1) & \cdots & R(p,p) \\ R(-1,-1) & R(0,0) & \cdots & R(p-1,p-1) \\ \cdot & \cdot & \cdots & \cdot \\ \cdot & \cdot & \cdots & \cdot \\ R(-p,-p) & R(-p+1,-p+1) & \cdots & R(0,0) \end{bmatrix}$$

$$a = [1 \;\; a_1 \;\; \cdots\cdots \;\; a_p]^T$$

$$b = [\beta \;\; 0 \;\; \cdots\cdots \;\; 0]^T$$

The matrix R is Toeplitz but in general is not symmetric. An essential condition for the representation in Eqn.(7.33) to exist for a causal $X(n)$ is that the polynomial

$$A(z) = 1 + \sum_{i=1}^{p} a_i\, z^{-i} \tag{7.34}$$

has all its roots inside the unit circle or eqivalently to the condition that the AR filter transfer function

$$H(z) = \frac{1}{A(z)} \tag{7.35}$$

is stable. It is well known that a sufficient condition for the stability of $H(z)$ is that R in addition to being Toeplitz is also symmetric and positive definite [7.25]. However, this is not a necessary condition. Thus, for all those processes whose third moments satisfy the sufficient condition above, stable AR representations of order p can be derived based on knowledge of the $2p+1$ moments $R(-p,-p), \ldots\ldots R(p,p)$.

Another representation is possible by letting k and l of Eqn.(7.32) run on portions of the triangle in Fig.7.1. The $p + 1$ equations corresponding to this representation are

$$R(-k,-l) + \sum_{i=1}^{p} a_i R(i-k, i-l) = \beta \delta(k,l) \tag{7.36}$$

where

$$k = 0, \ldots\ldots, L_1$$

and

$$l = 0, \ldots\ldots, k \qquad \text{for } k < L_1$$

and

$$l = 0, \ldots\ldots, L_2 \qquad \text{for } k = L_1$$

where L_1 and L_2 are chosen such that $L_2 \leq L_1$ and

$$p = 1 + L_2 + \frac{(L_1 - 1)(L_1 + 2)}{2}$$

The matrix corresponding to the equations in Eqn.(7.36) does not posses the Toeplitz structure of R in Eqn.(7.33).

The bispectrum of the AR process $X(n)$ in Eqn.(7.31) is given by [7.24],

$$B(\omega_1, \omega_2) = \beta H(\omega_1) H(\omega_2) H^*(\omega_1 + \omega_2) \qquad |\omega_1|, |\omega_2| \leq \pi \tag{7.37}$$

where $B(\omega_1, \omega_2)$ is the bispectrum of $X(n)$ and $H(\omega)$ is $H(z)$ of Eqn.(7.35) evaluated at $z = \exp(+j\omega)$. It is easily verified that $B(\omega_1, \omega_2)$ satisfies the properties described by Eqn.(7.31).

Given $2p + 1$ samples of the true third moment sequence of a process, one at the origin and the rest at p points on either side of it on the $m = n$ line in Fig.7.1, Eqn.(7.33) can be used to fit a p-th order AR model. Fast algorithms that make use of the Toeplitz structure exist for solving this equation [7.26]. More than $2p + 1$ samples are required to fit such a model using Eqn.(7.36). If the samples are from the third moments of a true p-th order process satisfying all the model assumptions then, the parameters $a_1, \ldots\ldots, a_p$ in both cases are the same. Otherwise the two solutions may be different. Eqns.(7.33),(7.36) and (7.37) form the basis for the parametric bispectrum estimation method proposed in [7.24].

Suppose $R(-p,-p), R(1-p, 1-p),.....,R(0, 0),.....,R(p, p)$ denote $2p + 1$ samples of the third moment sequence of a process. Let $G(m, n)$ be the third moment sequence of the output of a p-th order AR process driven by a Non Gaussian White Noise (NGWN) whose third moment is β. If we insist that $2p + 1$ values of the third moment sequence namely $G(-p,-p)$ through $G(p, p)$ match exactly the third moment sequence of the given process at corresponding lags i.e.

$$C(k, k) = R(k, k), \quad k = -p, 1-p,.....,0,....., p-1, p \tag{7.38}$$

then the third order recursion in Eqn.(7.33) follows as a necessary condition. It is in this sense that AR model is fitted to the third moment sequence.

7.3.3 Third order recursion method for bispectrum estimation

Suppose now that we are given only a finite length of data and it is required to estimate the bispectrum of the underlying discrete random process. For this purpose, a parametric method that involves fitting of an AR model driven by a NGWN has been proposed [7.24]. The method is based on Eqn.(7.33) and (7.37) where estimated third moments are substituted in place of true moments which are not known. Let $[X_1, X_2, ..., X_{N=KM}]$ be the given data set. Then:

(i) Form the biased third moment estimates as follows:

(a) Segment the data into K records of M samples each.

(b) For each record obtain $r^{(i)}(m, n)$, the biased estimate of the third moment at lags (m, n), as

$$r^{(i)}(m, n) = \frac{1}{M} \sum_{l=\max(1,\,1-m,\,1-n)}^{\min(M,\,M-m,\,M-n)} X_l^{(i)} X_{l+m}^{(i)} X_{l+n}^{(i)} \qquad i = 1, ..., K \tag{7.39}$$

(c) Average $r^{(i)}(m, n)$ over all records to obtain the overall estimate $R(m, n)$ as

$$R(m, n) = \frac{1}{K} \sum_{i=1}^{K} r^{(i)}(m, n) \tag{7.40}$$

(ii) Substitute the estimated moments in place of the true moments in Eqn.(7.33) to obtain

$$\hat{R}\,\alpha = \hat{b} \tag{7.41}$$

where

$$\alpha = [1 \;\; \alpha_1 \;\; \ldots\ldots\ldots \;\; \alpha_p]^T$$

and $[\alpha_i]_{i=1,\ldots\ldots,p}$ are the estimates of the AR parameters.

$$b = [\beta \;\; 0 \;\; \ldots\ldots\ldots \;\; 0]^T$$

and where β is the estimate of the third moment of the driving noise.

Fast algorithms can be used to solve the equations for α and β.

(iii) Form the bispectrum estimate by substituting α for a in Eqn.(7.37), i.e.,

$$B(\omega_1, \omega_2) = \beta H(\omega_1) H(\omega_2) H^*(\omega_1 + \omega_2) \tag{7.42}$$

or more conveniently the normalized estimate

$$\frac{B(\omega_1, \omega_2)}{\beta} = H(\omega_1) H(\omega_2) H^*(\omega_1 + \omega_2) \tag{7.43}$$

where

$$H(\omega) = \frac{1}{[1 + \sum_{n=1}^{p} \alpha_i \exp(-j\omega n)]}, \quad |\omega| \le \pi$$

$B(\omega_1, \omega_2)$ needs to be evaluated only at frequency pairs in the triangular region of Fig.7.2. The flow chart in Fig.7.3 summarizes the proposed parametric bispectrum estimation procedure.

Several comments about the above procedure are in order.

(1) An assumption made in using this procedure is that the process whose samples are given is third order ergodic. It has been shown in the paper [7.24] that if the process is in fact of type in Eqn.(7.31), then the parametric method provides consistent estimtes of the AR parameters $[a_i]$ $i=1, \ldots, p$.

(2) The matrix $\hat{R}$ is in general neither symmetric nor positive definite. Since no orthogonal vector spaces are involved, Eqn.(7.31) are not normal equations. In their place "third order recursion equations" is the term used.

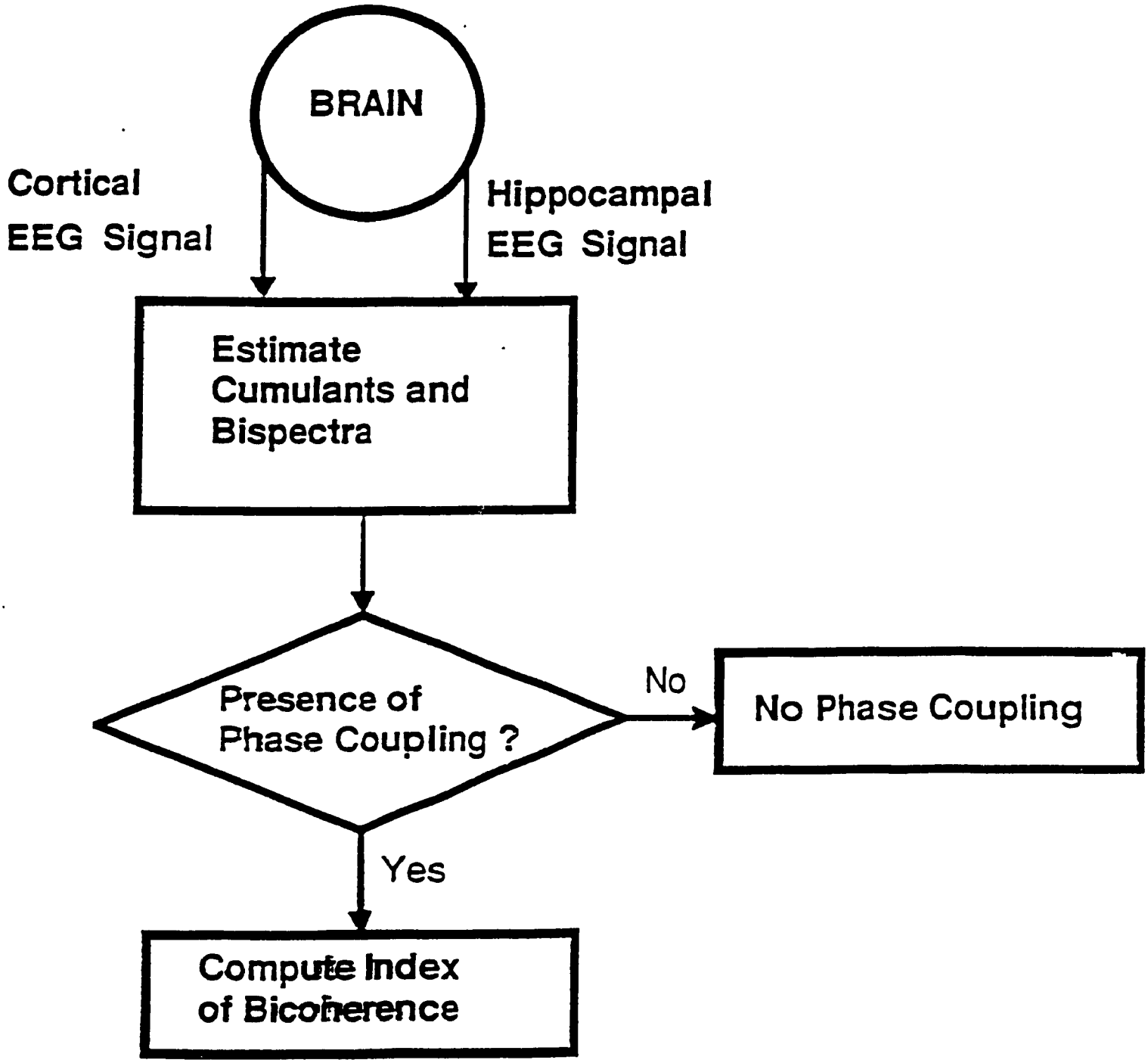

Fig.7.3 Flowchart of parametric bispectrum estimation method (Raghuveer and Nikias, 1984)

(3) Even when the given samples are from a stable AR process satisfying all the assumptions of the model in Eqn.(7.31), the parameter estimates from the proposed parmetric method do not necessarily provide a stable model. Only asymptotically is stability guaranteeed. Since in this method they are interested in using the AR parameter estimates for bispectrum estimation and not for filtering or prediction, stability is not a required property. In fact it is desirable in case of a process with a vanishing bispectrum, to have the poles of the fitted AR model go to infinity asymptotically so that the bispectrum estimate formed from Eqn.(7.43) tends to zero.

(4) It is not always necessary in step (i) of the estimation procedure to segment the data into records i.e. we can set $K = 1$ and $M = N$. However a single record cannot be used for detecting quadratic phase coupling between pairs of sinusouds. An example has been discussed in literature [7.24] how having independent records ensures consistent estimates of third moments in such situations.

(5) Instead of using Eqn(7.33), one can use Eqn(7.36) to form the AR parameter estimates. The corresponding matrix would not have a Toeplitz structure and is not appealing from analytical and computational viewpoints. It has been reported in [7.24] that the Toeplitz type exhibits lesser bias and provides smoother bispectral estimates.

(6) This is only an AR bispectrum estimation method. Since no entropy considerations are involved, it is not a maximum entropy bispectrum estimation method [8.27].

(7) In this method use of biased third moment estimates is proposed. No reason is given why unbiased third moment estimates can not be used.

(8) The conventional methods use FIR filters whose taps are the given samples of the process. The parametric method uses an IIR filter. Both make use of the same "data" i.e. the third moment sequence or its estimate of the process. In the case of conventional methods this is done by averaging triple products of the frequency responses of various FIR filters while in the case of the proposed parametric method, estimates of the third moments via average lagged triple products in the time domain are used to determine the filter parameters.

(9) AR parameters obtained by second order methods (e.g. the Yule-Walker method) model the power spectrum of the process and not its bispectrum and therefore can not be used for bispectrum

estimation.

(10) In this method they do not deal with AR model order selection for bispectrum estimation. Generally, the appropriate model order will be different from that for AR power spectrum estimation. Some of the well known AR model order selection criteria such as the AIC, FPE and Parzen's CAT [7.28] depend on autocorrelations and hence can not be used. However the AR part of the criteria of Chow [7.29] and Chan and Woods [7.30] may be adapted to the third order case.

(11) In a general context the problem under consideration can be seen as one of bispectral matching. Suppose a process has spectrum $P(\omega)$ and bispectrum $B(\omega_1, \omega_2)$. Then finding a linear filter with treansfer function $H(\omega)$ to match the power spectrum amounts to solving

$$P(\omega) = |H(\omega)|^2 \tag{7.44}$$

whereas finding a linear filter with tramsfer function $T(\omega)$ to match the bispectrum is equivalent to solving

$$B(\omega_1, \omega_2) = T(\omega_1)\, T(\omega_2)\, T(-\omega_1 - \omega_2) \tag{7.45}$$

The solution to Eqn.(7.45) when it exists is generally different from that of Eqn.(7.44).

The concept of linear models for bispectral matching follows from the discussion in section III of [7.24].

7.4 Detection of Quadratic Phase Coupling

7.4.1 Introduction

Consider the process

$$X(n) = \sum_{i=1}^{6} \cos(\lambda_i\, n + \phi_i) \tag{7.46}$$

where $\lambda_1 > \lambda_2 > 0$, $\lambda_4 > \lambda_5 > 0$, $\lambda_3 = \lambda_1 + \lambda_2$, $\lambda_6 = \lambda_4 + \lambda_5$, and $\phi_1, \phi_2, \ldots\ldots, \phi_5$ are all independent, uniformly distributed random variables over $(0, 2\pi)$ and $\phi_6 = \phi_4 + \phi_5$. In Eqn.(7.46) while $(\lambda_1, \lambda_2, \lambda_3)$ and $(\lambda_4, \lambda_5, \lambda_6)$ are at harmonically related positions, only the component at λ_6 is a result of phase coupling between those at λ_4 and λ_5 while the one at λ_3 is an independent harmonic component. The

power spectrum of the process consists of impulses at λ_i ; $i = 1, 2, 3, ..., 6$. Looking at the spectrum one can not say if the harmonically related components are in fact involved in quadratic phase coupling relationships. The third moment sequence $R(k, l)$ of $X(n)$ can be easily obtained as

$$R(k,l) = 0.25\,[\cos(\lambda_5 k + \lambda_4 l) + \cos(\lambda_6 k - \lambda_4 l) + \cos(\lambda_4 k + \lambda_5 l) + \cos(\lambda_6 k - \lambda_5 l) + \cos(\lambda_4 k - \lambda_6 l) + \cos(\lambda_5 k - \lambda_6 l)] \quad (7.47)$$

It is important to observe that in Eqn.(7.47), only the phase coupled components appear. Consequently, the bispectrum evaluated in the triangular region of Fig.7.2 shows an impulse only at (λ_4, λ_5) indicating that only this pair is phase coupled. In the total absence of phase coupling, the third moment sequence and hence the bispectrum are both zero. Thus the fact that only phase coupled components contribute to the third moment sequence of a process is what makes the bispectrum a useful tool for detecting quadratic phase coupling and discriminating phase coupled components from those that are not. All that is required of the bispectrum estimation technique is that it adequately recovers this information in the third moment sequence and as long as a linear model does so, it can be used for detecting phase coupling. The AR bispectrum estimation method described in [7.24] models accurately the third moment sequence of a process of the type given in Eqn.(7.46).

7.4.2 Quadratic Phase Detection in EEG Signals

In this study quadratic phase coupling was studied by computing the bispectra of EEG's recorded from the hippocampus of the rat. The data was obtained from the Montreal Neurological Institute.

The bispectrum which is the Fourier transform of the third order cumulant (TOC) sequence is capable of detecting phase coupling and the degree of phase coupling can be quantified using the bicoherence index, i.e. a normalized bispectrum.

In this study, EEG's were collected from two different regions of the rat brain namely, the hippocampus and the frontal cortex. These EEG's were sampled at 128 Hz. and digitized into 8 second epochs, and each epoch was manually scored by experts as one of four different sleep stages i.e. rapid

eye movement sleep (REM) sleep, quiet waking (QW) , slow wave (SW1) sleep 1 and slow wave (SW2) sleep 2. During the study, EEG's were collected from five adult rats, and 32 epochs of each sleep stage were scored for analysis for each animal.

The TOC sequence was first estimated via the equation

$$\hat{R}(m\ ,\ n) = \sum_{k \epsilon K} [X(k)\, X(k+m)\, X(k+n)]$$

where K is the region of support of the data, and the bispectrum is approximated by a summation over a finite region:

$$\hat{B}(\omega_1\ ,\ \omega_2) = \sum_{(m\ ,\ n) \epsilon S} \hat{R}(m\ ,\ n)\, W(m\ ,\ n)\, e^{-j(\omega_1 m\ +\ \omega_2 n)}$$

where S is the region of support of the estimated $\hat{R}(m\ ,\ n)$. In the above equation $W(m\ ,\ n)$ represents a two dimensional tapering function which is employed to reduce the variance of the bispectrum estimate. Also, to save computation time, the symmetric characterstic of the TOC sequence was taken into account when computing the bispectrum [7.17], [7.24]. To quantify the degree of quadratic phase coupling, the bicoherence index [7.24], [7.27] is computed. This index is a function of the Bispectrum $B(\omega_1\ ,\ \omega_2)$ and the power spectrum $P(\omega)$ and is defined as

$$bic(\omega) = \frac{B(\omega_1\ ,\ \omega_2)}{P(\omega_1)\, P(\omega_2)\, P(\omega_1\ ,\omega_2)}$$

If quadratic phase coupling was observed in the bispectrum, the bicoherence index was computed to indicate the significance level.

Our results showed that the bispectra of hippocampal EEG's during REM sleep exhibit a significant phase coupling between frequencies in the 6-8 Hz. range as seen in Fig.7.5. Bispectra of EEG's obtained from the frontal cortex during QW, on the other hand, exhibit only a weak phase coupling between frequencies in the 2-3 Hz. range (Figure 7.7). Howver no consistent phase coupling was observed during SWS. These results show a strong consistent phase coupling only exists for the hippocampal EEG during REM sleep where the presence of a sharp peak in the bispectrum occurs between frequencies 6-8 Hz. associated with the theta rythm generated in the hippocampal formation. The significance levels are summarized in Table 7.1.

7.5 Conclusions

In this chapter various bispectrum methods disussed in literature have been presented. These methods hold promise in terms of detecting quadratic phase coupling information and a study is done to detect phase coupling in the cortical and hippocampal EEG of the rat during varoius sleep stages. For EEG's recorded from the hippocampus, significant phase coupling was obtained during REM sleep between the frequency components assocaited with the theta rythm.

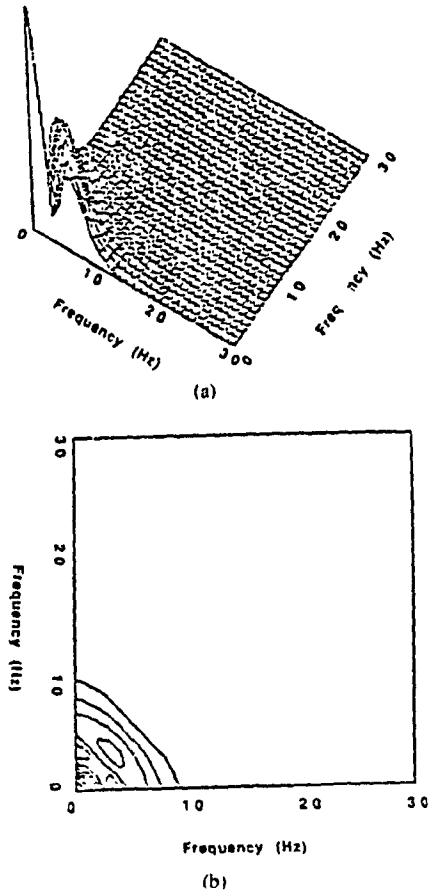

Fig.7.4 Detection of quadratic phase coupling in EEG signals using bispectrum. (a) Bispectrum of cortical EEG during quiet waking , (b) Contour of bispectrum indicates peak at (3 Hz., 3 Hz.)

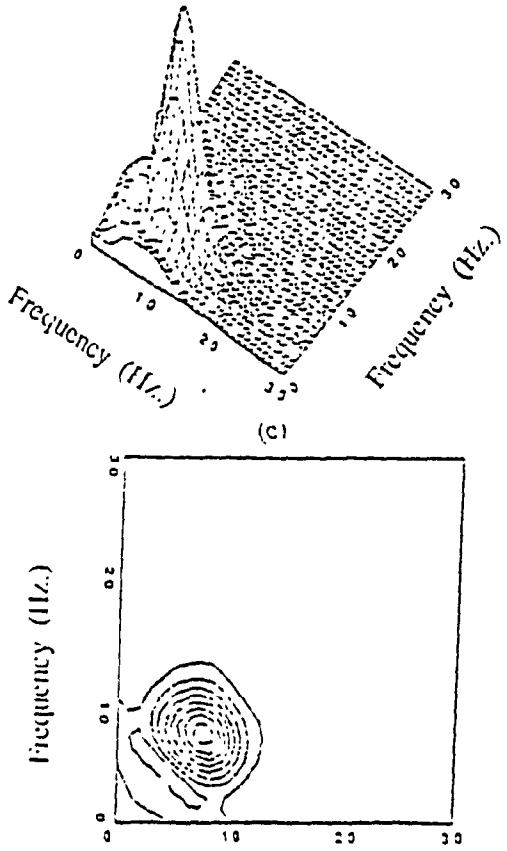

Fig. 7.4 Detection of quadratic phase coupling in EEG signals using bispectrum. (c) Bispectrum of hippocampal EEG during REM sleep, (d) Contour of bispectrum indicates peak at (7 Hz., 7 Hz.) i.e. in the theta range.

Table 7.1 Degree of phase coupling of the Hippocampal EEG during REM sleep.

Rat	R321	R351	R352	R354	R502
peak freq. (Hz.)	(7,7)	(6.6)	(7.7)	(7.7)	(6.5)
deg. coupling	1.07	0.81	0.88	1.07	1.29

7.6 References

[7.1] Brillinger,D.R., 1975, Time series , New York , Holt

[7.2] Brillinger,D.R., 1965, An Introduction to Polyspectra, Ann. Math. Stat., Vol.36, pp. 1351-1374.

[7.3] Huber,P.J., Kleiner,B., Gasser,T., and Dumermuth,G., 1971, Statistical Methods for investigating phase relations in stationary stochastic processes, IEEE Trans. Audio and Electroacoustics, pp. 78-86.

[7.4] Rosenblatt,M., and Van Ness,J.W., 1965, Estimation of the bispectrum, Ann. Math. Stat., Vol.36 pp. 1120-1136.

[7.5] Brillinger,D.R., and Rosenblatt,M., 1967, Asymtotic theory of Estimates of K-th Order Spectra, in Spectral Analysis of Time series, B.Harris, Ed. New York: Wiley.

[7.6] Brillinger,D.R., and Rosenblatt,M., Computation and interpretation of K-th order spectra, Op. Cit.

[7.7] Hasselmann,K., Munk,W., and MacDonald,G., 1963, Bispectra of Ocean Waves, in Time series analysis, M.Rosenblatt, Ed. New York: Wiley.

[7.8] M.D. Godfrey, 1965, An Exploratory study of the Bispectrum of Economic Time Series, Appl. Stat., Vol. 14, pp. 48-69.

[7.9] Kim,Y.C., and Powers,E.J., 1979, Digital Bispectral Analysis and it's applications to nonlinear Wave interactions, IEEE Trans. Plasma Science, pp. 120-131.

[7.10]Lii,K.S., Rosenblatt,M., and Van Atta,C., 1976, Bispectral Measurements in Turbulence, J. Fluid Mech., Vol.77, 45-62.

[7.11]Haubrich,R.A., 1965, Earth Noise, 5 to 500 Miliicycles per Second, J. Geophys. Res., pp. 1415-1427.

[7.12]Hinich,M.N., and Clay,C.S., 1968, The Application of the Discrete Fourier Transform in the Estimation of Power Spectra, Coherence and Bispectra of Geophysical Data, Rev. Geophys. Vol.6, pp.347.

[7.13]McComas,C.H., and Briscoe,M.G., 1980, Bispectra of Internal Waves, J. Fluid Mech., Vol. 97, pp. 205-213.

[7.14]Zadro,M.B., and Caputo,M., 1980, Spectral, Bispectral Analysis and Q of the Free Oscillations of the Earth, Supplemento al Nuovo Cimento, Vol. 6, No. 1, pp. 205-213.

[7.15]Korein,J., Tick,L.J., Zeitlin,R.A., and Randt,C.T., 1968, Linear and Non-Linear Spectral Analytic Techniques Applied to the Human Electroencephelogra, Carrier Sci. Health Res. Council, Vol. 44, pp. 1126-1128.

[7.16]Matsuoka,T., and Ulrych,T.J., 1984, Phase Estimation using the Bispectrum, Proc. IEEE, pp. 1403-1411.

[7.17]Brillinger,D.R., 1982, The Identification of Polynomial Systems by means of Higher Order Spectra, J. Sound Vib., 12, pp. 199-213.

[7.18]Lii,K.S., and Rosenblatt,M., 1982, Deconvolution and Estimation of Transfer Function Phase and Coefficients for non-Gaussian Linear Processes, Ann. Statist., Vol. 10, pp. 1195-1208.

[7.19]Rosenblatt,M., 1980, Linear Processes and Bispectra, J. Appl. Prob., 17, pp. 87-93.

[7.20]Huzii,M., 1981, Estimation of Coefficients of an Autoregressive Process by using a Higher Order Moment, J. Time Ser. Analysis, Vol. 2, pp. 87-93.

[7.21]Lohmann,A.W., and Wirnitzer,B., 1984, Triple Correlations, Proc. IEEE, Vol. 72, No. 7, pp. 889-901.

[7.22]Sato,T., and Sasaki,K., 1982, Bispectral Holography, J. Acoust. Soc. Amer., Vol. 70, pp. 1055-1096.

[7.23]Kay,S.M., and Marple,S.L., 1981, Spectrum Analysis: A Modern Perspective, Proc. IEEE, Vol. 69, No.11, pp. 1380-1418.

[7.24]Raghuveer,M.R., and Nikias,C.L., 1984, Bispectrum Estimation: A Parametric Approach, IEEE Trans. ASSP., ASSP-32, No.3, pp. 1024-1031.

[7.25]Makhoul,J., 1975, Linear Prediction: A Tutorial Review, Proc. IEEE, Vol. 63, pp. 561-580.

[7.26]Zohar,S., 1974, The Solution of a Toeplitz set of Linear Equations, J. ACM, Vol. 21, pp. 272-276.

[7.27]Nikias,C.L., and Raghuveer,M.R., 1985, Discussion: Higher Order Auto-Spectra by Maximum Entropy Method, Geophysics, 50(1).

[7.28]Kay,S.M., and Marple,S.L., 1981, Spectrum Analysis: A Modern Perspective, Proc. IEEE, Vol. 69, No. 11, pp. 1380-1418.

[7.29]Chow,J.C., 1972, On Estimating the Orders of an ARMA Process with uncertain observations, IEEE Trans. Automat. Contr., Vol. AC-17.

[7.30]Chan,Y.T., and Wood,J.C., 1984, A New Order Determination Technique for ARMA Processes, IEEE Trans. ASSP., Vol. ASSP-32, No.3, pp. 517-521.

CHAPTER 8

CONCLUSIONS

The spectral feature extraction of EEG signals by parametric approach is presented in this thesis. The parametric approach considered mainly involves spectral feature extraction of EEG signals by pole-zero modeling methods based on a combination of homomorphic filtering and linear prediction, sequential adaptive spectral modeling of EEG and spectral feature extraction of EEG when it is associated with muscle noise.

The studies on pole-zero spectral modeling of EEG by homomorphic prediction and pole-zero decomposition methods indicate that the advantages of linear prediction technique can be exploited by modeling the minimum phase equivalent of the EEG signal obtained by homomorphic filtering. However, when the EEG signal is directly used for spectral modeling, erroneous spectral estimates are obtained by the linear prediction based methods and this is due to incorrect estimation of zeros.

For the same number of parameters, the EEG spectral estimates obtained by these methods are found to be much superior to those obtained by all pole modeling method of Burg, with respect to the width of the spectral peaks and valley regions. The pole-zero decomposition method has been found to provide a better spectral fit to the logmagnitude spectrum than that obtained by homomorphic prediction, particularly with respect to bandwidth of the spectral peaks. It has been found that for the methods used, 12 parameters (8 poles - 4 zeros for homomorphic prediction and 12 cepstral coefficients for the pole-zero decomposition method) are sufficient to get a satisfactory spectral fit to the logmagnitude spectrum of the EEG.

The estiamtes of zero location by direct pole-zero modeling, for some EEG signals which has been found to lie outside the unit circle indicate that the EEG in general cannot be assumed to be a minimum phase signal.

The spectral modeling of EEG considered in the present study is general and application of these methods to specfic studies like infant maturity developement, effects of medication and to

represent different sleep stages are interesting possiblities. Since cepstral coefficient representation of EEG signals has found to be quite satisfactory and also as cepstral coeeficients are known for their good distance measure properties, their performance in EEG classification in different cases may be considered.

The contribution to the sequential adaptive approach involves extension of LMF adaptive algorithm to lattice structure. For the EEG signal, the LMF-TDL is found to be superior in providing better spectral fit to Burg's block data spectrum. The LMS-TDL and LMS-lattice both are found to be inferior to LMF-TDL and LMF-lattice respectively, with respect to providing resolvability and good spectral fit to Burg's block data spectrum for the same speed of convergence. However, from the point of view of accuracy of peak frequency estimation, both LMS and LMF adaptations show similar performance.

These algorithms can be extended to handle nonstaionary EEG signals which are encountered during transitions of eyes open to eyes closed, change in background activity that occurs prior to an epileptic crisis, changes in sleep records etc.

Also, the spectral feature extraction of EEG signals in presence of muscle noise, which is quite common with EEG recordings and which severely affects the EEG signal analysis is considered. The study illustrates the performance of the LMS-TDL and LMS-lattice sequential adaptive predictors in combination with a 4th order Butterworth lowpass filter, for muscle noise cancellation. The performance of these methods is assessed by computing Burg's spectra for the filtered EEG signals and the results indicate that for a valid parametric spectral representation of EEG associated with muscle noise, mere lowpass filtering is not sufficient and adaptive filtering is essential to minimize the EEG inband muscle noise. The results obtained from the method used in the study are found to be quite satisfactory from the EEG spectral estimation point of view.

The adaptive algorithm used in the present study for eliminating muscle noise could be used for cancelling other noises like the EOG and the ECG which also effect the EEG spectral estimation.

A parametric bispectrum estimation scheme proposed by Raghuveer and Nikias [7.24] was studied. When we are given samples of the true third moment sequence of a process, the method fits an

AR model in the sense of perfect matching between the output third moment sequence and third moment samples at given lags. For a finite time sample of the process, the method fits an AR model to biased third moment estimates obtained by forming averaged, lagged triple products in the time domain. Quadratic phase coupling was studied for different types of sleep patterns and bipectrum estimation was used to identify it. The results obtained are encouraging and qualify bispectrum estimation as a means to study sleep stages which are of great clinical importance.